Force Measurement of Kinesin Propelled Microtubules in Swarming Using an Electromagnetic Tweezer

(電磁ピンセットを用いたキネシンにより推進する微小管の群れにおける力測定)

Mst. Rubaya Rashid
モサンマッ ルバヤ ラシヅ

Material Chemistry Laboratory
Graduate School of Chemical Sciences and Engineering
Hokkaido University, Japan

2023

Contents

Chapter 3: Force determination of the MT swarm ring using magnetic bead and electromagnetic tweezer

Chapter 1
General Introduction

1.1 Purpose

The swarm is the collective movement of a large number of self-propelled entities, in particular insects, such as ants, bees, flocks of birds, or schools of fish, and even microorganisms such as bacteria that aggregate, moving in the same place or moving in the same direction.[1,2] This self-organization emerges through local interactions between self-propelled objects, rather than being controlled by a leader whose swarm is induced as a collective motion with a specific energy.' Swarming has several advantages that a single entity cannot achieve, such as parallelism, robustness, and flexibility.[3,4] Researchers in the fields of biotechnology and materials science have been motivated by natural swarms and attempts to replicate them in exploiting their advantages in different nanotechnological applications.[5,6]

Recently, a research group has demonstrated DNA-based controllable swarming of MT driven by multiple kinesins that exhibits translational and rotational motions.[7,8] The swarming of MTs with rotational and translational motion holds great potential as their motion can be harnessed to perform work for nanotechnological applications, e. g. in molecular machines or devices, molecular robotics, etc. To ensure real-life applications of the MT swarms it is a prerequisite to quantify the amount of work that can be harnessed from the swarms. In this work, we attempt to quantify the force associated with the swarming of MTs driven by kinesins. The force-velocity relationship of a single kinesin, as well as for a few numbers (1 to 10 kinesin) of kinesins against an increasing opposing load, has been well studied.

For single molecular force study in biological system, an optical tweezer is a commonly used tool that provides the forces in the piconewton range depending on the laser setup.[9] The force associated with the swarming of MTs propelled by multiple kinesins is higher compared to the single molecule system.[10–12] Recently, it has become popular to utilize magnetic beads as cargo for applying controlled forces using a magnetic source, providing ease of handling and magnetic force from zero to hundreds of pN.

Dynabeads^{TM} M-270 Amine is a superparamagnetic, bead with a uniform size (diameter 2.8 um) and has the chemical functional group such as carboxyl, amino, and streptavidin in the surface.

Recently they are used for applying hundreds of piconewton forces in presence of a magnetic field.[13–15] A custom-made electromagnetic tweezer system has been established in this work to apply electromagnetic force (emf) to the beads. By utilizing the recognition ability of DNA, beads can be easily attached to MT swarms[16] and emf can be easily applied to the swarm system. A ring-shaped swarm of MT's was constructed, bead was attached by DNA interaction, and controlled emf was applied to determine the force of the swarm. The rotational motion of the swarm ring allows it to change its direction of motion repeatedly and emf was applied. The directional change of the swarm ring allowed the EMTw to apply different amplitudes of force dependent on the angles between the applied emf and the direction of motion of the swarm ring. The systematic manipulation of the velocity applying emf and using the force calibration curve I determined the force of the swarm. The density of the involved kinesin was also estimated to compare the forces obtained from the swarm rings of different sizes propelled by multiple kinesins. The sub-additive force was found involving the increasing number of active kinesins with increasing the size of the swarm rings. Such estimation of the force of the swarm of MTs will widen applications of the MT swarm in nanotechnology as well as in robotics.

I also investigated the structural details of the packing and alignments of MTs in a swarm using a high speed atomic force microscopy combined with a fluorescence microscopy.[17–20] It was found that, the multiple MTs not only self-organize laterally but also form multiple layers with an increasing number of MTs in a swarm. These results provide new insight into the structure of the ring-shaped MT swarms and the alignment of MTs in the swarms.

1.2 Swarming in nature

Swarming is one of the most fascinating phenomena in nature exhibited by a large number of same individual self-propelled entities, from animals to microorganisms, such as the flocks of birds, school of fishes, colonies of ants and bacteria (Figure 1.1).[3,4] It is the self-organization or self-assembly of thousands to millions or even trillions of individual agents moves at the same time with same speed. Swarming pattern moving in a particular direction is generally formed by local interaction among the nearest neighbors in a decentralized manner. Instead of having a sophisticated controller for the entire swarm system, mutual interactions between individual entities play an important role in swarming. The dynamic coordination of the single entities into larger patterns and redistributing them into individual entities, the whole system works in a more sophisticated way. The advantages gained by the swarming are the protection from predators, forage of foods, migration from one place to another etc.

Figure 1.1 Swarm of living entities in nature

1.3 Swarming in artificial environment

Inspired by natural swarming, rescarchers in the field of material sciences and engineering introduced artificial swarm robots in different scales.[5,6] Swarm robotics is a new method of coordinating multi-robot systems consisting of multiple physical robots through inter-group cooperation and has the advantages of reusability of common agents and low cost of construction and maintenance compared to single conventional ones. The swarm robot can complete a sophisticated task or solve problems involving large amount of time, space or targets, and a certain danger that may exist in the environment. For example, the mergeable nervous system robotics in the size of meter range.[21] These robots can merge to form larger bodies with a single central controller, split into separate bodies with independent controllers, and self-heal by removing or replacing malfunctioning body parts (Figure 1.2a).

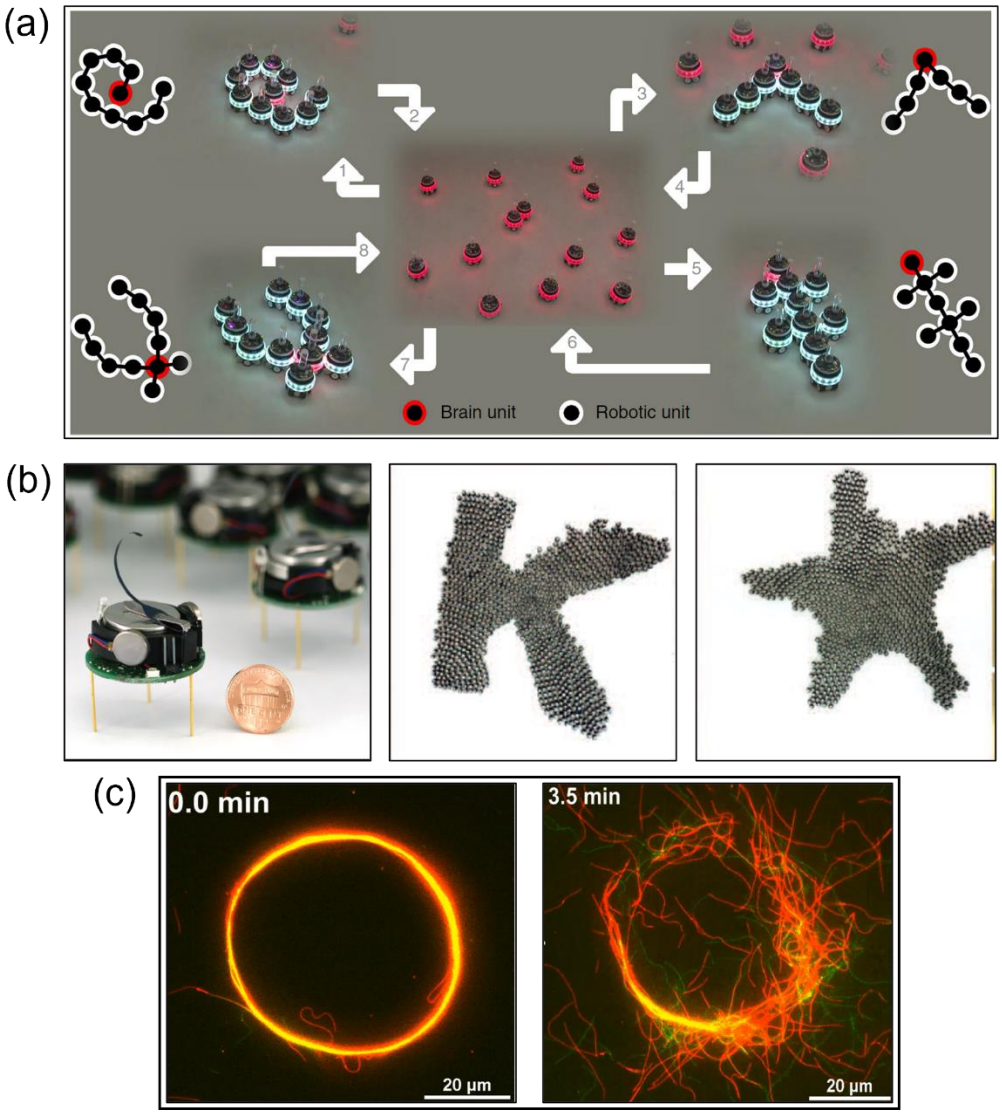

Figure 1.2 Artificial swarm robots by local interaction into different swarming patterns (a) The mergeable nervous system concept, MNS-robots physically connect to one another and thereby merge into larger MNS robots of different shapes and sizes.[21] (b) A Kilobot robot, shown alongside a U. S. penny for scale, and self-assembly from the individual entities to the final self-assembled shape.[22] (c) Molecular swarm robot: MT swarm propelled by kinesins, Regulation of MTs from swarm to single by employing DNA into the structure.[8]

Kilobot, another artificial swarm robot, demonstrates programmable self-organization of complex two-dimensional shapes by swarms of thousand robots (Figure 1.2b).[22] This was enabled by creating autonomous robots designed to operate in large groups and to cooperate through local interactions and by developing a collective algorithm for shape formation that is highly robust to the variability and error characteristic of large-scale decentralized systems. Recently a group of researchers introduced DNA based molecular swarm robot of microtubule (MT) and kinesin that

is in the micrometer size range (Figure 1.2c).[7,8] These molecular swarm robots draw the attention due to their small size, controllability, and flexibility. MT swarms demonstrates translational and rotational motion that holds potential to perform work in the nanotechnological applications. Recent advances in MT swarm robots have been reported for collaborative cargo transportation in a controllable manner by the translation of motion of MT swarm.[16] However to ensure more real-life applications of the MT swarms, it is a prerequisite to quantify the amount of work that can be harnessed from the swarms i.e. understand the force associated with the swarm.

1.4 Biomolecular motor system in *in vivo*

Within all eukaryotic cells, it is needed to transport vesicles, membrane-bound organelles, and nutrients through the viscous cytoplasm of the cell. Active transportation is required to move these essential cellular components over distances of up to a meter within the cell where diffusion alone is insufficient.[23] This active transport is carried out by many classes of molecular motors such as kinesins, dyneins and myosins on different filaments like actin and microtubule as a rail.[23,24] They will undergo dramatic conformational changes as they bind and hydrolyze ATP and release the products in a cyclic process. Motors, such as myosin and kinesin, operate in conjunction with cytoskeletal filaments - actin filaments and MTs, respectively. Kinesin was first observed in 1985 in giant squid axoplasm extracts and it's superfamily makes up one class of motor proteins with 14 subgroups, all of which are microtubule associated proteins.[25–27]

Microtubule polymerization requires the hydrolysis of guanosine triphosphate (GTP). The energy released from hydrolysis of GTP bound to β tubulin is used to bind α and β tubulin together. During polymerization, tubulin dimers bind head-to-tail to form linear protofilament (PF) with an 8 nm repeat distance and a variable number (10-18, often 13) of PFs assemble into a cylindrical structure with an outer diameter of about 25 nm and a length of many micrometers (Figure 1.3).[31] The tubulin monomers polymerize most rapidly on the (+) end of the microtubule, which in vivo typically leads away from the cell nucleus.

In order for a kinesin motor to be active, defined as able to hydrolyze adenosine triphosphate (ATP) and move along a microtubule filament, the motor domain kinesin must be bound to the β - tubulin of a microtubule for the gliding, [32–36] The lateral inter-PF contacts are mostly electrostatic, but the intra-PF interactions (-αβ -αβ -) are basically hydrophobic.[37] The structural properties of MTs are critical to their cellular functions as well as their nanotechnological applications.[38] MTs serve as

scaffolds for a wide variety of MT-associated molecular motors or trucks (i.e. kinesin's and dynein's families) in cell.

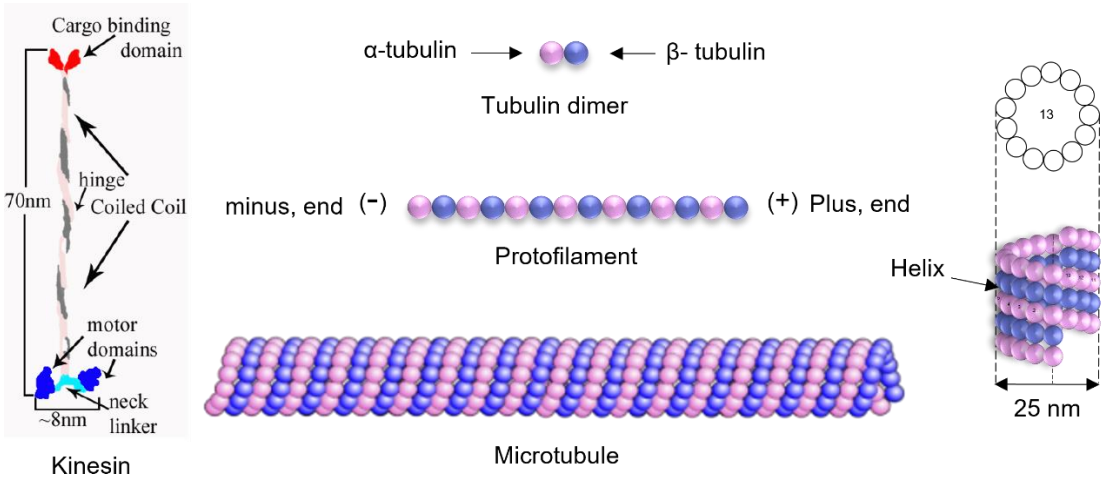

Figure 1.3 Model of a conventional kinesin dimer (left). Schematic image of the helical structure of a filament protein (microtubule) formed 13 protofilament of tubulin dimers (middle, right). Kinesin moves along microtubules, known as cytoskeletal 'track' are hollow cylinders polymerized from two heterodimer subunits: α and β tubulin (see figure 1.3).[23,24] Microtubules are formed of 12-14 protofilaments of tubulin and have an outer diameter of between 24-26 nm and an inner diameter of approximately 18 nm.[29]

The motors utilize chemical energy to generate mechanical motion. The molecular motor kinesin is a homodimer containing two heads-globular domains each of which has an ATP and a MT binding site.[39] It is a tetramer of two identical 'heavy chains' and two associated light chains. The heavy chains fold into two globular heads at one end a stalk, with a hinge in the middle, and a tail domain at the other end (Figure 1.3 left). The heads step on the binding sites along the MT protofilaments (PFs). These sites are spaced 8 nm apart and the kinesin is moving 8 nm in each step in a hand-over-hand mechanism.[40] For every step, kinesin consumes one ATP molecule (Figure 1.4b). Kinesin-1 motors are primarily involved in intracellular transport of vesicles and organelles, cell division and the organization of cilia and flagella.[41] The kinesin-1 (conventional kinesin) is of utility in nanotechnology because their primary function is the exertion of force. Micromechanical recordings from single kinesin molecules indicate that one motor can exert a force as great as 5 pN.[42] The efficiency of kinesin is in the order of 50%, considering the free energy available from ATP hydrolysis. Because of its high degree of processivity, even a single kinesin molecule is capable e propelling MTs along a surface. The small size and high efficiency

of MT-kinesin system makes it fascinating to apply it as molecular devices for a wide range of purposes which bane possible in synthetic environment such as motility assay system.[43,44]

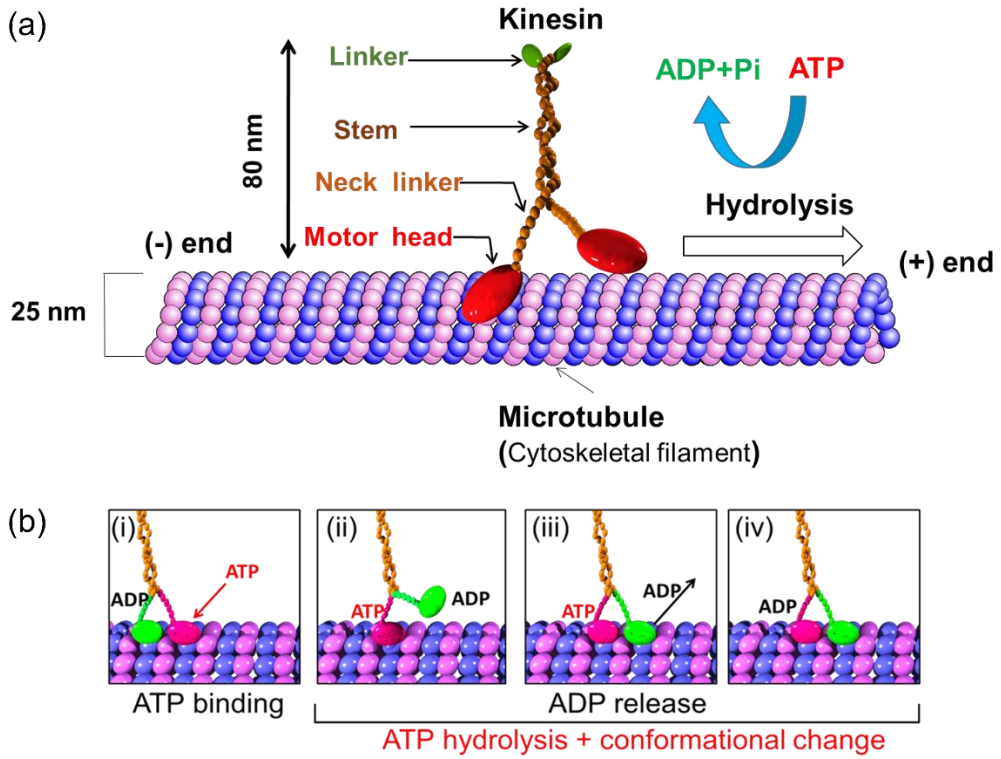

Figure 1.4 (a) Schematic image of kinesin on a MT track, (b) The stepping mechanism of kinesinon the MT track by hydrolysis of ATP to ADP.

1.5 *In vitro* motility assay of biomolecular motor system

The in vitro motility assay is the most promising setup for nanotechnological usage of biomolecular motor system in the artificial environment (Fig. 1.5).[45,46] To investigate the property of biomolecular motor systems in vitro, motor proteins and their associated cytoskeletal filaments were fabricated successfully by latest technological advancements. In this way at first, movement of myosin coated fluorescent beads were successfully observed on F-actin fixed substrate by Sheet and Spudich.[47] Vale and his colleagues discovered uni-directional gliding motion of MT in the cell extract from squid axon on a substrate driven by biomolecular motor (kinesin and dynein).[48] They named this method "in vitro motility assay" as gliding of filaments was observed which helps to investigate property of biomolecular motor systems. Later, Spudich has also developed a similar *in vitro* motility assay where motility of F-actin on a myosin coated glass surface was

demonstrated.[49] These works have opened the door for understanding how biomolcular motors transport cargo molecules involved in numerous cellular processes, including cell polarity, cell division, cellular movement, and signal transduction.

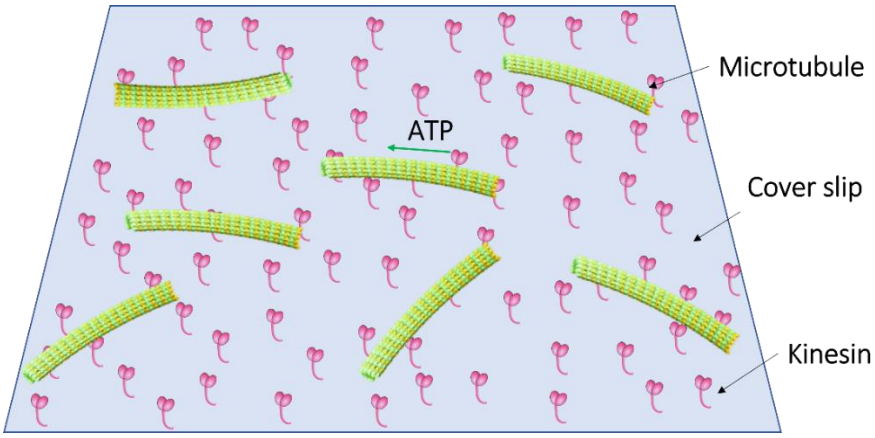

Fig. 1.5 Schematic image of in vitro gliding assay of MTs on kinesin coated surface.

With recent progress in the nanotechnology, in vitro gliding assay has been attracting interest for serving the smallest autonomous moving objects.[24] They provide transport of various nano- or micro-sized cargo molecules. This function is applicable for development of various kinds of micro devices which sort, separate, concentrate, probe, analyze and assembled materials (Figure 1.6a).[50–53] For example, Hess et al. used in vitro motility assay as piconewton force meter.[54] By considering one MT as a molecular cantilever, they calculated the force from bending of the cantilever when moving MTs collided with cantilever (Figure 1.6b). Furthermore, Hess et al introduced in vitro motility assay into a new method of surface imaging.[55] Further exploration with this system has been made with considerable efforts to achieve directed motility, control of moving direction by employing either chemical patterning of biomolecular motors or fabricated topographic patterns by using photolithography technique.[56,57] The direction of the moving filaments has been also controlled by employing electric field or magnetic field (Figure 1.6c).[58,59] The directional motion of filaments can be applied to sense mechanical deformation of surface which is advancement for soft surface induced nanotechnological applications reported by Inoue *et al*.[60]

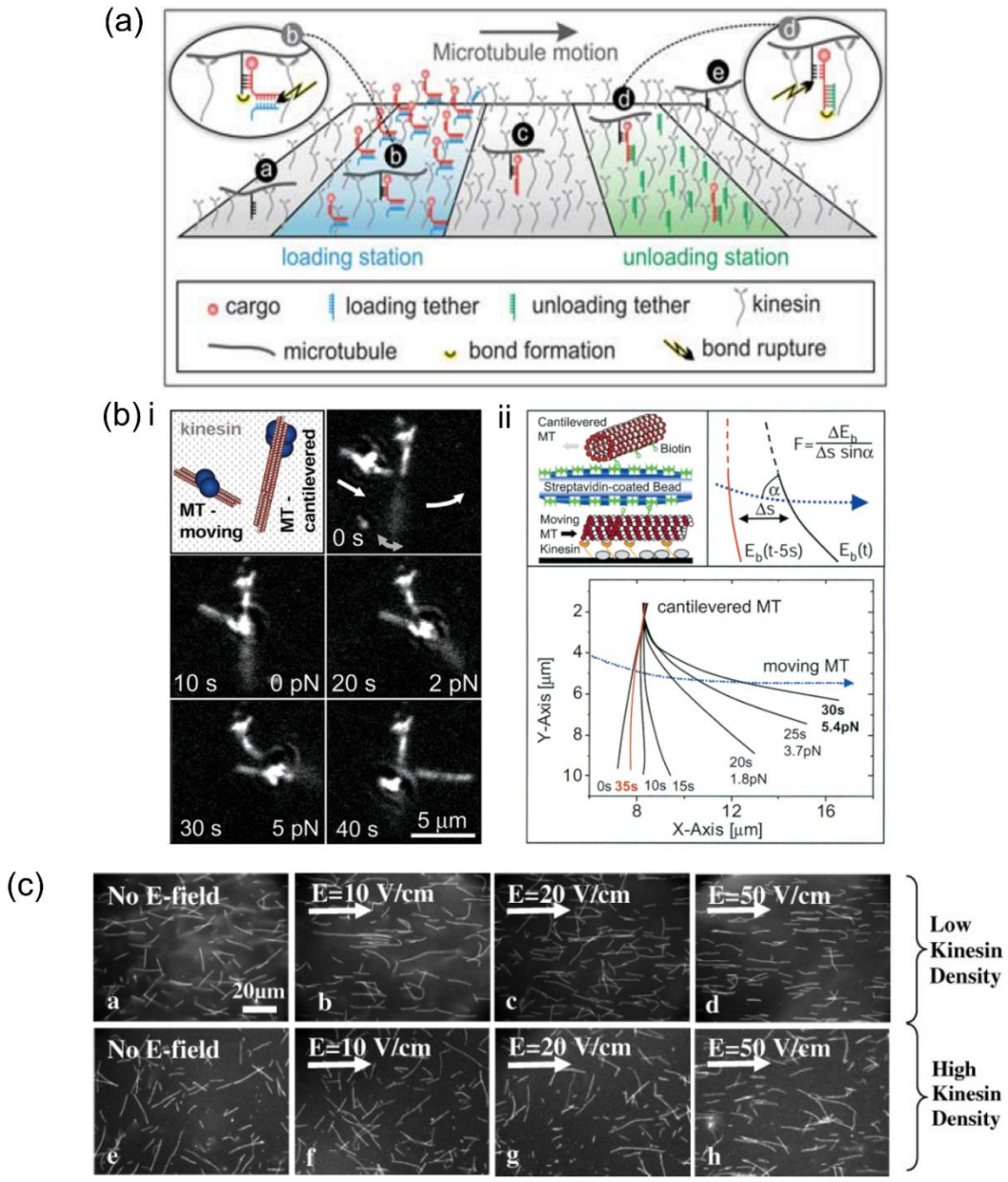

Fig. 1.6 (a) Cargo pick-up from loading station, transport and discharge at unloading station by molecular shuttles,[53] (b) (i) The cantilevered microtubule is attached on one end to a clump of beads, while the other end is suspended above the surface.[54] (ii) The moving microtubule (bottom) iS transported on a kinesin-coated surface, while connected through biotin linkers and a streptavidin- coated bead to the cantilevered microtubule (right top) (c) Gliding assay response to the application of various electric fields.[58]

Alongside with many applicable features of self-propelled MTs, this molecular shuttle was also applied to demonstrate swarm in a discrete level controlled by external stimuli or guiding direction. For example, investigation on the control over molecular shuttles by sequestration of enzyme

activities was studied by Hess et al using gliding assay of MTs. Localized release and enzymatic sequestration of the substrate ATP creates a spatially and temporally well-defined concentration profile, which in turn leads to controlled activation of a small number of molecular shuttles suggesting that these nano-systems are most efficiently addressed as a swarm rather than as individuals.[61] Hess and Nitta also reported the mechanisms responsible for the dispersion of a swarm of "molecular shuttles", consisting of functionalized Mis propelled by surface-adhered kinesin motor proteins.[62] It was revealed that, overall the dispersion of such molecular shuttles is comparable to the dispersion of a sample plug transported by electroosmotic flow. Besides this, an extensive study on swarming or collective behavior of biomolecular motor systems has been found in the literature which is based on energy dissipative self-organization process.

1.6 Self-organization of propelling filaments in *in vitro* motility assay

Nanotechnological applications of biomolecular motor systems have been possible to further amplify by integrating them using active self-organization (ACSO). The self-organization is accomplished through introducing attractive interaction between the cytoskeletal filaments driven by biomolecular motors using chemical energy of ATP hydrolysis allowing the creation of non-equilibrium structures. Recent studies have demonstrated some aspects of swarming behavior by controlling the mutual interactions of the propelled filaments using associated proteins, depletion agents, crowding effects, or ligand-receptor-based crosslinking.[11,63–68] These interactions lead to the emergence of fascinating swarm patterns, such as bundles, spools, vortex lattices, zigzag patterns as well as circular or polar patterns(Figure 1.7).[69–72]

Self-assembly of moving MT has been developed and vastly studied based on the in vitro motility assay by using strong non-covalent interaction e.g., streptavidin-biotin interaction or by using some kinds of cytoskeletal filament related proteins.[1,11,70,73] By using this method, a wide variety of assembled structures was obtained e.g. bundle, network, and ring-shaped structures that differ in size or shape. It was found that stiffer MTs with high bending rigidity favored the production of linear bundles while larger and longer bundles require more building blocks i.e; higher initial density of MTs. On the other hand, MT spools assembled from longer and flexible one is an example of such non-equilibrium structures, capable of storing bending energies on the order of 105 kT.[74,75] Phase diagram of ordered structures has thoroughly investigated and determined by

changing the experimental conditions such as the density of MTs and the strength of interaction of streptavidin/biotin.[70]

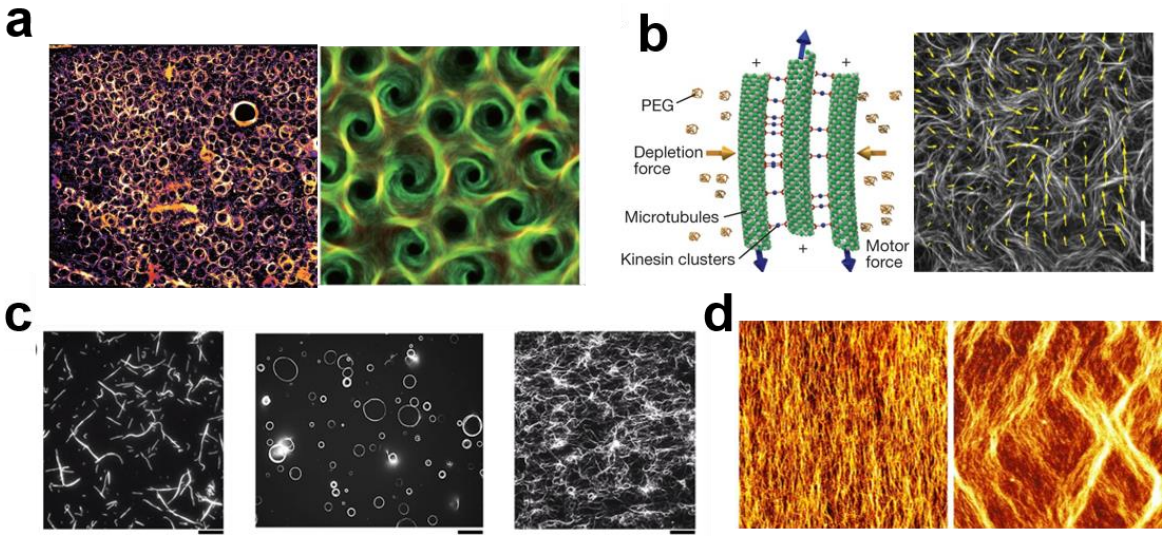

Figure 1.7 (a) Large sale vortex formation of collectively moving microtubules,[69] (b)Fluorescence image of an active microtubule network, scale bar: 80 um.[72] (c) Fluorescence microscopy images of MT bundles, rings, and networks produced in active self-assembly using streptavidin-biotin interaction. Scale bar: 10 μm.[70] (d) Zigzag pattern formation of MTs under cyclic stretching stimuli.[71] Images are used with permissions from references.

However, control over their collective behavior through a programmable manner is required to open an extensive opportunity for demonstrating tunable swarming with computing properties, which has not yet been achieved in these systems.[76] However, to get suitable linkers with the ability to combine with sufficient interaction strength, selectivity, reversibility, and capability to provide sensing and processing to the biomolecular motors systems have been always the biggest challenge.[77] In this way, a natural programmer DNA could be the most appropriate linker with all the capability to program swarming in the biomolecular motor system.

1.7 Incorporation of DNA in artificial swarming

DNA, a versatile tool to store genetic information with high molecular recognition ability has enormous potential for molecular computing depending on base sequence information.[78] Biomolecular engineering mainly depends on the programmability of Watson-Crick base pairing combining with a decrease in the cost of synthesis. Structural simplicity and controllable binding interactions of DNA by four base units (adenine, (A), cytosine (C), guanine (G), thymine (T))

result in a simple structure and predictable behavior (Figure 1.9).[79] Other than these structural features two important and exclusive properties make DNA suitable for molecular level constructions such as molecular recognition and self-assembly.[80]

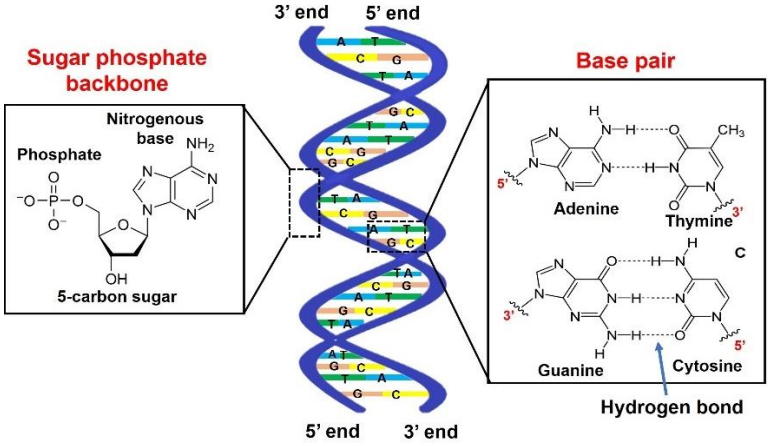

Figure 1.8 Schematic representation of the DNA double helix showing the sugar phosphate backbone and base pair.

The pioneering efforts of Seeman in DNA nanotechnology[81–83] and the revolutionizing work of Rosemond on DNA origami[84–86] paved the way to enable the rational design of DNA nanostructures. Adleman demonstrated the use of DNA to perform logical operations by solving a complex mathematical problem using only DNA oligonucleotides.[78] The self-assembly behavior of DNA was further computed to design different logical operations for engineering complex structures and exploit their functions. This attractive phenomenon of programming of DNA was further used for engineering the self-assembly of different building blocks to enhance their functionalities with higher-ordered structures. DNA programming was also successfully applied in DNA template self-assembly of other functional materials like nanoparticles and proteins.[87] Higher-order structures that originate from the specific and reversible DNA-directed self-assembly of microscopic building blocks hold great promise for future technologies. Applications of these self-assembly strategies span from photonics and plasmonics to biosensing and gene therapy.[88–90] Moreover, the same self-assembly strategy has been applied to compliant Brownian units, including emulsion droplets, lipid vesicles, time dependent assembly of functional clusters that result in rationally designed mesoscopic structures.[91] The concept of molecular robotics is also rooted in DNA molecular computing and then facilitated by the development of DNA origami.[92] The first step in molecular robotics was the development of DNA walkers, which have developed from being non-autonomous to being capable of directed but brief motion on the one-dimensional

track.[93,94] These walkers are powered by energy derived from DNA hybridization, consuming fuel oligonucleotides as they move from one binding site to another on a DNA-modified surface.

DNA has been used in combination with biomolecular motors either as a glue to assemble motors into multimers, or to connect motors to DNA origami scaffold, or being conjugated to MTs for cargo loading/unloading.[50,53,77,95] In spite of extensive studies on DNA based microrobotics, before 2018 there was no such report of DNA programmed swarming of biomolecular motor based microrobots.[7,8]

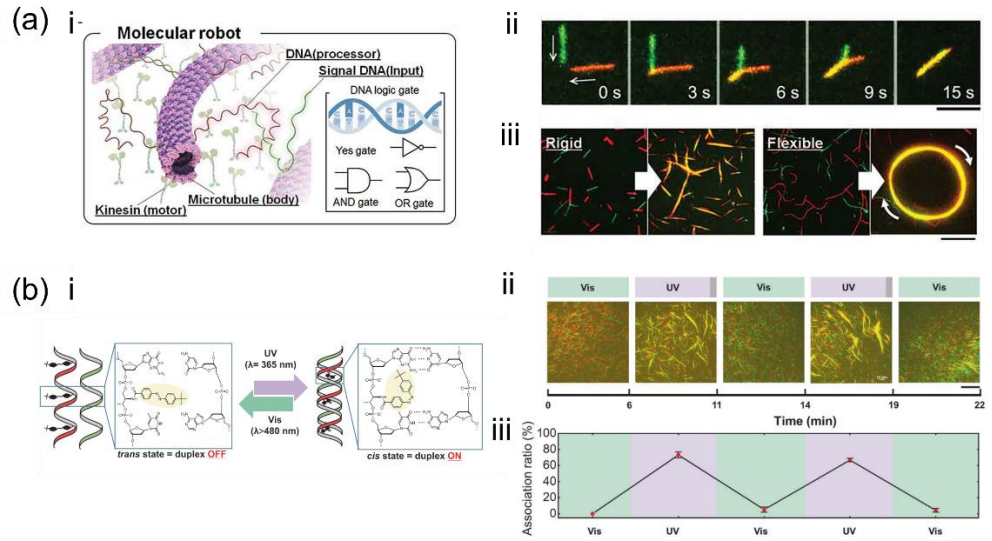

Figure 1.9 (a) (i, ii) Swarming mechanism of photoresponsive DNA (complementary sequence) conjugated microtubules, (iii) The pattern of swarm can be tuned by simply changing the mechanical properties of MTs,[8] (b) (i) DNA duplex formation by UV light-induced trans- to- cis isomerization of para tert-buty1-substituted azobenzene and (ii, iii) reversible regulation of MT swarming through photoirradiation.[96]

For the first time, biomolecular motor based microrobot 'molecular robot' was constructed using DNA as information processor where DNA can program the swarming in a reversible manner to form 'molecular swarm robot' (Figure 1,10).[7,8,96] Swarming of molecular robots was realized by utilizing the molecular recognition ability of DNA in controlling local interactions between molecular robots. DNA-based computation was used not only for swarm formation, but also for dissociation of the swarms into single molecular robots. The input signal of dissociation DNA prompted the groups of molecular robots to separate into single robots through strand displacement reaction of the complementary DNA of neighbor robots. But these systems limit the reversible regulation of the swarming. By incorporating photosensitive azobenzene moiety into DNA strands, the swarm formation by molecular robots and dissociation of swarms was controlled using light.

1.8 Cooperative cargo transportation by MT swarm robot

It has been always a challenge to construct a micro-sized robot at a molecular level with the ability to work miniaturing the macro robot.[97] Modern-day factory assembly lines often feature robots that pick up, transport and unload components in a programmed manner.[98] The transport of molecules, supramolecular complexes, and nano- or microparticles by a molecular robot could be a prime application in nanotechnology and also in bioengineering and healthcare.[97,99–105]

The idea of manipulating molecular cargo similarly has to date only been explored using chemical synthetic atoms or biological building blocks. Leigh et al, reported on a molecular robot that could selectively transport molecular cargo in either direction between two spatially distinct, chemically similar sites on a molecular platform.[106] Each robot can manipulate a single molecule and is made up of just 150 carbon, hydrogen, oxygen and nitrogen atoms. Xie et al. reported on microrobot swarm formation from the colloidal particles energized by external magnetic fields.[107] A variety of intriguing microrobotic swarm was exhibited ranging from dynamic self-organization to coherent motion; i.e. liquid, chain, vortex, and ribbon that enabled fast and reversible transformations between them. The reconfigurable microrobot swarms provide versatile collective modes to address environmental variations or multitasking requirements by passage through narrow channels (chain formation), coordinated handling of large loads (vortex formation), and large-area synchronized manipulation (ribbon formation). However, these chemically powered microrobots could limit its further application in a nanotechnological engineered system, which could be improved by using natural molecular devices.

A cargo sorting DNA molecular robot was reported recently with the ability to perform autonomous cargo transport using three modular building blocks.[108] The robot explored a two-dimensional testing ground on the surface of DNA origami, could pick up multiple cargos from unordered locations, and delivered each type to a specified destination until all cargo molecules are sorted into two distinct piles. But the slow-motion and poor efficiency of cargo sorting are the main drawbacks of this system which could be achieved by integrating motor proteins and launching simple communication between the robots for performing even more sophisticated tasks.[108] With more effort in developing modular and collective microrobots, and with simple and systematic approaches, molecular robots could eventually be easily programmed like macroscopic robots but working in microscopic environments. Recently a DNA based swarming of microrobots

was introduced in response to the visible-UV light in a reversible manner which has been reported to transport and unload cargoes efficiently responding to the photo signal are also described.

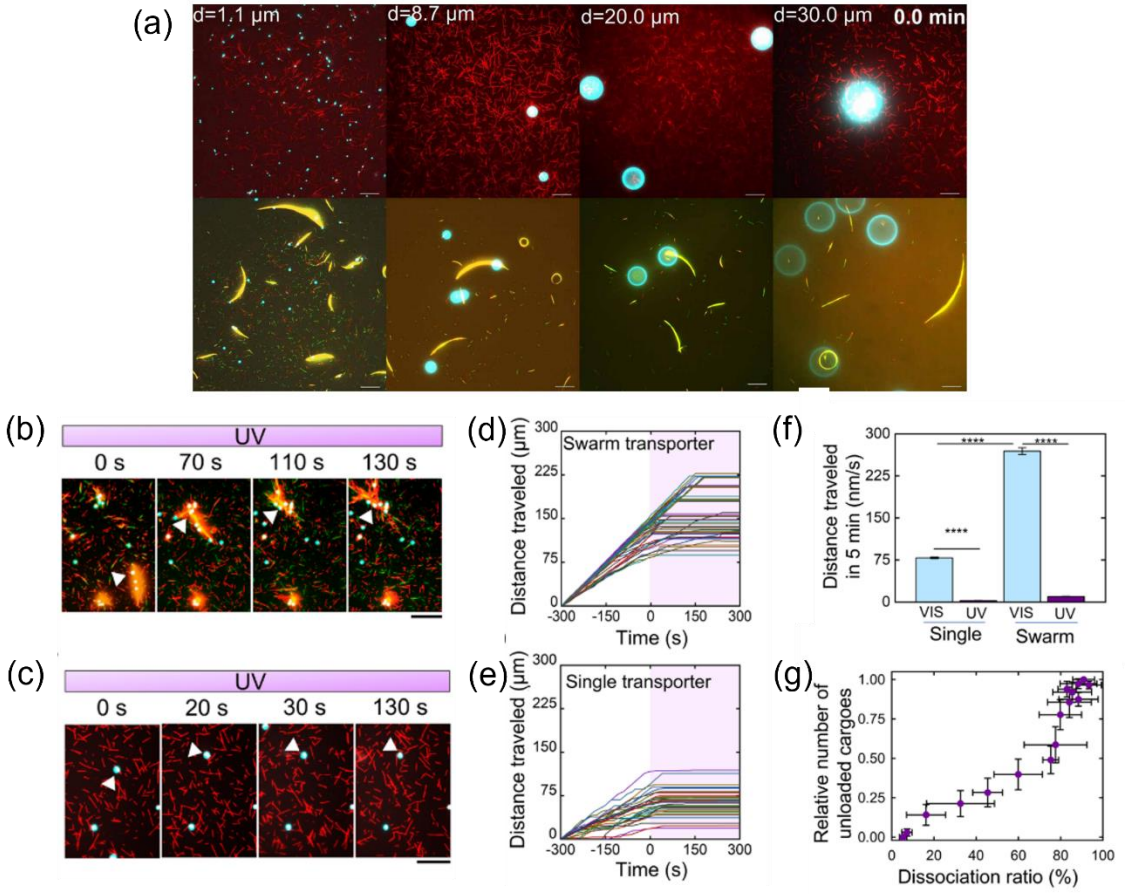

Figure 1.10 (a) Different diameters of cargo loading and transporting by single and swarm transporters. (b-g) Unloading of the transported cargo from the swarm and single transporters under UV light irradiation.[16]

1.9 Force determination of single and multiple Kinesin

Despite several extensive studies on the developing and controlling of swarm MT has been studied, the practical use of the swarm is yet to be obscured. The rotational and translational motion holds great potential as their motion can be harnessed to perform work for nanotechnological applications. It is necessity to quantify the efficiency i.e. force determination of the swarm to ensure the probable future application, as multiple kinesin and microtubules involved.

Several theoretical and experimental studies on force determination of single and a few kinesins (2- 10) propelling a microtubule or other cargoes are found in the literature. One of the examples is the force-velocity curve for multiple motors proposed by Klump and Lipowsky, where the

average velocity of the kinesin and the rate at which it unbinds from the MTs were predicted.[10] According to their model, each motor unbind from the filament after a finite number of steps but can also rebind to it again, the actual number of pulling motors is not constant but varies with time between zero and to multiple motor. The number of acting kinesin decreases as the opposing force increases. The stall force of an object pulled by many motors would increase linearly with the number of motors (i.e. stall force for one motor is 6 pN, the stall force for 2 motors is 12 p) but the velocity of the object would be negligible against higher forces. The detachment rate of the kinesins from the MTs is very low when the applied force is shared equally among all the kinesin motors. This model is comparable with the Shared-Force model proposed by Kunwar *et al.*[109]

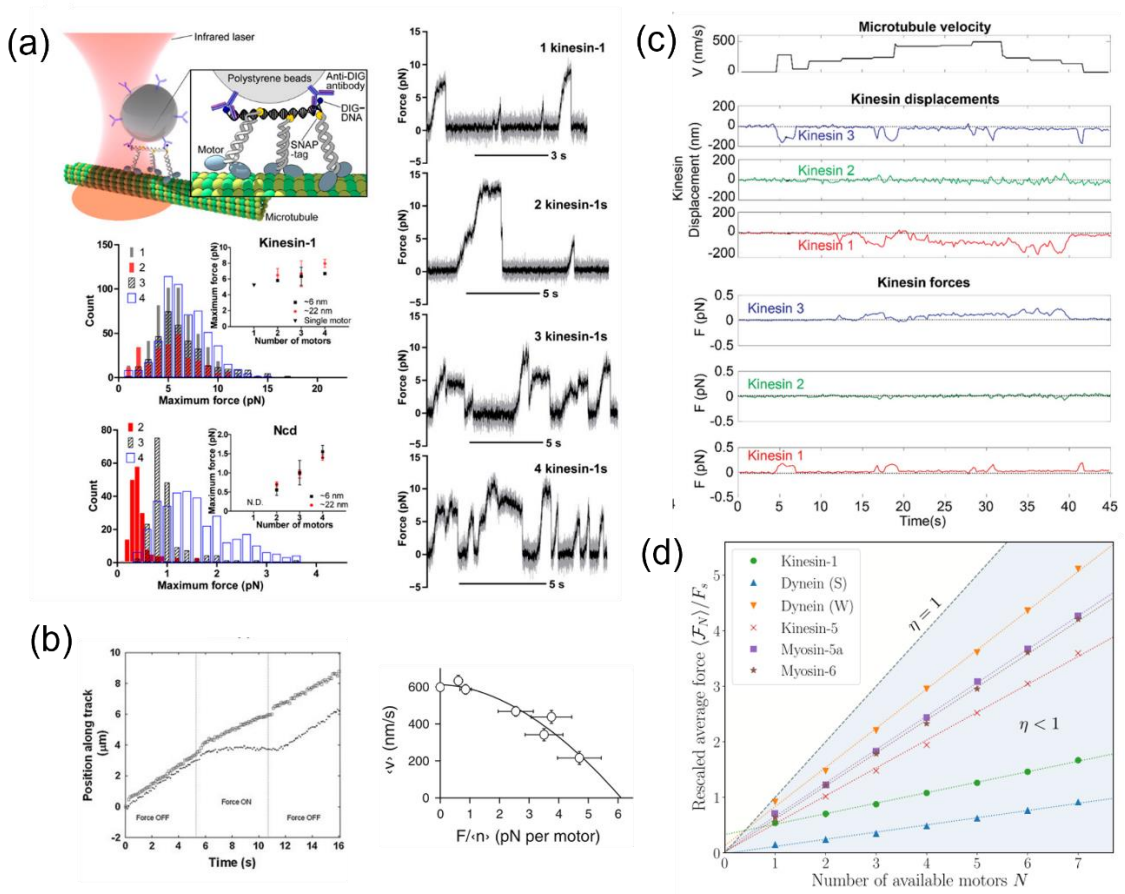

Figure 1.11 (a) Optical trapping assays for one to four kinesins.[112](b) The magnetic force slowed the microtubule down, and average velocity of gliding microtubules as a function of magnetic force.[15] (c) Force measurement of individual kinesins during multi-motor transport, microtubule velocity, kinesin dis-placements, and individual forces.[114] (d) Collective force generation by different types of different numbers of available motors.[113]

In contrast to these models, Hendricks *et al*. proposed a mechanistic model where kinesin synchronization increases with increased cargo linker stiffness or opposing force.[110] The kinesin motors are loosely synchronized at normal conditions and under low load, however, the synchronization increases to overcome obstacles or to deal with higher load. When the kinesin motors experience a higher load, the force against the opposing load increases linearly with the increasing number of kinesins. Another model called the shared-load model was proposed by Hill *et al*.[111] According to the model, the behavior of multiple motors under load is similar to the single motors when the load is shared equally to the motors. Fallesen *et. al.* reported the force-velocity relationship for multiple motors which was similar to the force-velocity relationship for a single motor, supporting a minimal load-sharing model.[15] The velocity distribution at low load has a single mode consistent with rapid fluctuations of number of motors. However, against a higher load on the multiple (2-7) motors, additional modes appeared resulting a lower velocity. Furuta *et al.* experimentally studied the forces generated by a controlled number of kinesin- 1 motors in a stationary optical trapping assay and the average collective force was increased sub additively with increasing the number of kinesins.[112] Their simulation results also showed similar results as the mean and median values of the forces generated by less than or equal to four kinesins increase with the number of kinesins, but the collective force generation was clearly sub additive. Another recent study by Mehmet *et al* reported the collective force generation by different motor types and kinesin-1 shows the sub-additive force generation in multiple motor assay.[113] Saurabh *et al* studied force generation by the kinesin in driving a MT and also overcoming obstacles. They reported that the kinesin exerts less than one pN force in average whiling gliding a MT and occasionally the force might increase while encountering obstacles.[114]

1.10 Dissertation outline

In this dissertation, I constructed kinesin propelled MT swarm using the recognition ability of DNA. An electromagnetic tweezers system has been developed and utilized it in the force determination of the swarm attaching with magnetic beads. The detailed studies and the results have been summarized in five chapters including general introduction and concluding remarks.

In **chapter 1**, the purpose of the dissertation and the background of the study have been explained.

In **chapter 2**, I reported the configuration and setup of a fluorescence microscope and a customized electromagnetic tweezer with micro-actuator for the fluorescence microscope observation under

controlled magnetic field. The force calibration was performed systematically by applying the magnetic beads in the liquid media by the electromagnetic tweezer. The bead was further attached to the MT swarms in a flow cell, and I observed the trajectory of the MT swarms by applying the magnetic field to the beads on the MT swarms. This study will enrich the understanding of the use of electromagnetic tweezers in biomolecular manipulations and dynamic control over the MT swarms.

In **chapter 3**, a new approach was taken to determine the force of kinesin on the substrate to propel the MT swarm with a magnetic bead by utilizing the system described in Chapter 2. The electromagnetic field was applied to the ring-shape MT swarms (MT ring swarms) attached with a magnetic bead by the electromagnetic tweezers. The continuous circular motion of the magnetic bead on the MT ring swarms allowed the tweezer to apply controlled positive and negative force dependent on the angles between the tweezer's tip and the magnetic bead. The applied force changed the velocity of the swarm ring. After the calibration, I determined the force of the MT ring swarms generated by ATP hydrolysis on the kinesin substrate. I systematically compared the forces of the MT ring swarms with different ring sizes. The force increased with increasing the size of MT ring swarms. This increase in force arose from the larger number of active kinesins propelling the MT ring swarms. The estimation of the force of the MT swarms will widen applications of the MT swarm in nanotechnology as well as robotics.

In **chapter 4**, I investigated the detail of the structures of the MT ring swarms and evaluated the number of MTs in the MT ring swarms by the combined system of HS-AFM and fluorescence microscopy. A combined HS-AFM and fluorescence microscopy in a single machine were used to investigate the packing and alignment of MT in an aqueous medium. It was found that in MT ring swarms, many MTs self-organized not only horizontally but also vertically to the substrate to form multiple layered structure, providing a new insight into the structure of the MT ring swarms and the alignment of MTs in the swarms. This will be indispensable in assessing the force associated with the MT swarms and allow for further regulation of the force by designing their structure, which will consequently further their applications.

In **chapter 5**, all the important results and future aspects of this research work have been summarized in the concluding remarks.

1.11 References

1. Whitesides, G. M. & Grzybowski, B. Self-assembly at all scales. *Science (80-.).* **295,** 2418–2421 (2002).
2. Palacci, J., Sacanna, S., Steinberg, A. P., Pine, D. J. & Chaikin, P. M. Colloidal Surfers. **339,** 936–941 (2013).
3. Beshers, S. N. & Fewell, J. H. Models of division of labor in social insects. *Annu. Rev. Entomol.* **46,** 413–40 (2001).
4. Niven, J. E. How honeybees break a decision-making deadlock. *Science (80-.).* **335,** 43–44 (2012).
5. Turgut, A. E., Çelikkanat, H., Gökçe, F. & Şahin, E. Self-organized flocking in mobile robot swarms. *Swarm Intell.* **2,** 97–120 (2008).
6. Wei, H., Chen, Y., Tan, J. & Wang, T. Sambot : A Self-Assembly Modular Robot System. *IEEE/ASME Trans. Mechatronics.* **16,** 745–757 (2011).
7. Keya, J. J., Kabir, A. M. R., Inoue, D., Sada, K., Hess, H., Kuzuya, A. & Kakugo, A. Control of swarming of molecular robots. *Sci. Rep.* **8,** 1–10 (2018).
8. Keya, J. J., Suzuki, R., Kabir, A. M. R., Inoue, D., Asanuma, H., Sada, K., Hess, H., Kuzuya, A. & Kakugo, A. DNA-assisted swarm control in a biomolecular motor system. *Nat. Commun.* **9,** 4–11 (2018).
9. Bustamante, C. J. & Wang, M. D. Optical tweezers in single-molecule biophysics. *Nat. Rev. Methods Prim.* (2021).
10. Klumpp, S. & Lipowsky, R. Cooprative cargo transport by several molecular motors. *Proc. Natl. Acad. Sci. U. S. A.* **102,** (2005).
11. Hess, H., Clemmens, J., Brunner, C., Doot, R., Luna, S., Ernst, K. H. & Vogel, V. Molecular self-assembly of 'nanowires' and 'nanospools' using active transport. *Nano Lett.* **5,** 629–633 (2005).
12. Liu, H., Spoerke, E. D., Bachand, M., Koch, S. J., Bunker, B. C. & Bachand, G. D. Biomolecular motor-powered self-assembly of dissipative nanocomposite rings. *Adv. Mater.* **20,** 4476–4481 (2008).
13. Fallesen, T., Hill, D. B., Steen, M., Macosko, J. C., Bonin, K., Holzwarth, G., Fallesen, T., Hill, D. B., Steen, M., Macosko, J. C. & Bonin, K. Magnet polepiece design for uniform magnetic force on superparamagnetic beads on superparamagnetic beads. **074303,** 1–6

(2018).

14. Fallesen, T. L., Macosko, J. C. & Holzwarth, G. Measuring the number and spacing of molecular motors propelling a gliding microtubule. **011918,** 1–8 (2011).
15. Fallesen, T. L., Macosko, J. C. & Holzwarth, G. Force – velocity relationship for multiple kinesin motors pulling a magnetic bead. *Eur. Biophys. J.* 1071–1079 (2011). doi:10.1007/s00249-011-0724-1
16. Akter, M., Keya, J. J., Kayano, K., Kabir, A. M. R., Inoue, D., Hess, H., Sada, K., Kuzuya, A., Asanuma, H. & Kakugo, A. Cooperative cargo transportation by a swarm of molecular machines. *Sci. Robot.* **7,** eabm0677 (2022).
17. Fukuda, S., Uchihashi, T., Iino, R., Okazaki, Y., Yoshida, M., Igarashi, K. & Ando, T. High-speed atomic force microscope combined with single-molecule fluorescence microscope. *Rev. Sci. Instrum.* **84,** (2013).
18. Ando, T., Kodera, N., Takai, E., Maruyama, D., Saito, K. & Toda, A. A high-speed atomic force microscope for studying biological macromolecules. *Proc. Natl. Acad. Sci. U. S. A.* **98,** 12468–12472 (2001).
19. Wijeratne, S. S., Marchan, M. F., Tresback, J. S. & Subramanian, R. Atomic force microscopy reveals distinct protofilament-scale structural dynamics in depolymerizing microtubule arrays. *Proc. Natl. Acad. Sci. U. S. A.* **119,** (2022).
20. Nasrin, S. R., Ganser, C., Nishikawa, S., Rashedul Kabir, A. M., Sada, K., Yamashita, T., Ikeguchi, M., Uchihashi, T., Hess, H. & Kakugo, A. Deformation of microtubules regulates translocation dynamics of kinesin. *Sci. Adv.* **7,** 1–12 (2021).
21. Mathews, N., Christensen, A. L., Grady, R. O., Mondada, F. & Dorigo, M. Mergeable nervous systems for robots. *Nat. Commun.* 1–7 (2017).
22. Rubenstein, M., Cornejo, A. & Nagpal, R. Programmable self-assembly in a thousand-robot swarm. *Science (80-.).* **345,** 795–800 (2014).
23. Schliwa, M. & Woehlke, G. Molecular motors. *Insight Rev. Artic. Nat.* **422,** 759–765 (2003).
24. U, H. H. & Vogel, V. Molecular shuttles based on motor proteins : active transport in synthetic environments. *Mol. Biotechnol.* 67–85 (2001).
25. Vale, R. D., Reese, T. S. & Sheetz, M. P. Identification of a Novel Force-Generating Protein , Kinesin , Involved in Microtubule-Based Motility. *Cell* **42,** 39–50 (1985).

26. Vale, R. D., Schnapp, B. J., Mitchison, T., Steuer, E. & Reese, T. S. Different Axoplasmic Proteins Generate Movement Opposite Directions along Microtubules In Vitro. *Cell* **43,** 623–632 (1985).
27. Lawrence, C. J., Dawe, R. K., Christie, K. R., Cleveland, D. W., Dawson, S. C., Endow, S. A., Goldstein, L. S. B., Goodson, H. V, Hirokawa, N., Howard, J., Malmberg, R. L., Mcintosh, J. R., Miki, H., Mitchison, T. J., Okada, Y., Reddy, A. S. N., Saxton, W. M., Schliwa, M., Scholey, J. M., Vale, R. D., Walczak, C. E. & Wordeman, L. A standardized kinesin nomenclature. *J. Cell Biol.* **10,** 19–22 (1985).
28. Case, R. B., Pierce, D. W., Hom-Booher, N., Hart, C. L. & Vale, R. D. The directional preference of kinesin motors is specified by an element outside of the motor catalytic domain. *Cell* **90,** 959–966 (1997).
29. Cooper, G. M. & Hausman, R. E. The Cell : A Molecular Approach , Seventh Edition. *Washint. DC, ASM Press*
30. Mickey, B. & Howard, J. Rigidity of Microtubules Is Increased by Stabilizing Agents. *J. Cell Biol.* 909–917
31. Zhang, R. & Nogales, E. A new protocol to accurately determine microtubule lattice seam location. *J. Struct. Biol.* **192,** 245–254 (2015).
32. Hackney, D. D., Levitt, J. D. & Suhan, J. Kinesin Undergoes a 9 S to 6 S Conformational Transition. *J. Biol. Chem.* **267,** 8696–8701 (1992).
33. Ruby, A. K., Hart, C. L., Ly, B., Hom-booher, N. & Vale, R. D. Microtubule Interaction Site of the Kinesin Motor. *Cell* **90,** 207–216 (1997).
34. Coy, D. L., Hancock, W. O., Wagenbach, M. & Howard, J. Kinesin ' s tail domain is an inhibitory regulator of the motor domain. *Nat. Cell Biol.* **1,** (1999).
35. Hackney, D. D. & Stock, M. F. Kinesin ' s IAK tail domain inhibits initial microtubule-stimulated ADP release. *Nat. Cell Biol.* **2,** 257–260 (2000).
36. Seeger, M. A. & Rice, S. E. Microtubule-associated Protein-like Binding of the Kinesin-1 Tail to Microtubules. *J. Biol. Chem.* **285,** 8155–8162 (2010).
37. Surrey, T., Frey, E., Florin, E., Pampaloni, F., Lattanzi, G. & Jona, A. Thermal fluctuations of grafted microtubules provide evidence of a length-dependent persistence length. *Proc. Natl. Acad. Sci. U. S. A.* (2006). doi:10.1073/pnas.0603931103
38. Bachand, G. D., Spoerke, E. D. & Stevens, M. J. Microtubule-Based Nanomaterials :

Exploiting Nature ' s Dynamic Biopolymers. *Biotecnol. Bioeng.* **112,** 1065–1073 (2015).

39. Howard, J. The movement of kinesin along microtubule. *Annu. Rev. Physiol.* (1996).
40. Coy, D. L., Wagenbach, M. & Howard, J. Kinesin Takes One 8-nm Step for Each ATP That It Hydrolyzes. *J. Biol. Chem.* **274,** 3667–3671 (1999).
41. Hirokawa, N., Noda, Y., Tanaka, Y. & Niwa, S. Kinesin superfamily motor proteins and intracellular transport. *Nat. Rev. Mol. Cell Biol.* **10,** 682–696 (2009).
42. Howard, J. The Movement of Kinesin Along Microtubules. *Annu. Rev. Physiol.* **58,** 703–729 (1996).
43. Diez, S. & Howard, J. Nanotechnological applications of biomolecular motor systems. *La Phys. au Canada* **65,** 7–12 (2009).
44. Sugita, S., Sakamoto, N., Ohashi, T. & Sato, M. Characterization of Motility Properties of Kinesin-Driven Microtubules Towards NanoScale Transporter: Focusing on Length of Microtubules and Kinesin Density. *J. Biomech. Sci. Eng.* **3,** 510–519 (2008).
45. Keya, J. J., Kabir, A. M. R. & Kakugo, A. Synchronous operation of biomolecular engines. *Biophys. Rev.* **12,** 401–409 (2020).
46. Korten, T., Tavkin, E., Scharrel, L., Kushwaha, V. S. & Diez, S. An automated in vitro motility assay for high-throughput studies of molecular motors. *Lab Chip* **18,** 3196–3206 (2018).
47. Spudich, J. A., Kron, S. J. & Sheetz, M. P. Movement of myosin-coated beads on oriented filaments reconstituted from purified actin. *Nature* **315,** 584–586 (1985).
48. Ma, J., Przibillat, E. & Hut, J. Yeast activators stimulate plant gene expression. *Lett. to Nat.* **334,** 631–633 (1988).
49. Kron, S. J. & Spudich, J. A. Fluorescent actin filaments move on myosin fixed to a glass surface. *Proc. Natl. Acad. Sci. U. S. A.* **83,** 6272–6276 (1986).
50. Agarwal, A., Katira, P., Hess, H. & Gaines, V. Millisecond Curing Time of a Molecular Adhesive Causes Velocity-Dependent Cargo-Loading of Molecular Shuttles 2009. *Nano Lett.* (2009).
51. Bachand, G. D., Rivera, S. B., Boal, A. K., Gaudioso, J., Liu, J. & Bunker, B. C. Assembly and Transport of Nanocrystal CdSe Quantum Dot Nanocomposites Using Microtubules and Kinesin Motor Proteins. *Nano Lett.* 1–5 (2004).
52. Unger, E. Motor protein-driven unidirectional transport of micrometer-sized cargoes

across isopolar microtubule arrays. *Nanotechnology* (2001).

53. Schmidt, C. & Vogel, V. Molecular shuttles powered by motor proteins: loading and unloading stations for nanocargo integrated into one device. *Lab Chip* **10,** (2010).
54. Hess, H., Howard, J. & Vogel, V. A Piconewton Forcemeter Assembled from Microtubules and Kinesins. *Nano Lett.* 1–3 (2002).
55. Hess, H., Clemmens, J., Howard, J. & Vogel, V. Surface Imaging by Self-Propelled Nanoscale Probes. *Nano Lett.* 8–11 (2002).
56. Reuther, C., Hajdo, L., Tucker, R., Kasprzak, A. A. & Diez, S. Biotemplated Nanopatterning of Planar Surfaces with Molecular Motors. *Nano Lett.* (2006).
57. Hiratsuka, Y., Tada, T., Oiwa, K., Kanayama, T. & Uyeda, T. Q. P. Controlling the Direction of Kinesin-Driven Microtubule Movements along Microlithographic Tracks. *Biophys. J.* **81,** 1555–1561 (2001).
58. Kim, T., Kao, M., Hasselbrink, E. F. & Meyh, E. Active Alignment of Microtubules with Electric Fields. *Nano Lett.* (2007).
59. Platt, M., Muthukrishnan, G., Hancock, W. O., Williams, M. E., Park, U. V & Pennsyl, V. Millimeter Scale Alignment of Magnetic Nanoparticle Functionalized Microtubules in Magnetic Fields. *J. Am. Chem. Soc.* 15686–15687 (2005).
60. Inoue, D., Nitta, T., Kabir, A. R., Sada, K., Gong, J. P., Konagaya, A. & Kakugo, A. Sensing surface mechanical deformation using active probes driven by motor proteins. *Nat. Commun.* 1–10 (2016).
61. Tucker, R., Katira, P., Hess, H. & Gaines, V. Herding Nanotransporters : Localized Activation via Release and Sequestration of Control Molecules. *Nano Lett.* (2008).
62. Nitta, T., Hess, H. & Gaines, V. Dispersion in Active Transport by Kinesin-Powered Molecular Shuttles. *Nano Lett.* (2005).
63. Inoue, D., Mahmot, B., Kabir, A. M. R., Farhana, T. I., Tokuraku, K., Sada, K., Konagaya, A. & Kakugo, A. Depletion force induced collective motion of microtubules driven by kinesin. *Nanoscale* **7,** 18054–18061 (2015).
64. Schaller, V., Schmoller, K. M., Karaköse, E., Hammerich, B., Maier, M. & Bausch, A. R. Crosslinking proteins modulate the self-organization of driven systems. *Soft Matter* **9,** 7229–7233 (2013).
65. Kraikivski, P., Lipowsky, R. & Kierfeld, J. Enhanced Ordering of Interacting Filaments

by Molecular Motors. *Phys. Rev. Lett.* **258103,** 1–4 (2006).

66. Schaller, V., Weber, C., Semmrich, C., Frey, E. & Bausch, A. R. Polar patterns of driven filaments. *Nature* **467,** (2010).
67. Tamura, Y., Kawamura, R., Shikinaka, K., Kakugo, A., Osada, Y., Gong, J. P. & Mayama, H. Dynamic self-organization and polymorphism of microtubule assembly through active interactions with kinesin. *Soft Matter* 5654–5659 (2011).
68. Kumar, S., Milani, G., Takatsuki, H., Lana, T., Persson, M., Frasson, C., Kronnie, G. & Månsson, A. Sensing protein antigen and microvesicle analytes using high-capacity biopolymer nano-carriers. *Analyst* **141,** (2016).
69. Sumino, Y., Nagai2, K. H., Shitaka, Y., Tanaka, D., Yoshikawa, K., Chate, H. & Oiwa, K. Large-scale vortex lattice emerging from collectively moving microtubules ´ 6 &. *Letter* (2012).
70. Rashedul, A. & Akira, K. Study of active self-assembly using biomolecular motors. *Polym. J.* (2018).
71. Inoue, D., Gutmann, G., Nitta, T., Kabir, R., Konagaya, A., Tokuraku, K., Sada, K., Hess, H. & Kakugo, A. Adaptation of Patterns of Motile Filaments under Dynamic Boundary Conditions. *ACS Nano* **13,** 12452–12460 (2019).
72. Sanchez, T., Chen, D. T. N., Decamp, S. J., Heymann, M. & Dogic, Z. Spontaneous motion in hierarchically assembled active matter. *Nature* **431,** 1–5 (2012).
73. Idan, O., Lam, A., Kamcev, J., Gonzales, J., Agarwal, A. & Hess, H. Nanoscale transport enables active self-assembly of millimeter-scale wires. *Nano Lett.* **12,** 240–245 (2012).
74. Lam, A. T., VanDelinder, V., Kabir, A. M. R., Hess, H., Bachand, G. D. & Kakugo, A. Cytoskeletal motor-driven active self-assembly in in vitro systems. *Soft Matter* **12,** 988–997 (2016).
75. Lam, A. T., Curschellas, C., Krovvidi, D. & Hess, H. Controlling self-assembly of microtubule spools via kinesin motor density. *Soft Matter* **10,** 8731–8736 (2014).
76. Yigit, B., Alapan, Y. & Sitti, M. Programmable Collective Behavior in Dynamically Self-Assembled Mobile Microrobotic Swarms. *Adv. Sci.* **6,** (2019).
77. Wollman, A. J. M., Sanchez-Cano, C., Carstairs, H. M. J., Cross, R. A. & Turberfield, A. J. Transport and self-organization across different length scales powered by motor proteins and programmed by DNA. *Nat. Nanotechnol.* **9,** 44–47 (2014).

78. Adleman, L. M. Molecular Computation of Solutions to Combinatorial Problems. *Science (80-.).* **266,** 1021–1024 (1994).
79. Crick, F. & Watson, J. Molecular structure of nucleic acids. *Nature* **171,** 737–738 (1953).
80. Lehn, J. M., Mascal, M., Decian, A. & Fischer, J. Molecular recognition directed self-assembly of ordered supramolecular strands by cocrystallization of complementary molecular components. *J. Chem. Soc. Chem. Commun.* **479,** 479–481 (1990).
81. Seeman, N. C. Biochemistry and structural DNA nanotechnology: An evolving symbiotic relationship. *Biochemistry* **42,** 7259–7269 (2003).
82. Zhang, Y. & Seeman, N. C. Construction of a DNA-Truncated Octahedron. *J. Am. Chem. Soc.* **116,** 1661–1669 (1994).
83. Tsu-Ju, F. & Seeman, N. C. DNA Double-Crossover Molecules. *Biochemistry* **32,** 3211–3220 (1993).
84. Rothemund, P. W. K., Papadakis, N. & Winfree, E. Algorithmic self-assembly of DNA Sierpinski triangles. *PLoS Biol.* **2,** (2004).
85. Maune, H. T., Han, S. P., Barish, R. D., Bockrath, M., Iii, W. A. G., Rothemund, P. W. K. & Winfree, E. Self-assembly of carbon nanotubes into two-dimensional geometries using DNA origami templates. *Nat. Nanotechnol.* **5,** 61–66 (2010).
86. Rothemund, P. W. K. Folding DNA to create nanoscale shapes and patterns. *Nature* **440,** 297–302 (2006).
87. Li, H., Park, S. H., Reif, J. H., LaBean, T. H. & Yan, H. DNA-Templated Self-Assembly of Protein and Nanoparticle Linear Arrays. *J. Am. Chem. Soc.* **126,** 418–419 (2004).
88. Zheng, Y. B., Kiraly, B., Weiss, P. S. & Huang, T. J. Molecular plasmonics for biology and nanomedicine. *Nanomedicine* **7,** 751–770 (2012).
89. Liu, N. & Liedl, T. DNA-Assembled Advanced Plasmonic Architectures. *Chem. Rev.* **118,** 3032—3053 (2018).
90. Shen, B., Kostiainen, M. A. & Linko, V. DNA Origami Nanophotonics and Plasmonics at Interfaces. *Langmuir* **34,** 14911–14920 (2018).
91. Parolini, L., Kotar, J., Di Michele, L. & Mognetti, B. M. Controlling Self-Assembly Kinetics of DNA-Functionalized Liposomes Using Toehold Exchange Mechanism. *ACS Nano* **10,** 2392–2398 (2016).
92. Hagiya, M., Konagaya, A., Kobayashi, S., Saito, H. & Murata, S. Molecular robots with

sensors and intelligence. *Acc. Chem. Res.* **47,** 1681–1690 (2014).

93. Lund, K., Manzo, A. J., Dabby, N., Michelotti, N., Johnson-Buck, A., Nangreave, J., Taylor, S., Pei, R., Stojanovic, M. N., Walter, N. G., Winfree, E. & Yan, H. Molecular robots guided by prescriptive landscapes. *Nature* **465,** 206–209 (2010).
94. Muscat, R. A., Bath, J. & Turberfield, A. J. A programmable molecular robot. *Nano Lett.* **11,** 982–987 (2011).
95. Hiyama, S., Inoue, T., Shima, T., Moritani, Y., Suda, T. & Sutoh, K. Autonomous loading, transport, and unloading of specified cargoes by using DNA hybridization and biological motor-based motility. *Small* **4,** 410–415 (2008).
96. Ishii, S., Akter, M., Murayama, K., Kabir, A. M. R., Asanuma, H., Sada, K. & Kakugo, A. Kinesin motors driven microtubule swarming triggered by UV light. *Polym. J.* (2022).
97. Abbott, J. J., Nagy, Z., Beyeler, F. & Nelson, B. J. Robotics in the Small, Part I: Microbotics. *IEEE Robot. Autom. Mag.* **14,** 92–103 (2007).
98. Kassem, S., Lee, A. T. L., Leigh, D. A., Markevicius, A. & Solà, J. Pick-up, transport and release of a molecular cargo using a small-molecule robotic arm. *Nat. Chem.* **8,** 138–143 (2016).
99. Li, J., Li, X., Luo, T., Wang, R., Liu, C., Chen, S., Li, D., Yue, J., Cheng, S. H. & Sun, D. Development of a magnetic microrobot for carrying and delivering targeted cells. *Sci. Robot.* **3,** 1–12 (2018).
100. Fischer, T., Santa, K. & Fatikow, S. Sensor system and powerful computer system for controlling a microrobot-based micromanipulation station. *J. Micromechanics Microengineering* **7,** 256–258 (1997).
101. Zhang, S., Scott, E. Y., Singh, J., Chen, Y., Zhang, Y., Elsayed, M., Dean Chamberlain, M., Shakiba, N., Adams, K., Yu, S., Morshead, C. M., Zandstra, P. W. & Wheeler, A. R. The optoelectronic microrobot: A versatile toolbox for micromanipulation. *Proc. Natl. Acad. Sci. U. S. A.* **116,** 14823–14828 (2019).
102. Xu, T., Yu, J., Yan, X., Choi, H. & Zhang, L. Magnetic actuation based motion control for microrobots: An overview. *Micromachines* **6,** 1346–1364 (2015).
103. Ceylan, H., Giltinan, J., Kozielski, K. & Sitti, M. Mobile microrobots for bioengineering applications. *Lab Chip* **17,** 1705–1724 (2017).
104. Corradi, P., Menciassi, a. & Dario, P. Space Applications of Micro-Robotics : a

Preliminary Investigation of Technological Challenges and Scenarios. *Proc. 5th Round Table Micro/Nano Technol. Space, Noordwijk, Netherlands* 11 (2005).

105. Donald, B. R., Levey, C. G., McGray, C. G., Paprotny, I. & Rus, D. An untethered, electrostatic, globally controllable MEMS micro-robot. *J. Microelectromechanical Syst.* **15,** 1–15 (2006).
106. Kassem, S., Lee, A. T. L., Leigh, D. A., Marcos, V., Palmer, L. I. & Pisano, S. Stereodivergent synthesis with a programmable molecular machine. *Nature* **549,** 374–378 (2017).
107. Xie, H., Sun, M., Fan, X., Lin, Z., Chen, W., Wang, L., Dong, L. & He, Q. Reconfigurable magnetic microrobot swarm: Multimode transformation, locomotion, and manipulation. *Sci. Robot.* **4,** eaav8006 (2019).
108. Thubagere, A. J., Li, W., Johnson, R. F., Chen, Z., Doroudi, S., Lee, Y. L., Izatt, G., Wittman, S., Srinivas, N., Woods, D., Winfree, E. & Qian, L. A cargo-sorting DNA robot. *Science (80-.).* **357,** (2017).
109. Kunwar, A., Vershinin, M., Xu, J. & Gross, S. P. Stepping , Strain Gating , and an Unexpected Force-Velocity Curve for Multiple-Motor-Based Transport. *Curr. Biol.* 1173–1183 (2008).
110. Hendricks, A. G. & Epureanu, B. I. Collective dynamics of kinesin. *Phys. Rev.* 1–12 (2009).
111. Hill, D. B., Plaza, M. J. & Holzwarth, G. Fast vesicle transport in PC12 neurites : velocities and forces. *Eur. Biophys. J.* **33,** 623–632 (2004).
112. Furuta, A., Toyoshima, Y. Y., Amino, M., Oiwa, K. & Kojima, H. Measuring collective transport by de fi ned numbers of processive and nonprocessive kinesin motors. **110,** (2013).
113. Lipowsky, R. Collective Force Generation by Molecular Motors Is Determined by Strain-Induced Unbinding. (2020).
114. Shukla, S., Troitskaia, A., Swarna, N., Maity, B. K., Tjioe, M., Bookwalter, C. S., Trybus, K. M., Chemla, Y. R. & Selvin, P. R. High-throughput force measurement of individual kinesin-1 motors during multi-motor transport. 12463–12475 (2022).

Chapter 2

Establishment of an electromagnetic tweezer and evaluation of its performance in the MT swarm system

Abstract

In recent years biomolecular motor kinesin-based swarms of microtubules have attracted attention due to its nanotechnological applications in *vitro* such as cooperative work in a controlled way. Although cargo transport has been successfully demonstrated by swarms, directional control over gliding toward specific locations or force determination of the swarms has not been achieved. In biomolecular manipulation in terms of deformation, controlling direction, force determination, etc., external forces are frequently employed. Here we report a custom-made setup of an electromagnetic tweezer with micro-actuators coupled to a fluorescence microscope to apply controlled force for the purpose of controlling the gliding direction, manipulating kinesin-MTs interaction, and force determination of MT swarms. The electromagnetic tweezer can generate a controlled magnetic field to apply spatial uniform magnetic force. I set up a custom-made electromagnetic tweezer to apply controlled force on a superparamagnetic bead attached MT swarm to control the kinesin MT interaction as well as gliding direction and force determination associate with the swarm

2.1 Introduction

Recently DNA-based biomolecular motor, kinesin-propelled microtubule (MT) swarm has gained attention in the field of nanotechnology and material science due to their cooperative task for cargo transportation.[1–4] The kinesin motors propel the MT swarms by converting the chemical energy of ATP into mechanical work.[5–7] The key factors of the molecular swarm are its small size, flexibility, and controllability, which play important roles to achieve the tasks.[8,9] Under normal conditions, the MT swarms glide in a random direction, and it has become a substantial challenge to their use in nanotechnological applications to convey the gliding route of MT swarms by applying an electromagnetic field. To date, single MT alignment and orientation have been achieved by incorporating or encapsulating magnetic particles in the MT system in presence of a magnetic field.[10,11] The reports evidence the placement or orientation of the MTs, however, dynamic control has not yet been achieved. In this chapter, I made a few trial approaches to control the kinesin MT interaction and the direction of a gliding MT swarm by applying external magnetic force.

For the force-related biological studies of single biomolecules in *vitro* and in vivo, a piconewton range of forces is required and the most widely used apparatus is the optical tweezer which can be employed to apply a force in the range of 1-50 pN depending on the laser setup.[12] For the MT swarms where multiple entities are involved, it is expected to hold much higher forces than a single-MT on the kinesin substrate.[13–15] Thus, for estimating the force (in chapter 3) of the swarm, a large range of forces is required.

Recently the commercially available superparamagnetic beads provide opportunities for magnetic experiments which can be used to apply magnetic forces in a controlled magnetic system. One of the examples is Dynabeads™ (M-270 Amine) a superparamagnetic, spherical, uniform in size (diameter 2.8 μm) with the chemical functionalization of carboxyl, amino, and streptavidin. Recently the magnetic beads are reported to generate hundreds of piconewton forces by the applied magnetic field.[16] Another essential tool to generate the controlled magnetic field is an electromagnetic tweezer.[17–19] A custom-made electromagnetic tweezer system has been established in this chapter to apply controlled magnetic force to the single bead loaded MT swarm in the purpose of manipulating the direction (to evaluate the performance of the EMTw), as well as the estimation of force (in chapter 3) associated with the kinesin-propelled MT swarm.

2.2 Results and discussion

2.2.1 Design of the electromagnetic tweezer

An electromagnetic tweezer was designed and established to apply controlled force to the magnetic bead-loaded swarm. The electromagnetic tweezer was designed using the software Autodesk inventor shown in figure 2.1.

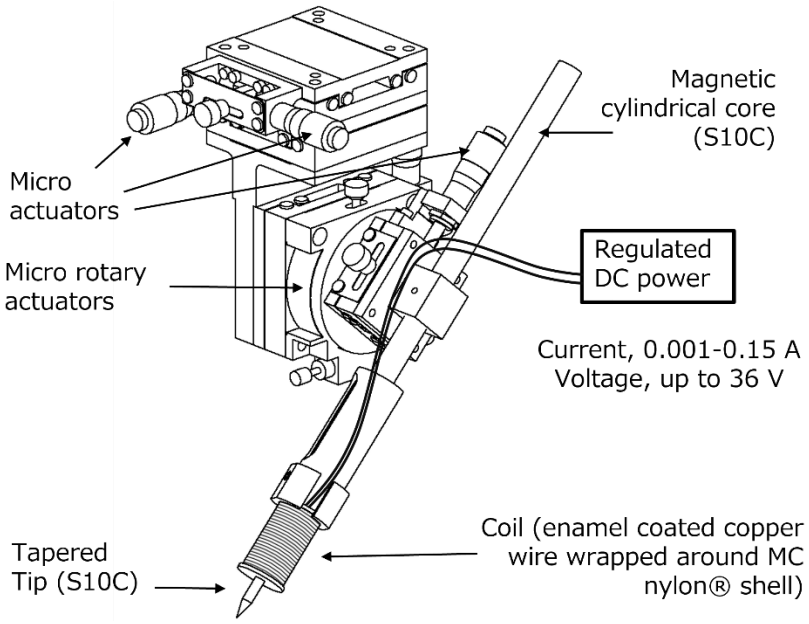

Figure 2.1 Design of electromagnetic tweezer with different parts assembled for laboratory setup.

2.2.2 Set-up of a custom-made electromagnetic tweezer combined with a fluorescence microscope

According to the design an electromagnetic tweezer system was established to can apply controlled magnetic force. The tweezer's system was built with combined with a fluorescence microscope to apply magnetic force and observe simultaneously. Figure 2.2 shows a photograph of the custom-made electromagnetic tweezer combined with the fluorescence microscope.

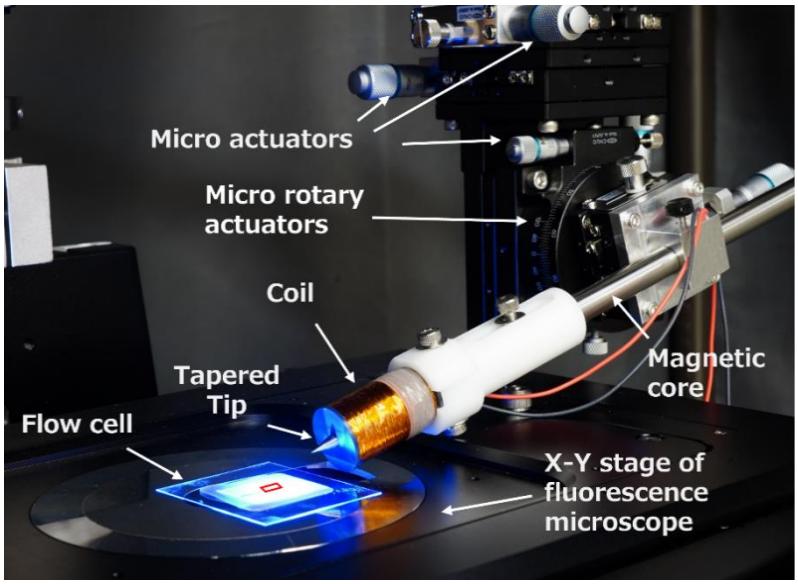

Figure 2.2 A photograph of the custom-made electromagnetic tweezer with different parts combined with the fluorescence microscope.

The micro-actuators in the body structure of the tweezer allowed it to adjust its height and position. The electromagnet employed consists of a solenoid with an enamel-coated copper wire (6500 windings of diameter 0.15) wrapped around a MC nylon® shell. There is a cylindrical core with a tapered tip made of S10C material in the electromagnet. There is an exchangeable cylindrical core with a tapered tip which allows easy replacement of cores by simply sliding them into the electromagnet. The magnetic core of the tapered tip is made of S10C material, contains 0.08-0.13% of carbon which provides higher electrical conductivity and low tensile strength. The micro rotary actuator allows the tip to bend at any angle to apply directed force. DC power supply from KIKUSHI PMX70-1A is used to tune the current and voltage. The magnitude of the force produced by the electromagnet is proportional to the current intensity flowing into the coil up to the saturation of the core material. The power supply can provide currents ranging from 0.001 to 0.15 A with the voltage up to 36 V where the coil resistance is 240 Ω. An increase in temperature due to large currents negatively affects the magnetic properties of the core. To keep the temperature low, the voltage and the current must be in the optimum range.

2.2.3 Estimation of magnetic field strength of the electromagnetic tweezer using a Gauss meter

A portable Hall-effect gauss/tesla meter from F.W. BELL (5100 series) was used to measure the magnetic field strength of the electromagnetic tweezer varying the current and voltage. There is a sensor in the gauss meter probe at 0.81 mm far from the edge. The distance between the sensor of the Gauss meter and the tip of magnetic tweezers was kept fixed (d = 2 mm) and the applied current was varied to observe the magnetic field strength. Figure 2.3a shows the magnetic field strength with the current. It is seen that the magnetic field strength value increases with increasing applied current.

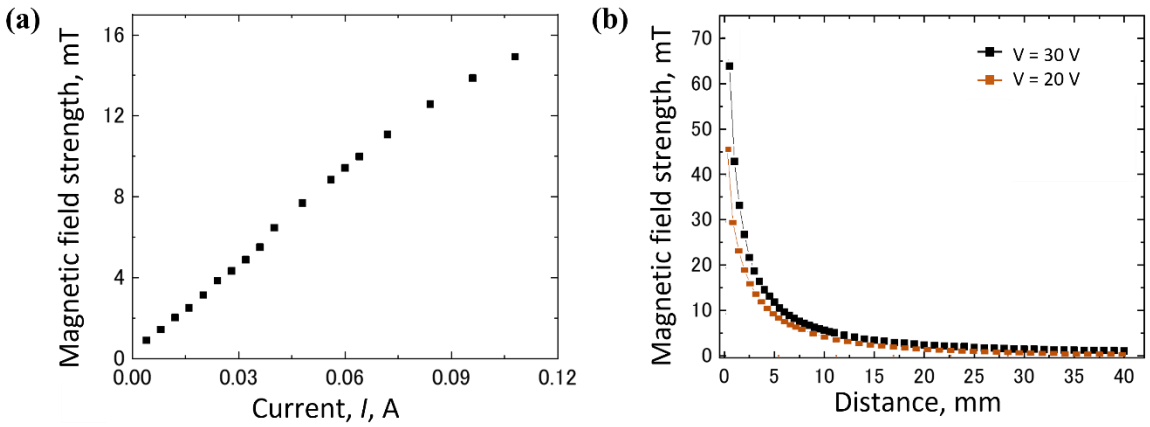

Figure 2.3 (a) Current vs magnetic field strength of the electromagnetic tweezers measured by the Gauss meter, (b) Magnetic field strength with distance at voltage 20 V (0.077 A) and at voltage 30 V (0.104 A).

The magnetic field strength was observed with distance when current and voltage were kept constant (figure 2.3b). With increasing distance between the sensor of the gauss meter and the tweezer's tip, the magnetic field strength decreases exponentially for both 20 V and 30 V applied voltage. The magnitude of the force produced by the electromagnet is proportional to the current intensity flowing into the coil.

2.2.4 Force calibration of the Dynabeads using EMTw

Dynabeads™ M-270 Amine (bead), a superparamagnetic spherical polymer particle of the consistent and amine functionalized surface was used. It was auto fluorescent with a diameter of 2.8 µm. Force calibration of these beads was performed for the applied magnetic field by the electromagnetic tweezers (EMTw). I prepared a suspension of Dynabeads in the viscous medium of glycerol (80 %), and used for the force calibration experiment. Table 2.1 shows the different

glycerol solutions (% (v/v) in water) with viscosity values. The viscosity of the glycerol solution was measured using a Rheometer.

Table 2.1 Glycerol solutions (% (v/v) in water) with viscosity values

Glycerol % (v/v) in water	Viscosity (Pa. s)
99.99	0.87800
90.00	0.21200
80.00	**0.07300**
70.00	0.03300
60.00	0.01600
100 % water	**0.00089**

A flow cell was prepared, the beads were dispersed in 80 % (v/v) glycerol (0.0737 Pa s) medium and force was applied using electromagnetic tweezers.

The tip position of the tweezer was set close to the flow cell (on the right side) to apply the force on the beads laterally as shown in figure 2.4a. The movement of the bead towards the tweezer's tip while applying force by the tweezer was captured by the fluorescence microscope. Figure 2.4b shows the fluorescence microscopy image of beads dispersed in 80 % glycerol and tip position where the tip and the beads are visualized in the same frame. The distance between the bead and the tip was determined from this fluorescence image. One of the trajectories of one bead applying 10 V is shown in figure 2.4b. From this trajectory, it is seen that the displacement of the beads increases as the distance decreases i. e. it comes closer to the tweezer's tip with time. From the trajectories of the beads, velocities were estimated, and finally the applied force, F was determined using Stokes' formula,

$$F = 6\pi \times \eta \times r \times v \qquad (1)$$

Where F is the force working on the beads in the dispersed medium applying electromagnetic tweezers, η = viscosity of the dispersed medium, r is the radius of the beads, and v = velocity of the beads applying emf.[17]

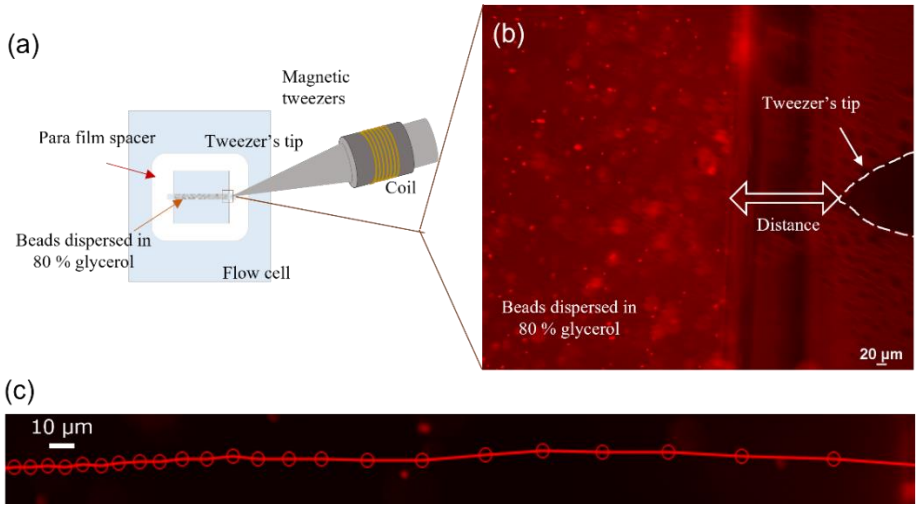

Figure 2.4 (a) Schematic representation of experimental setup for force calibration of beads, (b) fluorescence microscopy image of dispersed bead in glycerol medium and the position of the tweezer's tip, (c) Trajectory of a bead applying emf (10 V).

Estimating the force applied to the beads by applied emf, the distance versus force was plotted in figure 2.5. With increasing the distance of the beads from the tip the velocity, as well as the active force decreases exponentially. This decrease in velocity with distance is due to the lowering of magnetic field strength at a larger distance. The error bars in the figure are the standard deviation of the mean from the measurement of a range of velocities as well as corresponding distances. Therefore, tuning the applied current-voltage and the distance between the bead and the tweezer's tip, the velocity as well as the active force can be optimized. Different approaches were carried out in the next section to evaluate the performance of EMTw in the kinesin-microtubule swarm system.

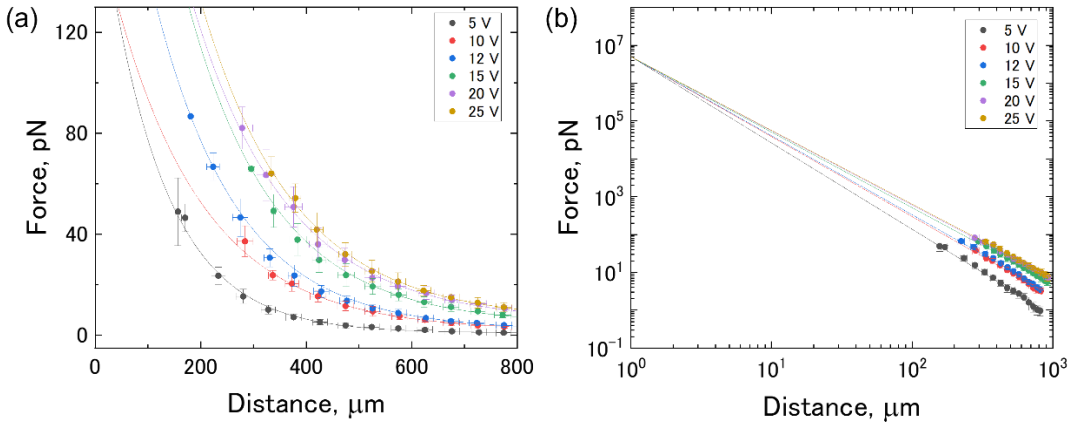

Figure 2.5 Bead's distance from tip versus active force applying emf in (a) linear (fitted exponentially) and (b) log scale (fitted linearly).

2.2.5 Preparation of MTs as a swarm unit

Two sets of MTs were polymerized from the azide and dye-labeled (ATTO488 dye in both cases) tubulin with a ratio of 1:4 in presence of GMPCPP (guanylyl-(α,β)-methylenedisphosphonate). After that, the complementary DNAs (250 μM of DNA1 and DNA2) were added to each set of MTs, and a click reaction was performed to modify the MTs by DNA.[20] This complementary DNA modification of the MTs allowed them to conjugate while propelled by kinesin in presence of ATP.

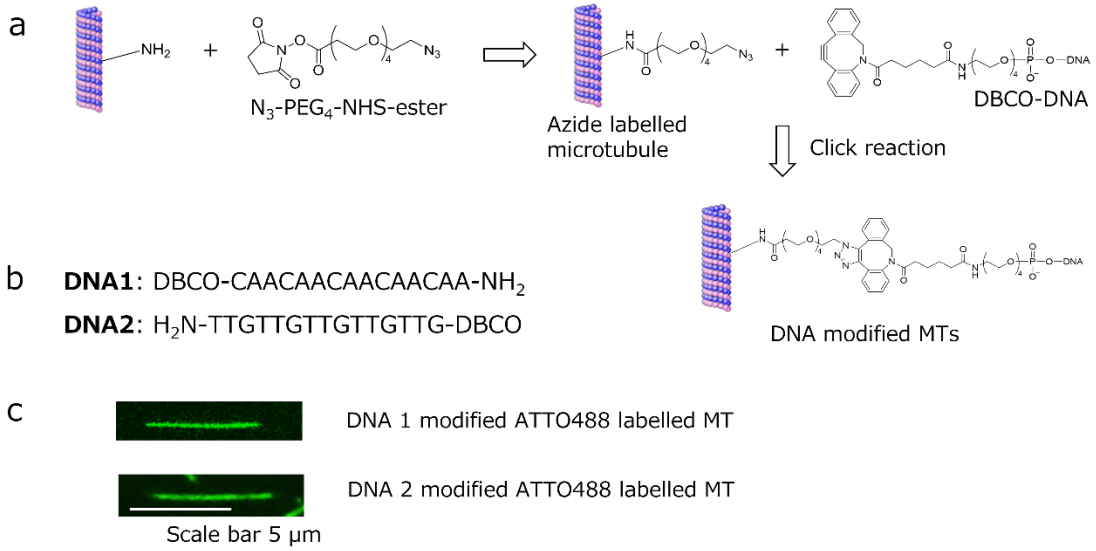

Figure 2.6 Schematic diagram of the preparation of swarm units through (a) conjugation of MT with DNA by click reaction, (b) DNA sequences, and (c) fluorescence microscopic images of the DNA conjugated MTs.

While click reaction for the preparation of DNA conjugated MTs, the DBCO at the 5′ end of DNA reacts with the azide functionalized MTs (figure 2.6).

2.2.6 Demonstration of swarm by active self-assembly of MTs

Swarm of MTs were constructed on the kinesin coated glass surface from two complementary DNA (DNA1 and DNA2) modified, green (ATTO 488 dye in both cases) MTs and the time lapse fluorescence images are shown in the figure 2.7. Upon the gliding of MTs on the kinesin coated glass surface, the complementary DNAs modified MTs tends to the conjugate with each other and finally form the bundle swarms.

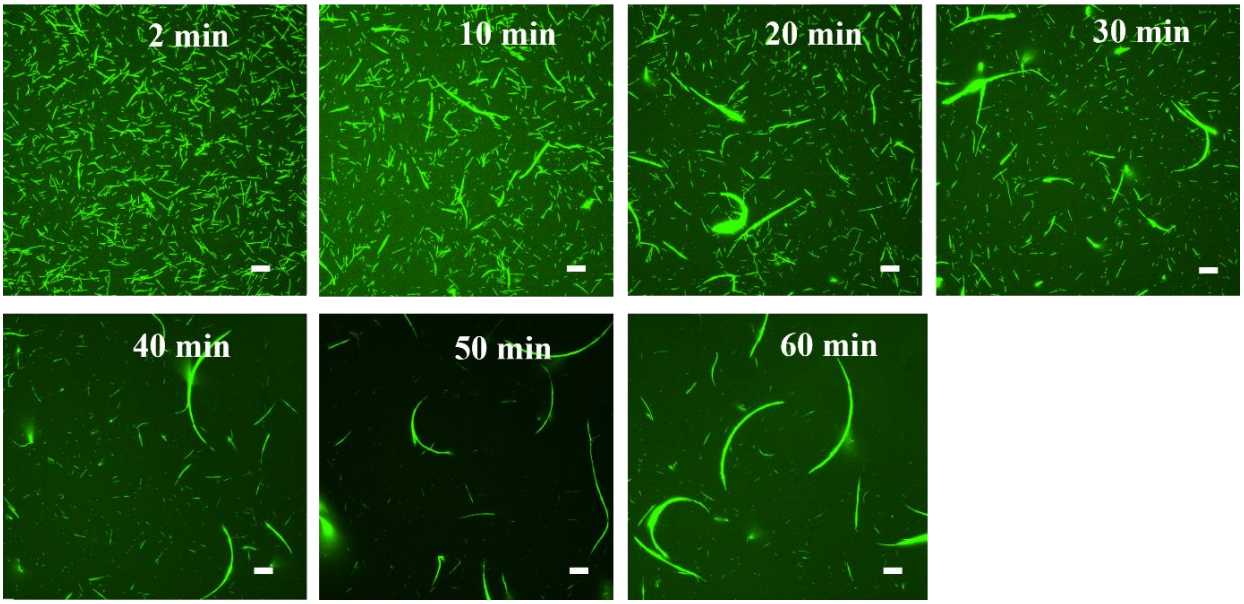

Figure 2.7 Time lapse fluorescence microscopy images of the swarm formation from the two complementary DNA (DNA1 and DNA2) modified and, green (ATTO 488 dye in both cases) MTs on the kinesin coated glass surface.

The labeling ratio of DNA to tubulin was determined from the concentrations of DNAs and tubulins measured. The molar extinction coefficient of the DNAs was determined by measuring the absorbance of different concentrations of the DNA at the wavelength of 260 nm using NanoDrop^{TM} 2000c. The DNA labeled MTs solutions were kept at 4 ^{o}C overnight and the concentration of DNA and tubulin were measured using **NanoDrop^{TM} 2000c** (Figure 2.8). The labeling ratio of DNA to tubulin is listed in the table 2.1.

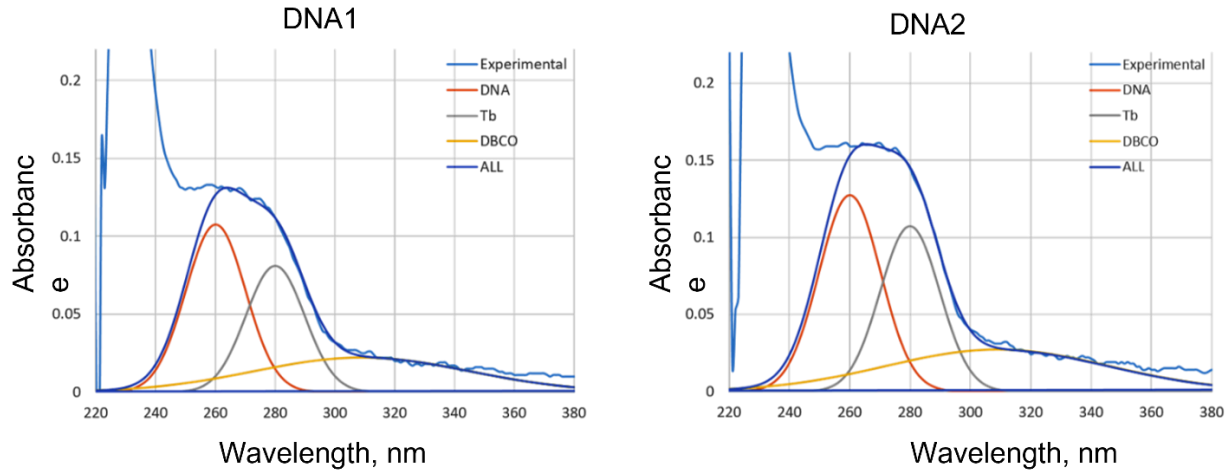

Figure 2.8 Deconvoluted absorption spectra of DNA1 and DNA2 modified MTs.

Table 2.1 Labeling ratio of DNA1 and DNA2 modified MTs

DNAs	Molar extinction coefficientε ($Lmol^{-1}cm^{-1}$)	Conc. of DNA at 260 (µM)	Conc. of tubulin dimer at 280 nm (µM)	DNA to Tubulin L. R. (%)
DNA1	159600	7.39	7.84	94.26
DNA2	134700	10.69	10.1	105.54

2.2.7 Modification of the beads by complementary DNA

To load and carry the bead (magnetic particle, **Dynabeads™ M-270 Amine)** by the swarm, the beads were modified by the DNA2, which is complementary to the DNA1. The bead (diameter, 2.8 µm) was employed to load and carry by the swarm for controlling the direction of the MT swarms. In the first step of modification the amine-functionalized beads were converted to azide-functionalized beads using N3-PEG4-NHS ester. In the latter case the DNA modification of the azide-beads were performed by click reaction (for more details see methods). Figure 2.9 shows the schematic representation of the DNA modification of the beads by click reaction.

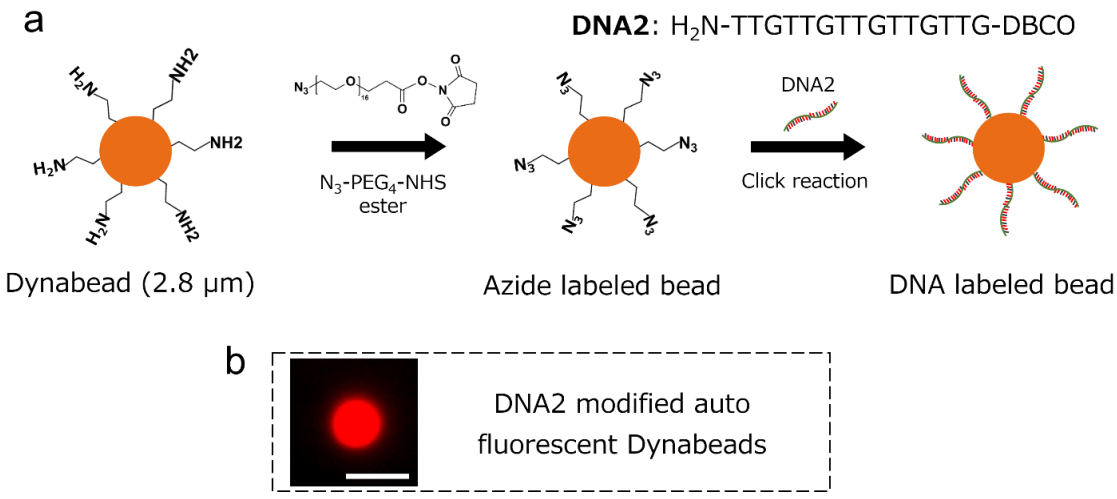

Figure 2.9 (a) Schematic representation of the azide labeling of beads and consequently DNA modification. Fluorescence microscopic image of the autofluorescence bead dispersed in 1×BRB80 solution after the modification using DNA2. Scale bar 5 µm.

After the modification, the beads were suspended in 1×BRB80 solution for preservation at 4 ºC for 1-2 weeks. Once the swarming is performed in a flow cell, the beads were diluted 30 times in the ATP buffer and applied to the flow cell to load and transport by the MT swarm. Usually, the

beads were added to the flow cell after 30 minutes of ATP addition, when most of the single MTs associated to form larger MT bundles.

2.2.8 Attaching and transporting of beads by the swarm

To attach the beads to the swarms, the beads (dispersed in ATP buffer) were added to the flow cell after the MT swarm formation (after 20-30 minutes of ATP addition). The beads are loaded to the swarm in a zipping geometry resulting in a 24 base pair overlapping of DNA1 and DNA2. When all the DNAs in MTs form the complementary base pair between DNA1 and DNA2, beads can no longer attach to the swarm. When a swarm resulting from the DNA1 modified and DNA2 modified, pass through the DNA2 labeled bead, it selectively attaches to the DNA1 modified MTs by complementary DNA interaction. This attachment resulted in the loading and carrying of beads by the MT swarm. Figure 2.10 shows time lapse fluorescence microscopy images of the bead transportation by the swarming of MTs. The observation was done after 30 minutes of ATP addition and several DNA2 modified beads were transported in random directions.

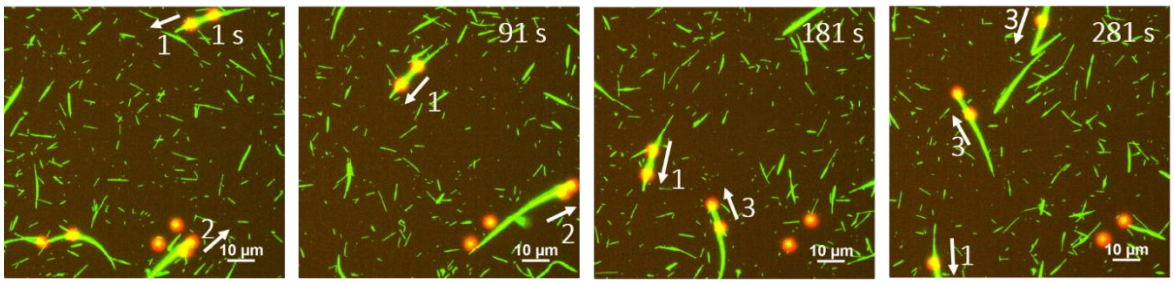

Figure 2. 10 Time lapse fluorescence microscopy images of bead transportation by MT swarm.

2.2.9 Vertical pulling and detaching of bead loaded MT swarm from kinesin coated surface applying emf

The beads were loaded and carried by the swarm located at the lower surface of the flow cell and the position of the tweezer's tip was positioned on the top of the flow cell (figure 2.11 right). Experimental setup for vertical pulling is shown schematically 2.11 (not in real scale).

Figure 2.12 shows the fluorescence microscopy time lapse images of lower surface of the flow cell where, several beads were attached and transported by the MT swarm. EMF, 5V was applied vertically from the top of the flow cell after 60 s of observation. The MT swarms has been started

pull vertically from lower surface to the bulk (or upper surface) of the flow cell by applying the emf.

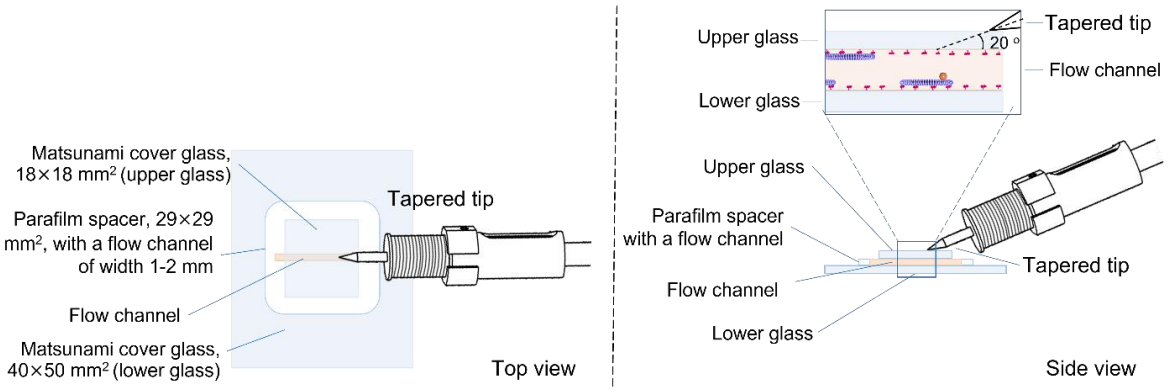

Figure 2.11 Schematic representation of the magnetic field applier system from the top view and bottom view (not in real scale). The inset image shows the scheme of flow cell in between the two glass surfaces and the swarm is formed at both surfaces.

After applying EMF 5 V the bead loaded MT swarms were attracted by the electromagnetic force and from figure it is seen that one of the beads loaded swarm disappeared with the swarming of MTs from kinesin surface. When EMF applied the beads with swarming of MTs pulled towards the tip and detached from the kinesin coated glass surface then might be destined to the upper surface of the flow cell.

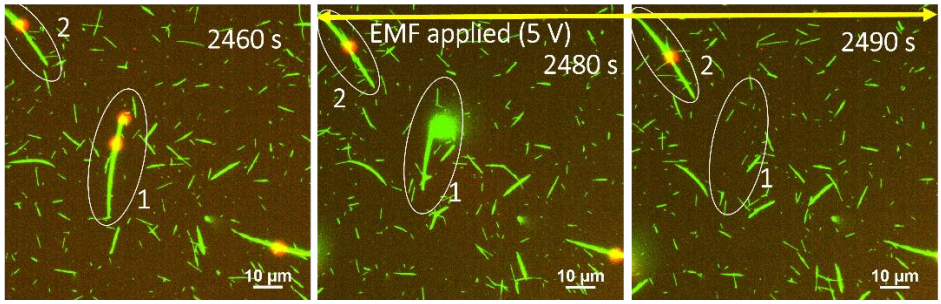

Figure 2.12 Time lapse fluorescence microscopy images of cargo transportation and application of EMF (5 V) vertically. EMF applied after 60 s of observation.

Distance between observation surface and electromagnetic tweezers tip was ~120 µm corresponding magnetic force is ~ 90 pN. From the multiple experiment of applying emf to the bead loaded swarm it was observed that small bundles take short time to detach, and larger bundles requires longer time and higher emf to detach. Larger bundles contain large number of MTs which interacts with large number of kinesins, so it takes longer time to completely detach from the kinesin surface.

2.2.10 Lateral pulling of bead loaded swarm of MTs on kinesin surface applying EMF

For the lateral pulling of the bead attached-MT swarms the tweezers tip position was kept similar to the force calibration experiment (section 2.2.4, figure 2.4). Figure 2.13 shows the lateral pulling of gliding MT swarms by applied emf and the change of the direction of MT swarm.

After applying EMF (5 V) the bead loaded MT swarm started to change the direction (after 180 s of observation) and follow the path toward the tweezer's tip. The beads attached to the leading position rather than lagging position of the MTs swarm, changes their direction towards the tip position under emf. Distance between the bead loaded MT swarm and the tweezer's tip was ~302 µm corresponds to magnetic force of ~10 pN.

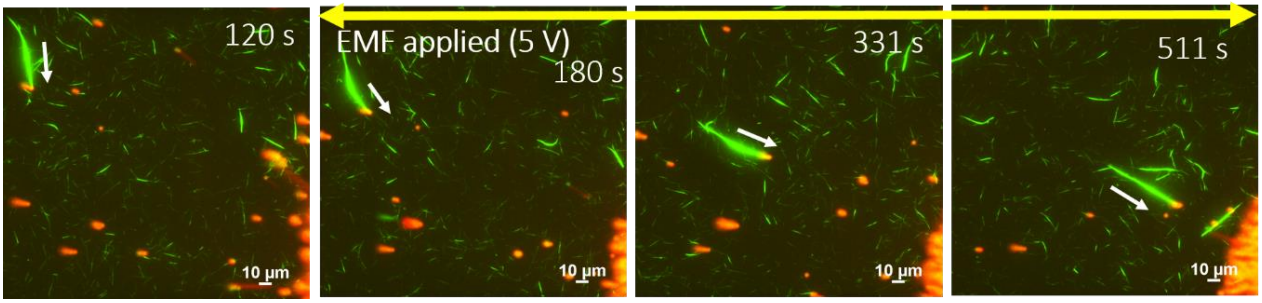

Figure 2.13 (a) Time lapse fluorescence microscopy images of controlling the gliding direction of swarm by lateral pulling of bead loaded MT swarm. emf 5 V applied at 180 s of observation.

For single MTs attached to a single bead, it was observed that only 1 or 2 V was sufficient to pull or detach from kinesin coated surface. In case of MTs swarm attaching with beads required large EMF ~5 to 10 V to be pulled or detached from kinesin coated surface. It is possible to change the gliding direction of beads loaded swarming of MTs applying emf when beads are attached to the leading position of the MTs swarm.

2.3 Conclusion

A simple electromagnetic tweezers system has been established to generate electromagnetic field which can apply hundreds of piconewton force to the superparamagnetic Dynabeads. The acting force on the beads was found to be controlled easily only changing the distance by micro-actuators and the voltage applied. Then the electromagnetic tweezer was equipped with the fluorescence microscope to observe the behavior of bead as well as MT swarm with the bead applying the external magnetic field. The detachment from kinesin surface or changing the gliding direction of the magnetic bead attached MT swarm was observed. Compared to the optical tweezers system the magnetic bead based EMTw system is found easier to handle and the range of applied force is larger. The detaching force of the MT swarms from the kinesin surface was found to be increased with increasing the size of the swarm which indicates the higher interaction between large number of MTs to the kinesins in a larger swarm. The beads attached to the leading position of the gliding MT swarms followed the direction designated by the emf applied. These results offers technical advantages for the setup of electromagnetic tweezers and systematic application of magnetic force spatially to the bead loaded swarm for distinct purposes. This study will enrich the current understanding the use of electromagnetic tweezers in biomolecular manipulations and dynamic control over the MT-kinesin swarming system.

2.4. Experimental

2.4.1 Preparation of the flow cell for the force calibration of Dynabeads

The beads were dispersed in 80 % glycerol medium (viscosity, 0.073 Ps. s) to apply magnetic field. To prepare a flow cell a parafilm was taken and cut in a 29×29 mm^2 with a channel 22×1.5 mm^2 in it. A flow cell with dimensions of 18 × 1.5 × 0.45 mm^3 (L × W × H) was assembled from two cover glasses (MATSUNAMI Inc.) using the parafilm as a spacer. The beads dispersed in glycerol medium was inserted into the flow cell and placed on the microscopic stage. The tweezer's tip was placed on the right side of the flow cell (similar to section 2.2.10) and emf was applied laterally to the beads. The time lapse images (5 seconds interval) were captured by the fluorescence microscope while different applied voltages by the EMTw.

2.4.2 Purification of tubulin and kinesin

Tubulin was purified from porcine brain using a high-concentration PIPES buffer (1 M PIPES, 20 mM EGTA, and 10 mM $MgCl_2$) and stored in BRB80 buffer (80 mM PIPES, 1 mM EGTA, 2 mM $MgCl_2$, pH adjusted to 6.8 using KOH).[21,22] Azide labeled tubulin was prepared using N_3-PEG_4-NHS following the established protocol of labeling tubulin with fluorescent dye.[20,23] The tubulin concentration was determined by measuring the absorbance at 280 nm using a UV spectrophotometer (Nanodrop 2000c). Recombinant kinesin-1 consisting of the first 573 amino acid residues of human kinesin-1 was prepared as described in the literature.[24]

2.4.3 Complementary DNA sequences for the modification of MTs

Two pairs of complementary DNA sequences were used in this chapter. For the demonstration of the MT swarm, the complementary DNAs, DBCO-CAACAACAACAACAA-NH_2 (DNA1) and H_2N-TTGTTGTTGTTG-DBCO (DNA2) were used (table 2.1). The DNA to tubulin labeling ratios were 93% and 102% for DNA1 and DNA2 modified MTs, respectively (table 2.1). The DNAs were purchased from Hokkaido System Science Co. Ltd. The DNAs were modified at the 5′ end with dibenzo cyclooctyne (DBCO). The molar extinction coefficient of the DNAs was measured by developing a calibration curve of the absorbance with different concentrations of individual DNAs.

2.4.4 Preparation of MTs

Dye-labeled tubulin (70 μM) and azide-labeled tubulin (70 μM) were mixed in the molar ration, 1:4 and polymerization buffer (80 mM PIPES, 1 mM EGTA, 1 mM $MgCl_2$, 1 mM guanylyl-(α,β)-methylenedisphosphonate (GMPCPP), pH~6.8) was added and the solution was incubated at 37 °C for 30 min. 1 μL of 4×BRB80 buffer and 0.5 μL of 1 mM taxol (in DMSO) were added to the MT solution just after polymerization to stabilize the MTs. A copper free click reaction of an azide-alkyne cycloaddition reaction was initiated by adding 3.5 μL DBCO conjugated DNA (250 μM) to the 10 μL azide-MTs (56 μM) and incubating the solution at 37 °C for 6 hours.[25] 100 μL of cushion buffer (BRB80 buffer supplemented with 60% glycerol) was added to separate the tubulin dimers or free DNAs from the DNA modified MTs by centrifugation at 54000 rpm for 1 hour at 37 °C. After discarding the supernatant, the MTs pellet was washed once with 100 μL BRB80P (BRB80 supplemented with 1 mM taxol) and dissolved in 15 μL BRB80P.

2.4.5 Measurement of the labeling ratio of DNA to tubulin

The DNA (DNA1 and DNA2) conjugated MTs in BRB80 were depolymerized to DNA conjugated tubulins by keeping the MTs solution in a tuble on ice overnight. The absorption spectrum of the DNA conjugated tubulin dimers was measured using a spectrophotometer (NanoDrop™ 2000c, Thermo Fisher Scientific Inc.) and deconvoluted using the normal distribution function with Microsoft Excel (Windows Edition, Microsoft Corporation) with peaks at 260 nm and 280 nm. The concentrations of DNA and tubulin dimers were calculated from the Beer-Lambert law using the molar extinction coefficient of tubulin dimers and DNAs from which the labeling ratio was determined and listed in the table 2.1.[4]

2.4.6 Azide and DNA modification of beads

10 μL beads (dispersed in water) were taken and centrifuged for 1 min to separate the beads from water. 32 μl, 20 mM N_3-PEG_4-NHS ester were added to the bead and mixed properly with micropipette. The solution was incubated on ice for 1 hour. 10 μL, 20 mM glycine added to the solution and kept on ice for 30 minutes. The solution then washed with 10 μl BRB 80 three times to remove free azide ester by centrifuging in a 0.22 μm porous filter tube. 10 μl BRB 80 solution was added to disperse the beads. 3.5 μl of 250 μM DNA1 was added to the beads solution and incubated on ice for 12/24 hrs. Then the beads were again washed with BRB 80 solution and

centrifuged. Finally, the DNA labelled beads were dispersed in 10 µl BRB 80 solutions and stored at 4 ^{o}C for 1-2 weeks. For the loading and carrying of the beads to the swarm, the bead solution was further diluted (~50 times) using ATP buffer (BRB80 buffer supplemented with dithiothreitol (1 mM), casein (0.5 mg/ml), d-glucose (4.5 mg/ml), glucose oxidase (50 U/ml), catalase (50 U/ml), taxol (10 µM), ATP (5 mM), and methylcellulose (0.2%; w/v)).

2.4.7 Flow cells preparation and motility assays for the swarming of MTs

A flow cell was prepared using two cover glasses and a parafilm spacer. A parafilm was taken and cut in a 29×29 mm^2 with a channel 22×1.5 mm^2 in it. A flow cell with dimensions of 18 × 1.5 × 0.45 mm^3 (L × W × H) was assembled from two cover glasses (MATSUNAMI Inc.) using the parafilm as a spacer.

To demonstrate the swarming, first the flow cell was filled with 5 µL casein buffer (BRB80 buffer supplemented with casein (0.5 mg/ml)). After incubating for 3 min, 5 µL, 800 nM kinesin solution was introduced into the flow cell and incubated for 5 min. The flow cell was washed with 10 µL of wash buffer (BRB80 buffer supplemented with dithiothreitol (1 mM), casein (0.5 mg/ml), d-glucose (4.5 mg/ml), glucose oxidase (50 U/ml), catalase (50 U/ml), and taxol (10 µM)) and 5 µL of one of the DNA modified MTs solution (diluted in BRB80P) was introduced and incubated for 2 min. The flow cell then washed with 10 µL of wash buffer and 5 µL of the complementary DNA modified MTs were introduced. After incubating for 2 min, the flow cell was washed with 10 µL of wash buffer and the motility of the MTs was initiated by applying 5 µL of ATP (wash buffer supplemented with ATP (5 mM), and methylcellulose (0.2%; w/v).[2] The time of ATP addition was set as 0 min. Soon after the addition of ATP buffer, the flow cell was placed in an inert chamber system and observed under a fluorescence microscope.[26] To associate almost all the single MTs into a bundle swarm, a waiting time of~30-40 min was found to be necessary.

2.4.8 Loading and carrying of beads by the swarm

After the formation of the MT swarm, 5 µl of beads (dispersed in ATP buffer, 50 times dilution) was introduced into the flow cell. After 5 minutes of incubation, the flow cell was washed two times by adding 5 µl of ATP buffer into the flow cell to wash the excess beads. Then, the flow cell was immediately taken to the microscopic stage and observation at the lower surface of the flow cell was performed by the EMTw combined fluorescence microscope.

2.4.9 Application of the emf to the swarm by electromagnetic tweezer

The controlled emf was applied to the flow cell controlling the distance from tip to the swarm, applied current and voltage of the tweezer. Swarming in the flow cell was positioned on the observation field of the fluorescence microscope. The EMTw's tip was set on the (2.2.9) and right side (2.2.10) of the observation field.

2.4.10 Fluorescence Microscopy Image Capture

The samples were visualized by an epifluorescence microscope (Eclipse Ti, Nikon) using an oil-coupled Nikon Plan fluor 60xN.A.1.4 objective (Nikon). UV cut-off filter blocks (TRITC: EX540/25, DM565, BA605/55; GFP-B: EX460-500, DM50S, BA510-560; Nikon) were used in the optical path of the microscope. Images were captured using a cooled-CMOS camera (NEO CMOS, Andor) connected to a PC.

2.4.11 Image Analysis

The fluorescence microscopy images were analyzed by NIS-Elements software (Nikon) and ImageJ software.[27] Velocity of the beads under emf was measured using the Image plugin MTrackJ. Statistical analysis and graphs were performed with the software OriginPro Version 2019, OriginLab, USA.[28]

2.5 References

1. Keya, J. J., Kabir, A. M. R., Inoue, D., Sada, K., Hess, H., Kuzuya, A. & Kakugo, A. Control of swarming of molecular robots. *Sci. Rep.* **8,** 1–10 (2018).
2. Keya, J. J., Suzuki, R., Kabir, A. M. R., Inoue, D., Asanuma, H., Sada, K., Hess, H., Kuzuya, A. & Kakugo, A. DNA-assisted swarm control in a biomolecular motor system. *Nat. Commun.* **9,** 4–11 (2018).
3. Ishii, S., Akter, M., Murayama, K., Kabir, A. M. R., Asanuma, H., Sada, K. & Kakugo, A. Kinesin motors driven microtubule swarming triggered by UV light. *Polym. J.* (2022).
4. Akter, M., Keya, J. J., Kayano, K., Kabir, A. M. R., Inoue, D., Hess, H., Sada, K., Kuzuya, A., Asanuma, H. & Kakugo, A. Cooperative cargo transportation by a swarm of molecular machines. *Sci. Robot.* **7,** eabm0677 (2022).
5. Palacci, J., Sacanna, S., Steinberg, A. P., Pine, D. J. & Chaikin, P. M. Colloidal Surfers. **339,** 936–941 (2013).
6. Xu, T., Soto, F., Gao, W., Dong, R., Garcia-gradilla, V., Magan, E., Zhang, X. & Wang, J. Reversible Swarming and Separation of Self-Propelled Chemically Powered Nanomotors under Acoustic Fields. **1,** 1–4 (2015).
7. Wang, W., Duan, W., Ahmed, S., Sen, A. & Mallouk, T. E. From One to Many: Dynamic Assembly and Collective Behavior of Self-Propelled Colloidal Motors. (2015). doi:10.1021/acs.accounts.5b00025
8. Beshers, S. N. & Fewell, J. H. Models of division of labor in social insects. *Annu. Rev. Entomol.* **46,** 413–40 (2001).
9. Niven, J. E. How honeybees break a decision-making deadlock. *Science (80-.).* **335,** 43–44 (2012).
10. Platt, M., Muthukrishnan, G., Hancock, W. O., Williams, M. E., Park, U. V & Pennsyl, V. Millimeter Scale Alignment of Magnetic Nanoparticle Functionalized Microtubules in Magnetic Fields. 15686–15687 (2005). doi:10.1021/ja055815s
11. Inaba, H., Yamada, M., Rashid, M. R., Kabir, A. M. R., Kakugo, A., Sada, K. & Matsuura, K. Magnetic Force-Induced Alignment of Microtubules by Encapsulation of CoPt Nanoparticles Using a Tau-Derived Peptide. *Nano Lett.* **20,** 5251–5258 (2020).
12. Bustamante, C. J. & Wang, M. D. Optical tweezers in single-molecule biophysics. *Nat. Rev. Methods Prim.* doi:10.1038/s43586-021-00021-6

13. Klumpp, S. & Lipowsky, R. Cooprative cargo transport by several molecular motors. *Proc. Natl. Acad. Sci. U. S. A.* **102,** (2005).
14. Liu, H., Spoerke, E. D., Bachand, M., Koch, S. J., Bunker, B. C. & Bachand, G. D. Biomolecular motor-powered self-assembly of dissipative nanocomposite rings. *Adv. Mater.* **20,** 4476–4481 (2008).
15. Hess, H., Clemmens, J., Brunner, C., Doot, R., Luna, S., Ernst, K. H. & Vogel, V. Molecular self-assembly of 'nanowires' and 'nanospools' using active transport. *Nano Lett.* **5,** 629–633 (2005).
16. Fallesen, T., Hill, D. B., Steen, M., Macosko, J. C., Bonin, K., Holzwarth, G., Fallesen, T., Hill, D. B., Steen, M., Macosko, J. C. & Bonin, K. Magnet polepiece design for uniform magnetic force on superparamagnetic beads on superparamagnetic beads. **074303,** 1–6 (2018).
17. Kollmannsberger, P. & Fabry, B. applications. **V,** 1–6 (2007).
18. Sarkar, R. & Rybenkov, V. V. A Guide to Magnetic Tweezers and Their Applications. **4,** (2016).
19. Gu, H., Boehler, Q., Ahmed, D. & Nelson, B. J. Magnetic quadrupole assemblies with arbitrary shapes and magnetizations. 1–8 (2019).
20. Akter, M., Keya, J. J., Kabir, A. M. R., Rashid, M. R., Ishii, S. & Kakugo, A. Functionalization of Tubulin: Approaches to Modify Tubulin with Biotin and DNA. *Methods Mol. Biol.* **2430,** 47—59 (2022).
21. Ishii, S., Akter, M., Keya, J. J., Rashid, M. R., Afroze, F., Nasrin, S. R. & Kakugo, A. Purification of Tubulin from Porcine Brain and its Fluorescence Dye Modification. *Methods Mol. Biol.* **2430,** 3–16 (2022).
22. Castoldi, M. & Popov, A. V. Purification of brain tubulin through two cycles of polymerization- depolymerization in a high-molarity buffer. *Protein Expr. Purif.* **32,** 83–88 (2003).
23. Peloquin, J., Komarova, Y. & Borisy, G. Conjugation of fluorophores to tubulin. *Nat. Methods* **2,** 299–303 (2005).
24. Case, R. B., Pierce, D. W., Hom-Booher, N., Hart, C. L. & Vale, R. D. The directional preference of kinesin motors is specified by an element outside of the motor catalytic domain. *Cell* **90,** 959–966 (1997).

25. Früh, S. M., Steuerwald, D., Simon, U. & Vogel, V. Covalent cargo loading to molecular shuttles via copper-free ‘click chemistry’. *Biomacromolecules* **13,** 3908–3911 (2012).
26. Kabir, A. M. R., Inoue, D., Kakugo, A., Kamei, A. & Gong, J. P. Prolongation of the Active Lifetime of a Biomolecular Motor for in Vitro Motility Assay by Using an Inert Atmosphere. *Langmuir* **27,** 13659–13668 (2011).
27. Sheffield, J. B. An introduction to ImageJ: A useful tool for biological image processing and analysis. *Microsc. Microanal.* **14,** 898–899 (2008).
28. Edwards, P. M. Origin 7.0: Scientific graphing and data analysis software. *J. Chem. Inf. Comput. Sci.* **42,** 1270 (2002).

Chapter 3

Force determination of the MT swarm ring using magnetic bead and electromagnetic tweezer

Abstract

The microtubule (MT)-kinesin system offers a promising route for the construction of molecular swarm robots by DNA conjugation. The MT-kinesin swarm robots have advantages over the single MT-kinesin system and are being used for nanotechnological applications. The swarming of MTs converts the chemical energy of ATP into rotational and translational motion, which holds great potential as the motion can be harnessed to perform work. To ensure real-life applications of the MT swarms it is a prerequisite to quantify the amount of work that can be harnessed from the swarms. In this chapter, I attempt to quantify the force associated with the swarming of MTs driven by kinesins using a magnetic bead and an electromagnetic tweezer. The force of the swarm has been found higher than in the motility of a single MT by kinesins and the force increases sub additively with the increasing number of kinesins. Understanding the force production by the swarm will support to rise new ideas for designing future biomolecular devices in nanotechnological applications.

3.1 Introduction

Swarming is one of the most fascinating phenomena observed in nature that demonstrates organized structures by multiple motile entities.[1] It offers several advantages, such as 'parallelism', 'robustness', and 'flexibility', that cannot be achieved by solitary individuals.[2,3] In recent years, much effort has been devoted to exploiting the advantages of swarming in an artificial environment.[4,5] To date, the swarming of mechanical devices or chemically fueled self-propelled objects has been demonstrated by mimicking the swarming of living organisms.[6–8]

Recently the swarming of biomolecular motor system microtubule (MT)-kinesin in in vitro has attracted much attention due to its micro size and controllability using DNA technology.[9,10] The swarming of kinesin-propelled MT demonstrates bundle-shaped and ring-shaped swarms only by changing the rigidity of the MTs.[11] The bundle-shaped MT swarms are found to be more useful in the transportation of cargo in an efficient manner compared to individual MTs.[12] It is quite clearly understood that the swarm of MTs provides integrated force from the hundreds of kinesin-propelled MTs which show better transportability of the cargo than the single MT- kinesin (Figure 3.1a). The ring-shaped swarm of MTs also holds great prospects for future applications due to its ability to produce rotational motion.[13,14]

Although the swarm of MTs is getting much attention due to its applications in vitro, the amount of work that can be harnessed from the MT swarm has remained obscure yet. So far, a few efforts have been devoted to investigating the force of single kinesin and few kinesins (up to 10) propelling a single MT, mostly based on optical tweezers.[15–17] For the motility experiment the kinesins are bound by DNAs and some opposing load was applied in the opposite direction of the gliding MTs. One of the examples for the force determination of the MTs in the motility experiment where *Fallson et. el.* bound a bead to the plus end i. e. lag position of the MT and applied opposite force applying electromagnetic force.[18] In case of the swarming one of the challenging tasks is to attach the bead at the specific position of the swarm, moreover, the bundle swarm changes its track randomly to apply the force from a certain direction. Another challenging task is to predict the amount force to be applied to the swarm which is a compatible to affect the velocity of the swarm.

In the previous chapter I discussed the bundle swarm and its random directional change, and I set up an electromagnetic tweezer which can redirect the route of a magnetic bead loaded swarm by applying EMF. In this chapter a ring-shaped swarm of MT was constructed and an EMTw and

magnetic bead was utilized to determine the force of the swarm (Figure 3.1b). The magnetic bead was loaded to the MT swarm ring to perturbate it's rotational motion. The swarm ring changes its direction of motion repeatedly. The circular motion of the swarm ring allowed the magnetic bead to be apply different amount of force to the swarm dependent on the angles between emf generated by the tweezer and the direction of motion of the swarm ring. Using the force calibration curve, I determined the force of a swarm. I also estimated the density of the involved kinesin to compare the forces obtained from the swarm rings of different sizes involving different numbers of kinesins. The force of the swarm ring increases sub-additionally with increasing the size of the circular swarm. This increase in force arises from the higher number of active kinesins driving the larger swarms. Such estimation of the force of the swarm of MTs will widen applications of the MT swarm in nanotechnology as well as in robotics.

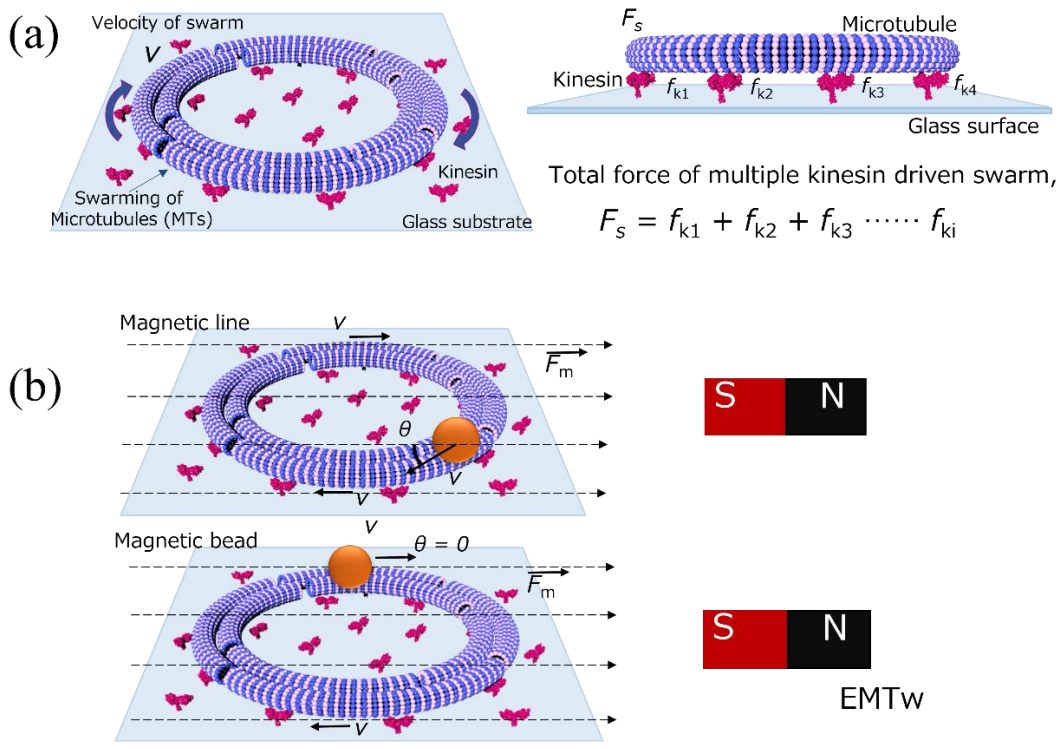

Figure 3.1 Schematic representation of (a) the force of a circular swarm associated with multiple kinesin and microtubules and (b) the model to determine the force using a magnetic bead and an electromagnetic tweezer (EMTw)

3.2 Results and discussion

3.2.1 Preparation of MTs as a swarm unit

MTs were polymerized from the azide and dye-labeled (ATTO550 and ATTO488 dye) tubulin with a ratio of 1:4 in presence of GTP (guanosine triphosphate). After that, the complementary DNAs (DNA1 and DNA2) were added to each set of MTs, and a click reaction was performed to modify the MTs by DNA.[19] This complementary DNA modification of the MTs allowed them to conjugate while propelled by kinesin in presence of ATP.

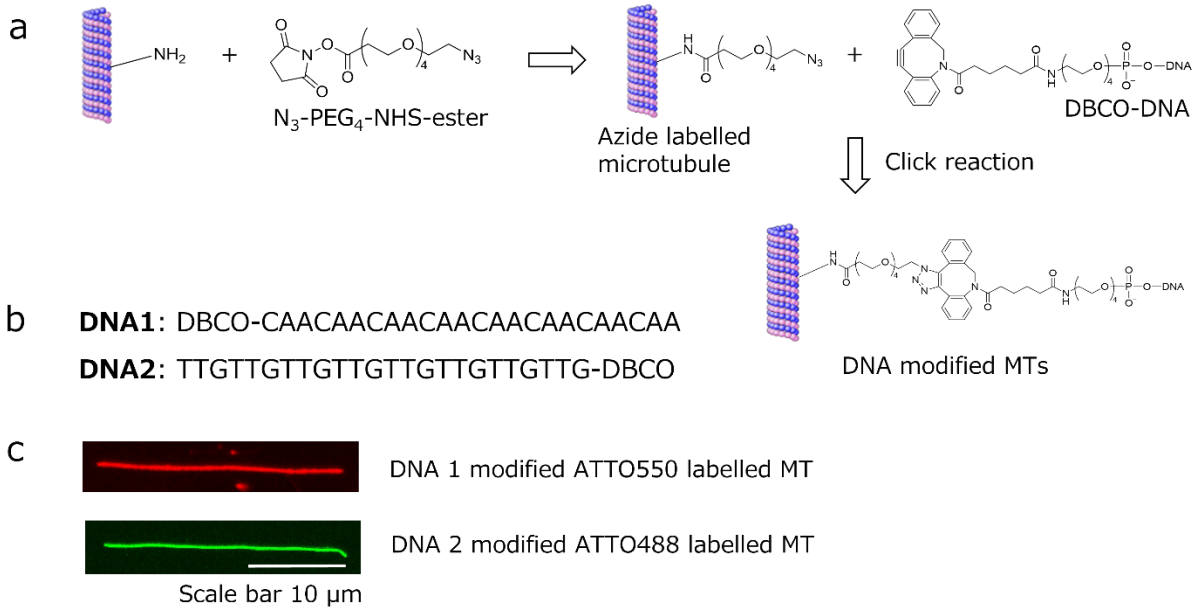

Figure 3.2 Schematic diagram of the preparation of swarm units through (a) conjugation of MT with DNA by click reaction, (b) DNA sequences, and (c) fluorescence microscopic images of the DNA conjugated MTs, scale bar 10 µm.

While click reaction for the preparation of DNA conjugated MTs, the DBCO at the 5′ end of DNA reacts with the azide functionalized MTs (figure 3.2). ATTO550 and ATTO488 labeled tubulins were used to distinguish the filaments as red and green.

3.2.2 Formation of swarm ring by active self-assembly of MTs

Ring-shaped swarm of MTs were constructed on the kinesin coated glass surface from two complementary DNA (DNA1 and DNA2) modified and, red and green (ATTO 550 and ATTO 488 labeled) MTs and schematically shown in the figure 3.2. Upon the gliding of MTs (figure

3.2a) on the kinesin coated glass surface, the flexibility of the MTs tends to the bend (figure 3.2b) and finally form a ring-shaped swarm (figure 3.2c) by DNA interaction.

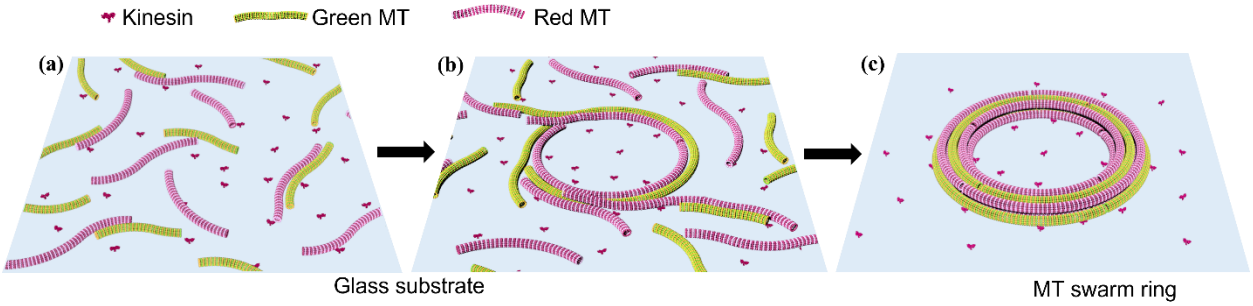

Figure 3.3: Schematic representation of the ring-shaped swarm formation by the two complementary DNA (DNA1 and DNA2) modified and, red and green (ATTO 550 and ATTO 488 labeled) MTs on the kinesin coated glass surface.

To demonstrate the swarming the ATTO 550 labeled DNA1 modified and ATTO 488 labeled DNA2 modified MTs prepared in section 3.2.1 were applied to the kinesin (400 nM) coated glass surface. The swarming was initiated in presence of ATP and observed by the fluorescence microscope. It should be mentioned that, in static condition i.e. in absence of ATP or kinesin swarming didn't take place but some static MTs or aggregation of MT were found (Figure 3.4a, b). In the absence of kinesin, the DNA modified MTs form aggregation due to the Brownian motion and the DNA interaction (Figure 3.4a). When, kinesin was present and there were no ATP present, the static MTs with zero displacement were found (Figure 3.4b).

In the presence of ATP, the MTs started gliding on the kinesin surface and the closer MTs started to interact with each other by complementary DNA sequences. Swarming is preferentially formed by the unidirectional moving swarm unis with similar velocity in active self-assembly process. However, for the MITs that collided while moving in the opposite direction, no successful swarm formation was observed. The DNA interaction between unidirectional MTs resulted in small groups or bundles and flexible GTP MTs rotated in a curved path to make a ring swarm.[9,11] The rings grew larger with time as new MTs unites to the existing swarms and stable rings were obtained from the single MTs. Figure 3.4c shows the time-lapse fluorescence microscopy image of the swarm ring of MTs from single DNA modified MTs. To understand the swarm behavior, different parameters like time dependency, kinesin concentration and DNA concentrations were studied in more details. Optimizing these parameters supports to choose the best conditions of the swarm for the force determination experiments.

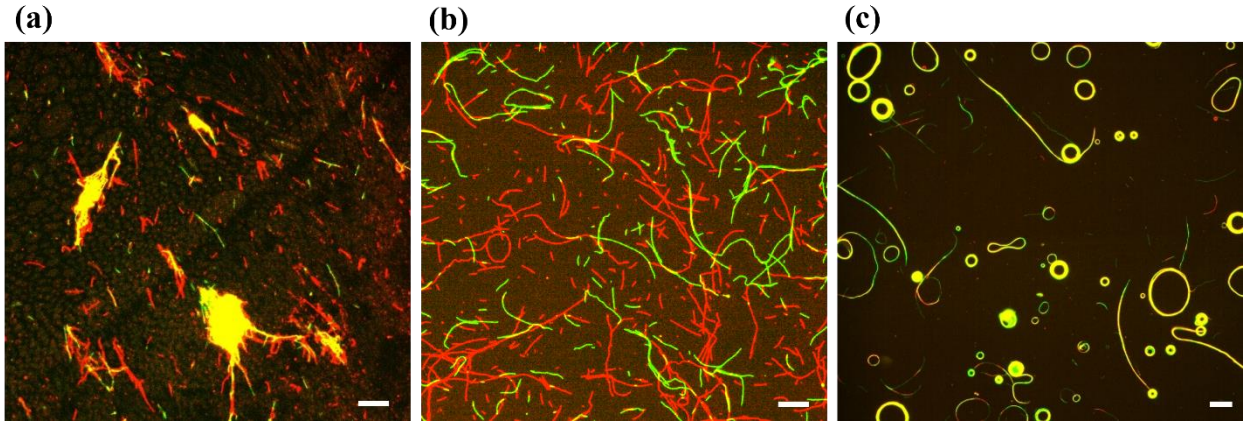

Figure 3.4 Fluorescence microscopic images of growth of MT swarm in different system: (a) MTs were found to form aggregates in a static system in absence of kinesin and ATP (no motor and fuel). (b) no swarm formation was observed in in presence of kinesin but absence of ATP (no fuel) (9) the dynamic system, swarming of MTs were formed on a kinesin coated surface in the presence of ATP. Scale bar: 10 µm.

3.2.3 Effect of kinesin concentrations on the formation of swarming

To investigate the effect of kinesin concentration on the demonstration of the ring-shaped swarming of MTs, the kinesin concentration was varied. The swarming was performed by the 100 nM, 200 nM, 400 nM, and 800 nM kinesin. Figure 3.5 shows the fluorescence microscopy images of the MT swarms under these conditions.

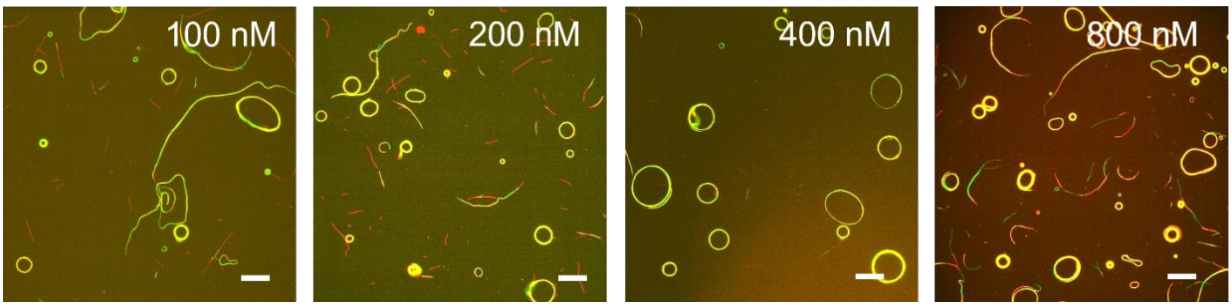

Figure 3.5 Fluorescence microscopy images of swarming of DNA modified MTs varying the kinesin concentrations. The concentrations of kinesins used to demonstrate the swarming was, 100 nM, 200 nM, 400 nM, and 800 nM. Scale bar: 20 µm.

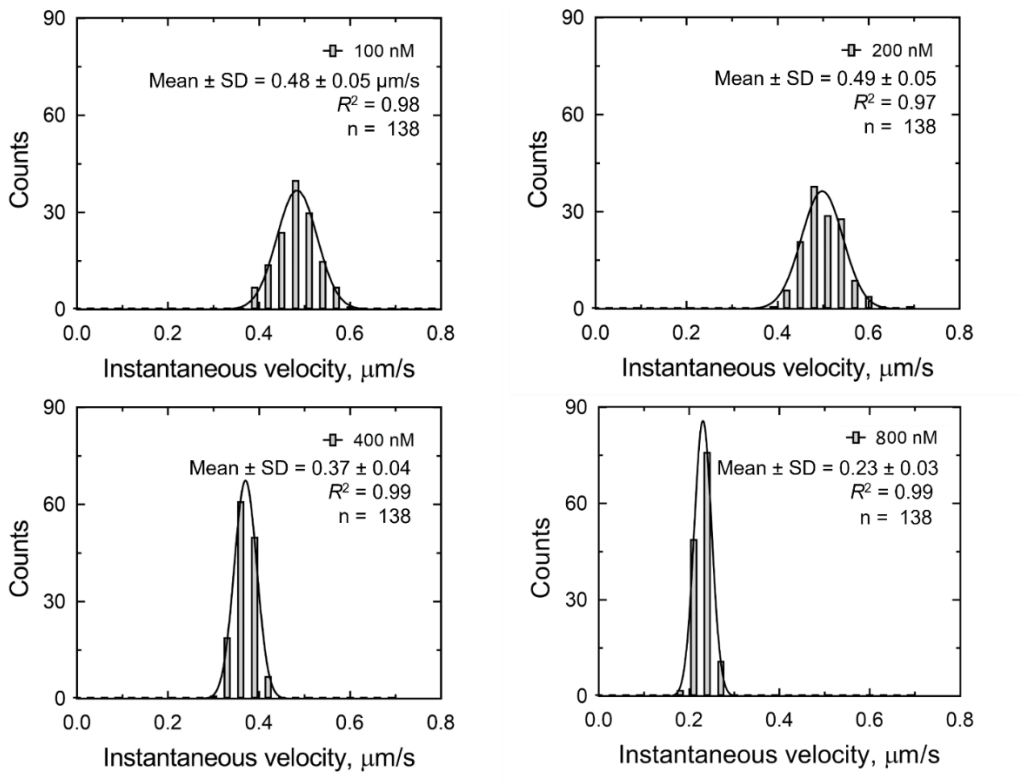

Figure 3.6 Comparison of mean instantaneous velocities of MT swarm ring propelled by kinesins of different concentrations. The number of instantaneous velocities considered 138 for each distribution. The events were normally distributed and were fitted to the normal Gaussian distribution. Mean velocities from the fits with standard errors and the goodness of fits (*R*-square) are provided in the legends of the graphs.

The images of the swarming were taken after 30 minutes of ATP addition for each of the kinesin concentrations. It is observed that the attachment of the MTs on the kinesin surface increases with increasing the kinesin concentration. The velocity of the swarm rings was determined from the swarming movies using ImageJ software. Figure 3.6 shows the Gaussian distribution of the instantaneous velocities of the swarm ring. The mean instantaneous velocity of the swarm rings was observed higher with decreasing kinesin concentration as clearly seen in figure 3.6. It is also observed that the velocity shows a broad distribution with lower kinesin concentrations (100 nM, 200 nM) whereas a narrow distribution is found with higher concentrations of kinesin (400 nM, and 800 nM). The swarming with a low concentration of kinesin show detachment in some cases, which coincides with the broad distribution of velocity. The kinesin concentration was chosen 400 nM for the further experiments for force determination as the velocity was stable in this concentration.

3.2.4 Optimization of the labeling ratio of DNA to tubulin

The melting temperature (T_m) was measured for the DNA duplex and shown in figure 3.7. From the experiment, T_m value was determined 68.04 ^oC, whereas the T_m value given by the supplier was 53.6 ^oC.

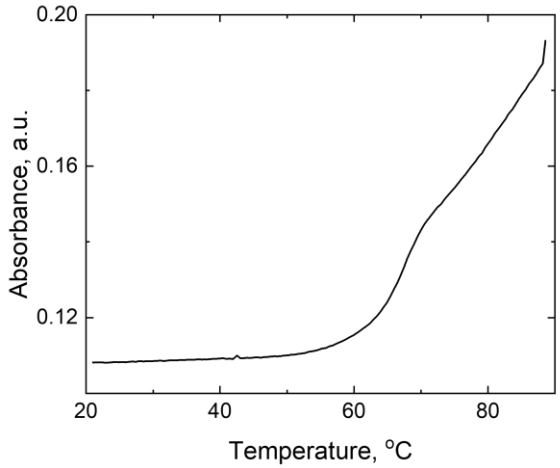

Figure 3.7 Melting temperature of DNA duplex. Condition: 10 µM DNA, 10 mM NaCl, 10 mM phosphate buffer (pH 7.0), absorbance at 260 nm

To optimize the labeling ratio of DNA to tubulin, the concentration of the DNA was varied for click reaction. MTs were conjugated with 3 different concentrations of DNAs listed in table 1.

Table 3.1. Labeling ratio of $(CAA)_8$ and $(TTG)_8$ modified MTs at different concentrations:

Concentration (in feed) (µM)	Molar extinction coefficient Ɛ ($Lmol^{-1}cm^{-1}$)	Conc. of DNA (µM) after depolymerization	Conc. of tubulin dimer (µM)	DNA to Tubulin L. R. (%)
$(CAA)_8$				
1000	210200	12.76	12.28	103.25
500		7.52	7.42	101.35
250		7.64	8.07	87.49
$(TTG)_8$				
1000	147400	17.06	15.05	113.25
500		12.59	10.78	116.57
250		12.49	11.65	107.29

After polymerization, swarming was performed with the MTs modified with different concentrations of DNA, as shown in figure 3.8. The figure indicates the successful swarm formation by the different concentrations of the DNA modified MTs.

The molar extinction coefficient of the DNAs was determined by measuring the absorbance of different concentrations of the DNA at the wavelength of 260 nm using **NanoDrop™ 2000c.** The DNA labeled MTs were kept at 4 ^{o}C overnight and the concentration of DNA and tubulin were measured using **NanoDrop™ 2000c.** The labeling ratio of DNA to tubulin was determined from the concentrations measured. The labeling ratio of DNA to tubulin was listed in the table 1.

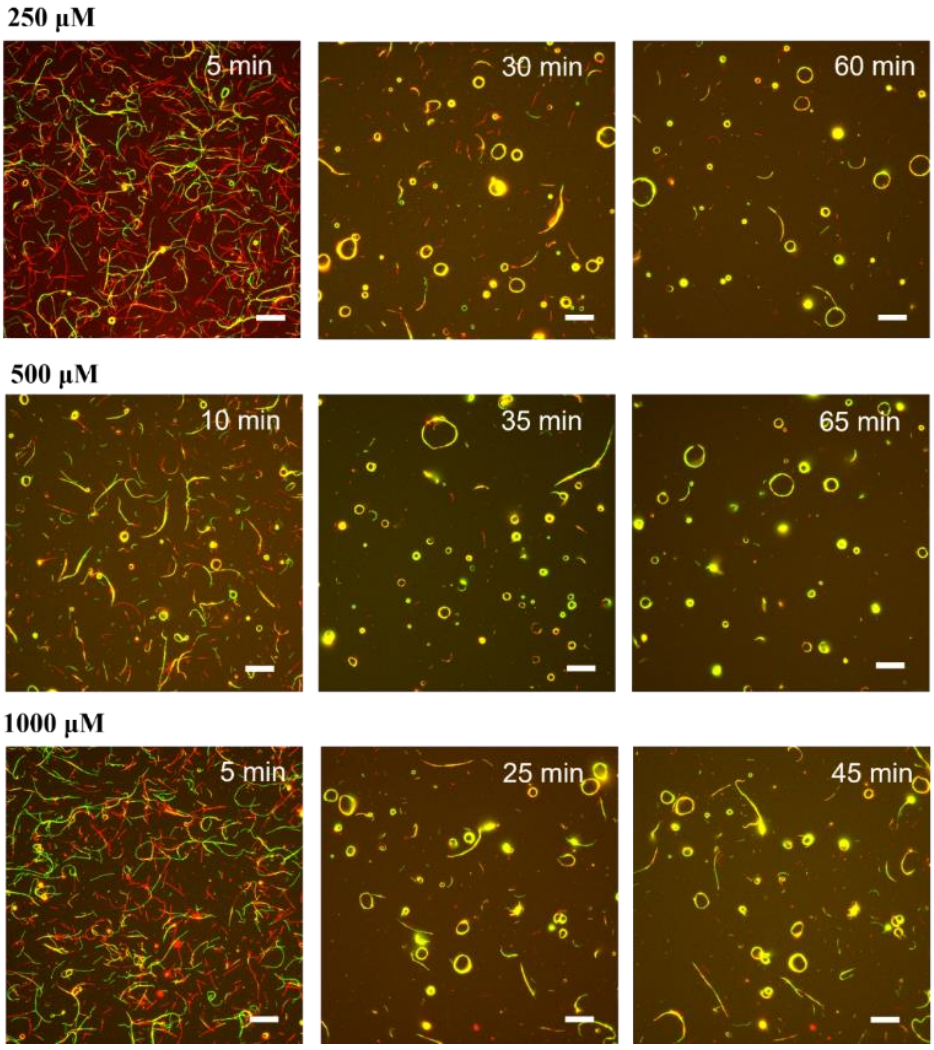

Figure 3.8 Time-lapse fluorescence microscopy images of swarming of $(CAA)_8$ modified, ATTO550 labeled and $(TTG)_8$ modified, ATTO488 labeled GTP MTs varying the DNA concentration for the modifications of MT. The concentrations of the DNAs used for the modification of MTs are 250 µM, 500 µM, and 1000 µM. Scale bar: 20 µm.

From figure 3.8 and table 3.1, it is seen that the labeling ratio values increases with increasing the concentrations of $(CAA)_8$ and $(TTG)_8$ labeled MTs. However, in all the cases the labeling ratio was around 100 % and the swarming was successful in all the 3 concentrations used. In the case of the higher concentrations of 500 and 1000 µM few aggregations were observed, whereas in the case of 250 µM DNA there were less aggregations and. For the demonstration of swarming, 250 µM was chosen for the DNA modification of MTs.

3.2.5 Effect of time on MT swarm ring formation

Time-dependent swarming was explored by the active self-assembly of the DNA modified MTs to observe the saturation and prolonged observation of the system. For the demonstration of swarming the MTs were modified by the complementary DNA1 and DNA2. The concentration used for the DNA modification was 250 µM with a labeling ratio of~90 % and~100% for DNA1 and DNA2 respectively. The kinesin concentration was fixed to 400 nM in presence of 5 mM ATP. After preparing the flow cell for the demonstration of swarming the fluorescence microscopic observation was performed. Figure 3.9 shows the time-lapse fluorescence microscopic images of the swarming.

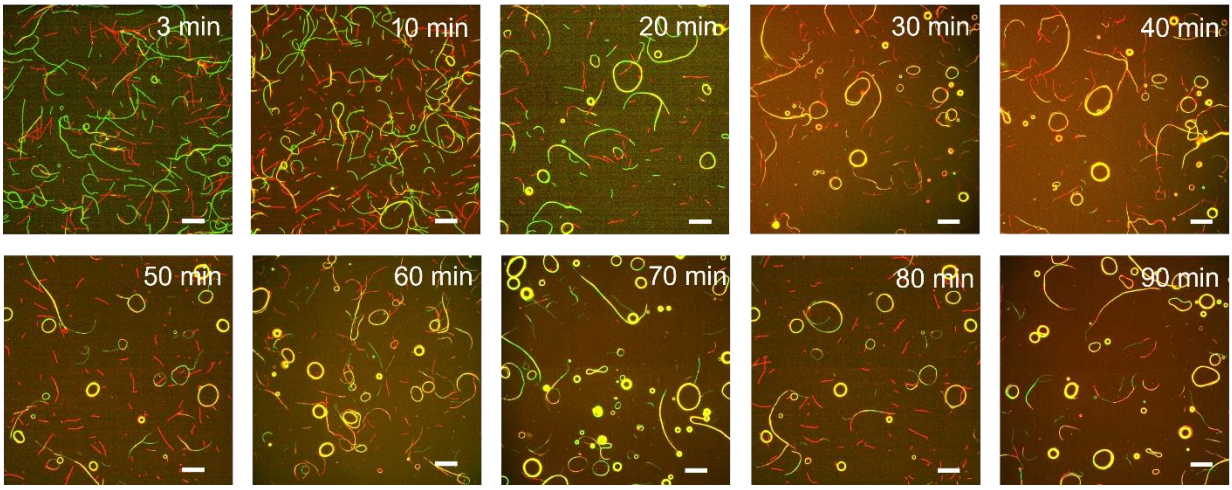

Figure 3.9 Time-lapse fluorescence microscopy images of swarming of $(CAA)_8$ modified, ATTO550 labeled and $(TTG)_8$ modified, ATTO488 labeled GTP MTs show the formation of the circular-shaped swarm from the single DNA modified MTs with time. Scale bar: 20 µm.

From the time-lapse images, it is observed that the gliding of flexible MTs forms small bundles which spool into a circular swarm with time. The number of single MTs and swarm rings over time were counted manually and association ratio and densities were determined (see methods).

The number of the circular swarm was found to increase with time which can be clearly seen from the association ratio shown in figure 3.10 (top).

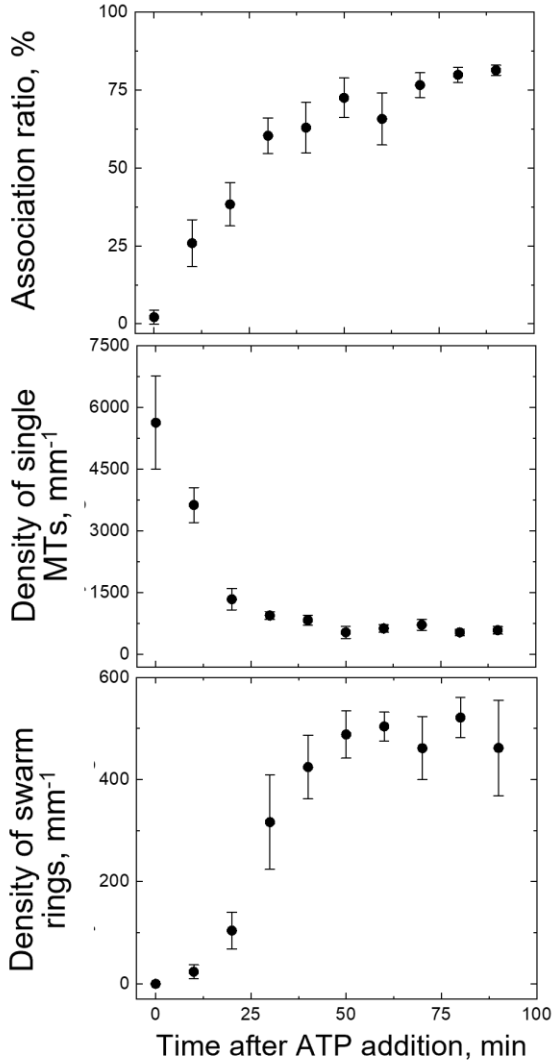

Figure 3.10 Time-dependent (top) association ratio, (middle) density of single MTs, and (bottom) density of MT swarm rings. Within the 60 minutes of ATP addition, the association ratio, and the number of single MTs and swarm reach the plateau which indicates the saturation of the system by this time. Error bar: S. E.

The density of the single MTs decreases with time, on the other hand, the number of the rings increases which has shown in figures 3.10 middle and bottom. After 60 minutes both the number of single MTs and the swarm ring reach a plateau. The number of single MTs decrease drastically after 20 minutes and the number of swarm ring shows a sharp increase at around 20-30 minutes of ATP addition. And after 20-30 minutes the lower rate of decreasing the number of single units and

the increasing the swarm is found. It can be said if single MTs are available the swarm formation continues to thicken the existing swarm rings or make a new swarm ring.

3.2.6 Modification of the magnetic particle by complementary DNA

To load and carry the magnetic particle, **Dynabeads™ M-270 Amine** by the swarm, the Dynabeads were modified by the DNA2, which is complementary to the DNA1. A superparamagnetic Dynabeads (simply termed as 'bead') of 2.8 µm was employed in this work to load and carry by the swarm for the force determination of the MT swarm. The beads are auto fluorescent and composed of highly cross-linked polystyrene with magnetic particles (Fe_3O_4) precipitated in pores evenly distributed throughout the beads. The beads are further coated with a hydrophilic layer of glycidyl ether which seals the iron oxide inside the beads and the surface is activated with primary amine functionality on a short hydrophilic linker.

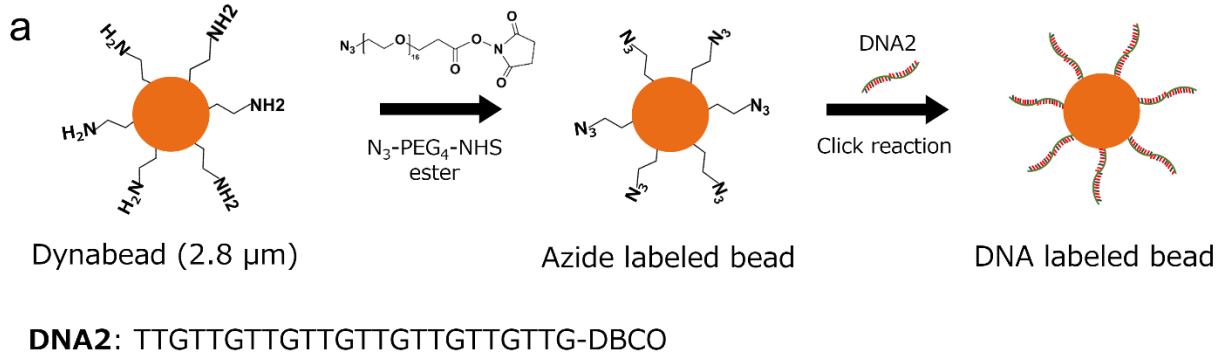

Figure 3.11 (a) Schematic representation of the azide labeling of beads and consequently DNA modification. Fluorescence microscopic image of the autofluorescence Dynabead dispersed in 1×BRB80 solution after the modification using DNA2. Scale bar 5 µm.

In the first step of modification the amine-functionalized beads were converted to azide-functionalized beads using N3-PEG4-NHS ester. In the latter case the DNA modification of the azide-beads were performed by click reaction (for more details see methods). Figure 3.11 shows the schematic representation of the DNA modification of the beads by click reaction.

After the modification, the beads were suspended in 1×BRB80 solution for preservation at 4 ^{o}C for 1-2 weeks. Once the swarming is performed in a flow cell, the beads were diluted 30 times in the ATP buffer and applied to the flow cell to load and transport by the MT swarm ring. Usually, after the addition of ATP buffer to the flow cell, it takes~30 minutes for the complete swarm ring formation. Usually, the beads were added to the flow cell after 30 minutes of ATP addition, when most of the swarm rings already formed.

3.2.7 Attaching the beads to the swarm ring

To attach the beads to the swarm rings, the beads (dispersed in ATP buffer) were added to the flow cell after swarm formation (after 20-30 minutes of ATP addition). Figure 3.12 shows the schematic representation of the loading and carrying of the beads by the swarm ring. The beads are loaded to the swarm in a zipping geometry resulting in a 24 base pair overlapping of DNA1 and DNA2. When all the DNAs in MTs form the complementary base pair between DNA1 and DNA2, beads can no longer attach to the swarm.

When a swarm ring resulting from the DNA1 modified red MTs and DNA2 modified green MTs, pass through the DNA2 labeled Dynabead, it selectively attaches to the DNA1 modified red MTs by complementary DNA interaction. This attachment resulted in the loading of beads by the swarm ring and carrying in the circular path by the swarm ring propelled by multiple kinesins.

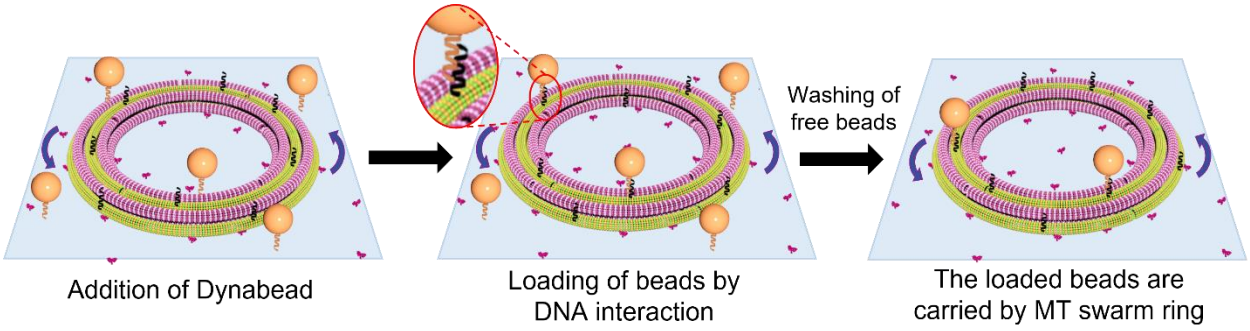

Figure 3.12 Schematic representation of the bead's attachment to the MT swarm by DNA zipping. After the attachment, the beads are loaded by the swarm and transporting in a circular path. The scheme is not in scale.

After loading and carrying of beads by the swarm ring, it was observed under the fluorescence microscopy. Figure 3.13 shows the time-lapse images of the loading and carrying of beads by the MT swarm rings. Here, the swarm is constructed by the DNA1 labeled red MTs and DNA2 labeled

green MTs, whereas the beads are labeled with DNA2. From the observation, it might be said that the DNA2 labeled beads were hybridized with the complementary DNA1 labeled red MTs and consequently loaded and transported by the swarm ring.

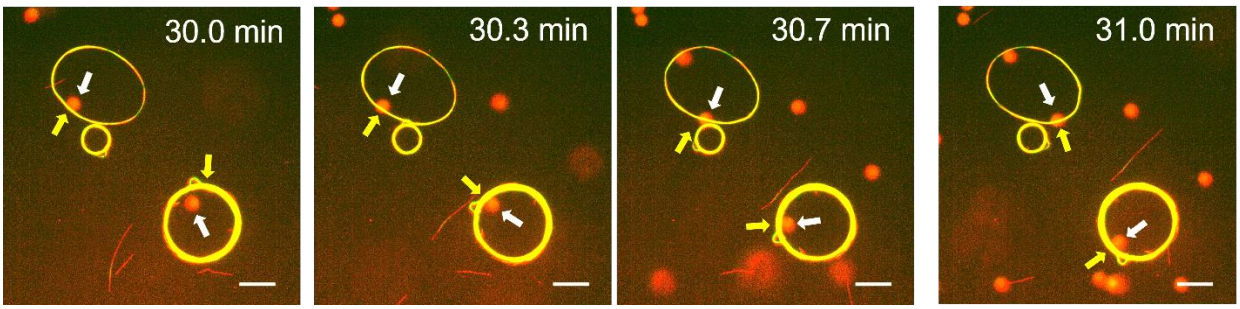

Figure 3.13 Time-lapse fluorescence images of the DNA2 labeled bead loading by the DNA assisted swarm ring of MTs. It is obvious that the DNA2 labeled beads attach to the DNA1 labeled red MTs and are loaded by the swarm and then carried in the circular path. Scale bar: 10 μm.

According to the experimental approach, the swarm is formed at both surfaces, the upper surface and lower surface of the flow cell. The beads itself have a weight of 0.13 μg and the beads sediment to the lower surface due to the gravity. Because of the gravity, the beads only become close to the swarming at the lower surface of the flow cell and loaded then carried by these swarms.

3.2.8 Application of electromagnetic force by electromagnetic tweezer to the bead-attached swarm

The electromagnetic force (emf) from the electromagnetic tweezer (EMTw) was applied to the bead attached MT swarm ring as an external field to control the circular motion of the swarm ring. A custom-made electromagnetic tweezer (EMTw) was built to introduce an external magnetic field. The electromagnet employed in the EMTw consists of a solenoid with an enamel-coated copper wire wrapped around an MC nylon® shell. There is a cylindrical core with a tapered tip made of S10C material into the electromagnet. DC power is used to tune the current and voltage within a range of 0.001 to 0.15 and the maximum voltage of 36 V where the coil resistance is 240 Ω. The magnitude of the emf produced by the tweezer is proportional to the current intensity flowing into the coil.

The force calibration was performed for the Dynabeads. The tip of the EMTw was very touched to the upper surface of the flow cell with a tilt angle of around ~20 ^{o}. The schematic representation

of the placement of the flow cell and the tip of the tweezer is shown in figure 3.14 (not in real scale).

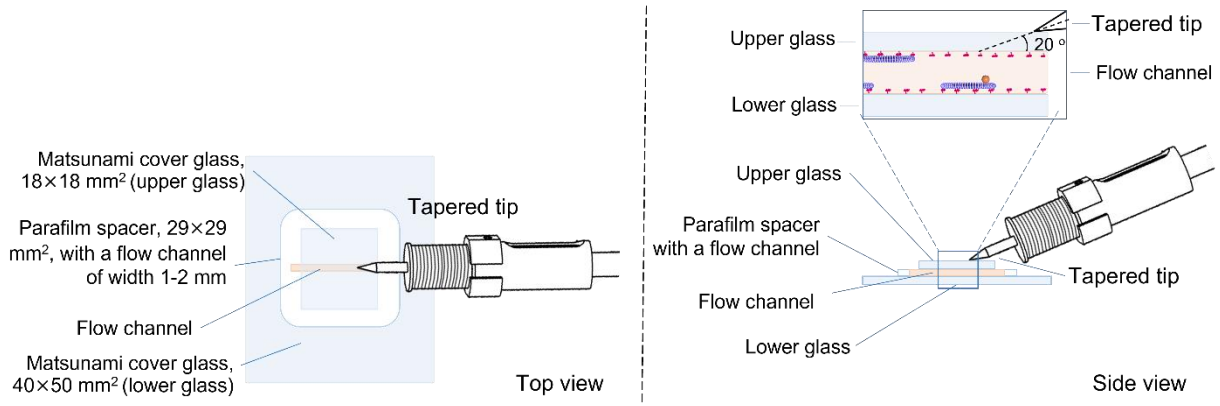

Figure 3.14 Schematic representation of the magnetic field applier system from the top view and bottom view (not in real scale). The inset image shows the scheme of flow cell in between the two glass surfaces and the swarm is formed at both surfaces.

3.2.9 Different approaches to applying the emf to the bead loaded swarm

3.2.9.1 Applying emf to the bead loaded swarm at the lower surface of the flow cell

Initially I attempted to apply the emf to the beads carrying by the swarm ring at the lower surface of the flow cell. The effect of the applied force on the MT swarm rings are shown in Figure 3.15.

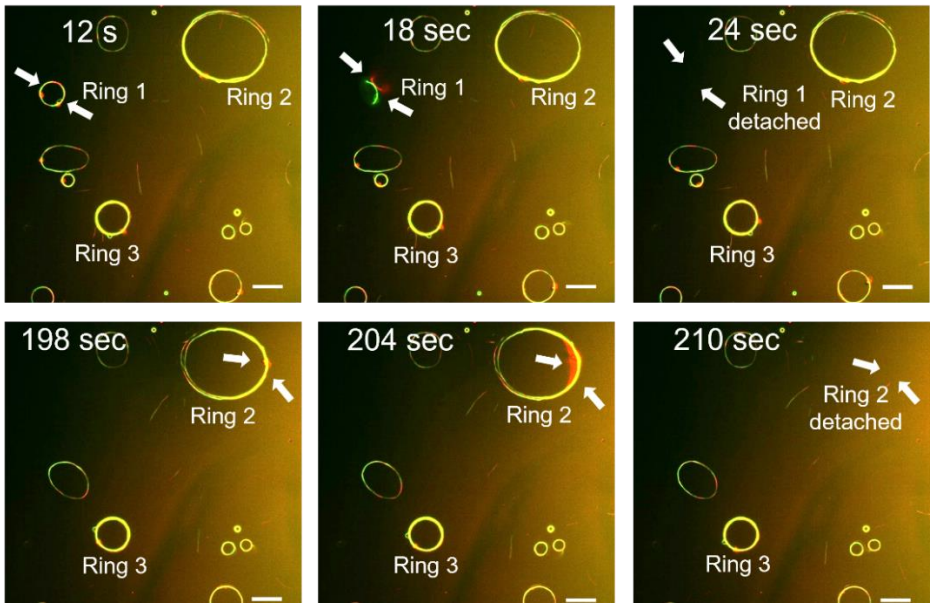

Figure 3.15 Fluorescence microscopic time-lapse images of applying emf to the MT swarm rings. The observation field was at the lower surface of the flow cell and the bead attached rings were detached by the vertical pulling by applying the emf (10 V). The time scale corresponds to the time after applying the emf.

Here, 10 V was applied to the swarm rings. Considering ring 1, it is seen that it started to detach from the kinesin surface after 12 seconds of applying emf and within 18 seconds, ring 1 has completely detached. The same phenomenon is observed in the case of ring 2, which started to detach after 204 seconds after applying emf and completely detached after 210 seconds.

In this experiment, the emf (10 V) has been successfully applied to the bead loaded circular swarm. No detachment of the single bead from the swarm was observed due to the strong interaction between DNAs of bead and MTs.

After applying the emf, the bead loaded swarms started to detach from the kinesin-coated glass substrate due to the vertical applied force. Some of the rings detached just after emf applied (ring 1), some took longer time (ring 2), and some did not detach at all even after the prolonged emf application (ring 3). However, the velocity of the swarm could not be controlled by applying emf. The solution is a bulk area between the slide glasses and the beads were attached to the MT swarm ring at the lower surface. and after applying emf the swarm detached from the kinesin-coated glass substrate (lower surface) and might moves towards the upper surface though the bulk area of the flow cell. This phenomenon is schematically described in figure 3.16.

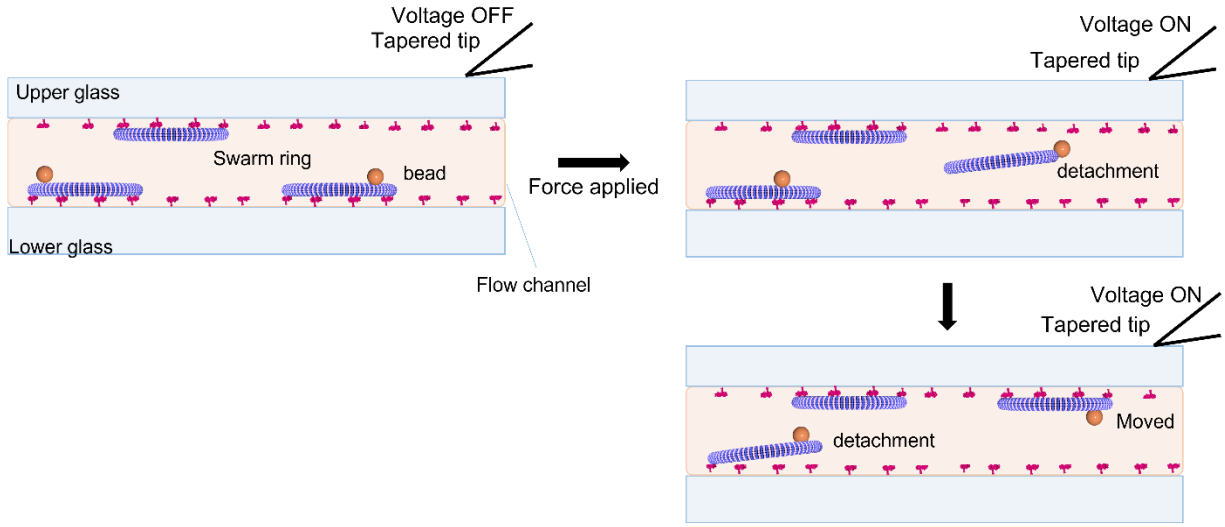

Figure 3.16 Schematic representation of applying the emf to the bead-loaded swarm ring located at the lower surface of the flow cell (not in real scale). Due to applying emf the bead-loaded swarm ring detached and might relocate towards the direction of the electromagnetic force applied.

3.2.9.2 Loading of beads to the swarm rings at the upper surface of the flow cell and applying emf

As described in the previous section, to avoid the detachment of the swarm by applied emf, the beads were attached to the swarm rings located at the upper surface of the flow cell. Figure 3.17 shows the schematic illustration of the steps to attach the beads to the swarm at the upper surface. The steps are listed here,

i. Beads dispersed in ATP buffer was added to the flow cell.

ii. Just after the addition of ATP the flow cell was flipped upside down and waited for 5 minutes.

iii. This flipping of the flow cell and waiting of 5 minutes allowed the movement of the beads towards the upper surface * (towards the ground), due to the gravitational force working on the beads.

iv. After the waiting time the flow cell was flipped to the initial orientation.

v. At this step the flow cell was washed with ATP buffer to remove all the free beads from the flow cell.

After washing, only the attached beads at the upper surface are remaining and carried by the MT swarm ring. To apply the force, I choose the swarm ring with single bead attached to it.

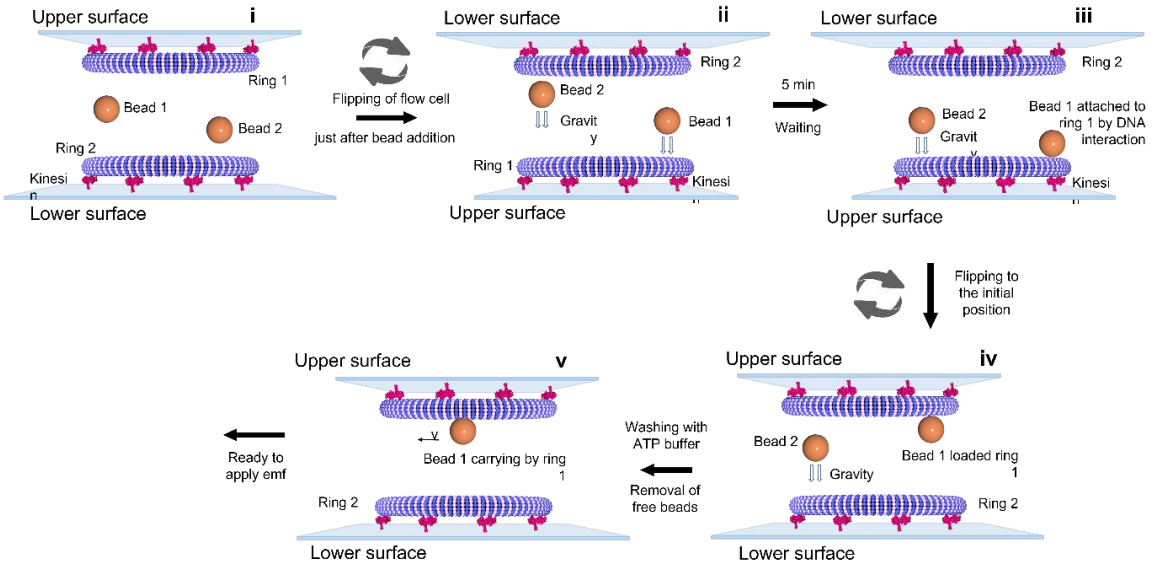

Figure 3.17: Schematic representation of loading of the beads to the MT swarm ring located at the upper surface of the flow cell. The flow cell was flipped after the addition of beads (i, ii), and 5 minutes of waiting time allowed the attachment of beads to the swarm at the upper surface i. e. towards the ground (iii). The flow cell was flipped to the initial position (iv) and washed with ATP buffer to remove the free beads from the flow cell (v). (Schemes are not in real scale).

After each event of applying force the velocity and the spatial fluctuation was observed to understand the compatibility of the force. Three types of behaviors were found during the application of magnetic force to the swarm ring,

(i) If the applied force is higher than the force of the swarm ring, the shape of the swarm might be distorted or detached from the kinesin surface

(ii) If the applied force is much lower than the force of a swarm the velocity of the swarm ring does not show any increasing or decreasing pattern and there is no translational motion as well.

(iii) If the applied magnetic force is compatible with the force of the swarm ring the velocity of the swarm ring shows increasing and decreasing pattern. Additionally, the swarm ring shows some translational motion toward the applied force.

Finally, I established the swarm-tweezer system to apply appropriately to the swarm ring. After the swarm formation, the beads were loaded, and carried by the swarm at the upper surface of the flow cell. Emf was applied to the swarm by the tweezer and the voltage was increased in a stepwise manner. Here I describe one of the force determination events of swarm ring. I choose a swarm with an outer diameter of around 9 μm and a ring width of 1.4 μm. From the fluorescence observation, no void space was found in its structure and the ring was rotating with a velocity of 0.26 ± 0.04 μm/s without applying emf. 10 V was applied to control the velocity of the bead-loaded swarm ring of MTs. The distance between the tip and the center of the swarm was around 260 μm. The distance was measured from the microscopic view of the magnetic lines induced by the free bead trajectory towards the tweezer's tip. Since the diameter of the swarm ring, 9 μm, much smaller than the distance between the tip to the center of mass of the swarm ring, it is assumed that the magnetic field lines are uniform in all the regions of the swarm ring. The displacement or velocity of the swarm ring was observed for 20 minutes. At the first 0-5 minutes the observation was performed without applying emf (no emf) and emf was applied from 5-10 minutes, again the emf was turn off from 10-15 minutes (no emf) and again emf was applied from 15-20 minutes.

Figure 3.18a shows the trajectory of the bead attached to the swarm ring during without applying emf and applying emf and the corresponding time-dependent velocity plot is shown in figure 3.18b. From the trajectory of the swarm ring, it is seen that the ring itself translocated towards the direction of the force applied by the EMTw. The trajectory of the ring velocity for the first 5 minutes, up to 3 cycles shows negligible displacement, which is also reflected in the time-

dependent velocity plot (Figure 3.18b). The velocity at 0-5 min, as well as 10-15 min, showed a smaller deviation than the average velocity. The velocity at 5-10 and 15 -20 min shows a periodic increasing and decreasing pattern, which is the reflection of the electromagnetic force applied to the bead-loaded swarm.

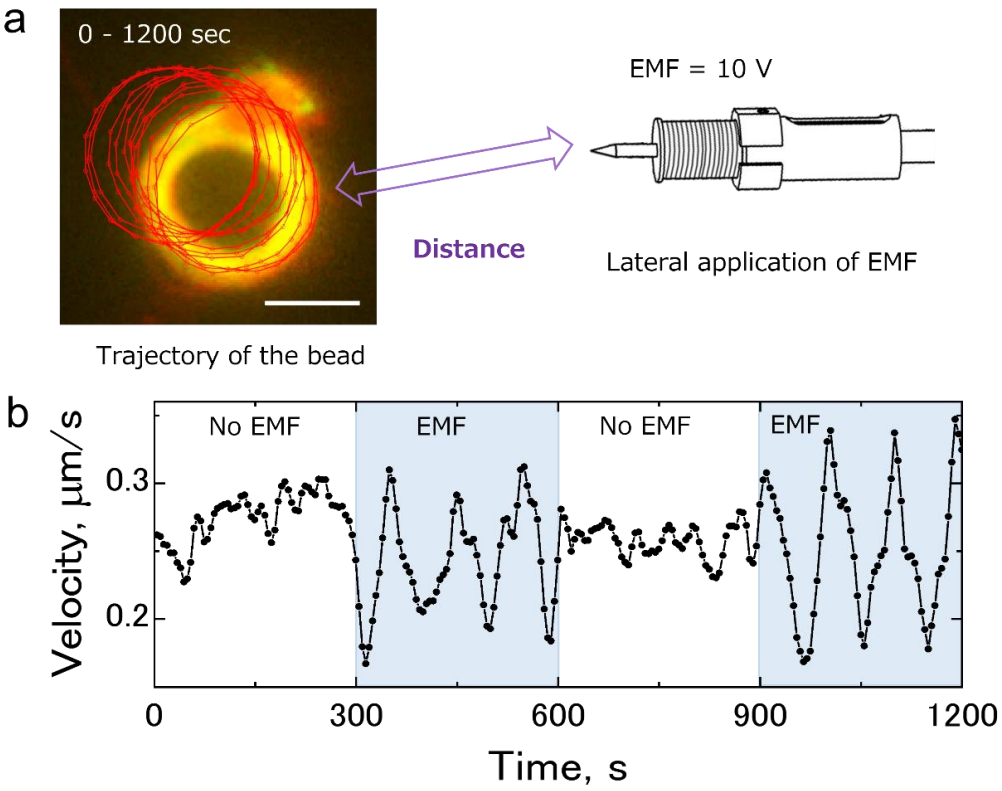

Figure 3.18: Application of the emf to control the velocity of the circular swarm, (a) Trajectory of the bead attached to the swarm ring without applying (0 V) and with applying emf (10 V).

3.2.10 Trajectory analysis of the bead-loaded swarm applying EMF

Figure 3.19b shows the trajectory of the bead attached to the swarm ring of one cycle and the corresponding velocity is shown in the red mark of figure 3.19a. The distance between the swarming ring of MTs and the tip of the tweezers was estimated by comparing full-frame fluorescence images and corresponding magnetic field lines produced by the trajectory of free beads. The yellow dashed lines in figure 3.19b represent the electromagnetic field produced by the applied magnetic field. The swarming ring was rotating in a clockwise direction and the EMTw was applied from the right side of the swarm ring. From the trajectory of one cycle, it is seen that

the lowest displacement was observed from 960-965 s and the highest displacement was obtained from 1105-1010 s.

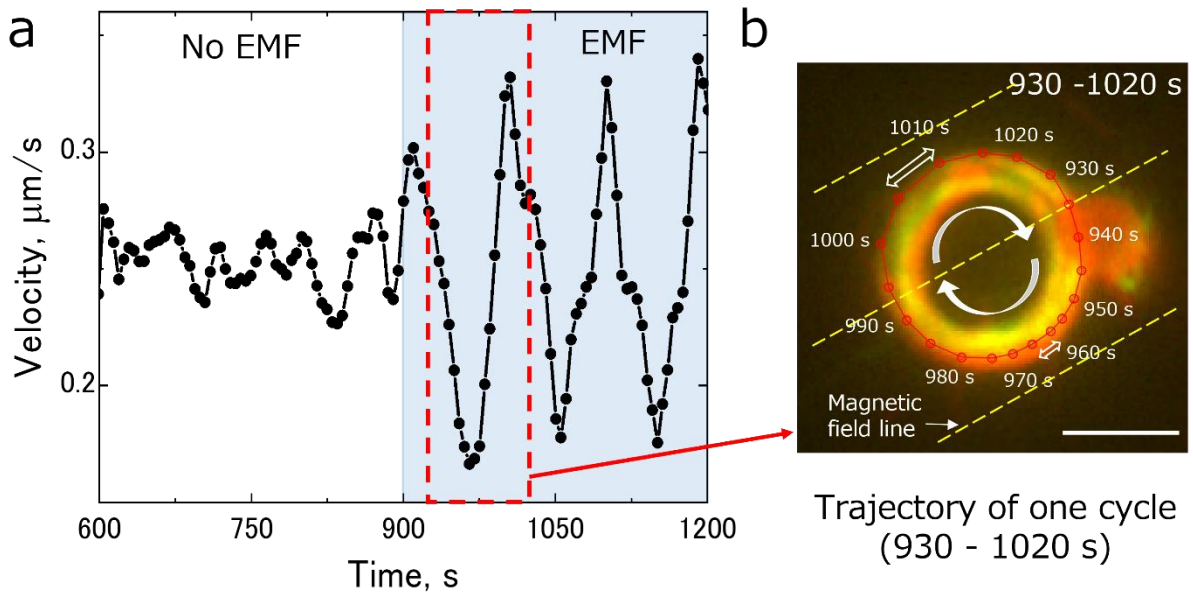

Figure 3.19: Velocity and corresponding one cycle trajectory of the bead-loaded swarm ring applying emf, (a) Velocity of the swarm ring without and applying emf, where the red marks correspond to the velocity of the swarm ring of (b) one cycle trajectory of the swarm ring during 930-1020s while applying emf. Scale bar 5 µm

The distance between the tip and the swarm ring was determined by comparing the dimensions of the fluorescence observation field. The applied force to the swarm ring was estimated from the force calibration curve of the beads discussed in chapter 2 (section: 2.2.4).

3.2.11 Determination of acting magnetic force on the rotating MT swarm ring

On the basis of the trajectory of the bead attached to the swarm ring I measured the velocity, *V*. The total force of the swarm ring is F_s corresponds to the total number of kinesin's force which is driving the swarm ring. It was assumed that the bead attached to the swarm ring (by DNA conjugation) circulates with the same velocity, *V* as of the swarm ring. The external magnetic force, F_m is applied to the bead-loaded swarm ring and the acting magnetic force, F_a depends on the direction of motion of the bead attached.

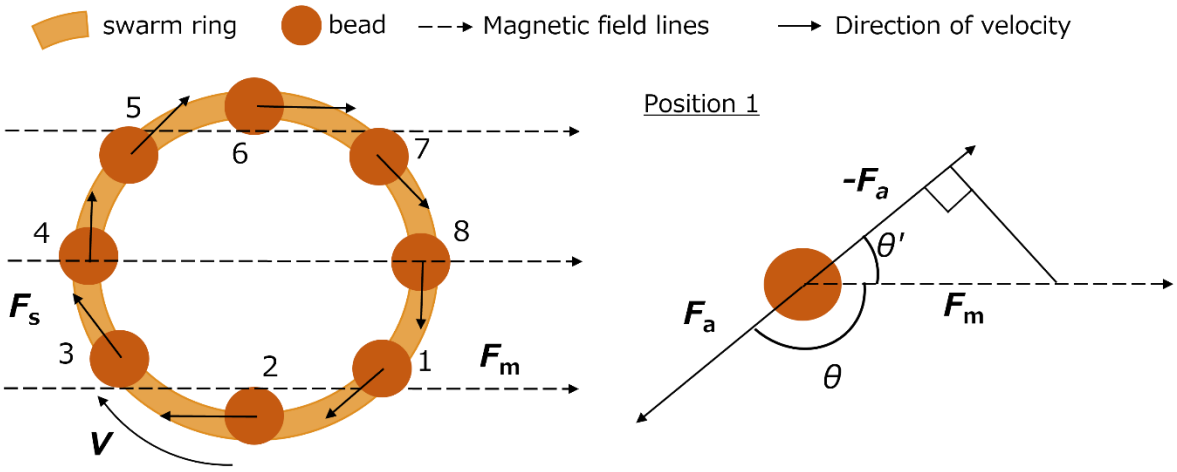

F_s: Force of the swarm, V: Velocity of the swarm, F_m: Magnetic force, F_a: acting force on bead along the direction of motion of the swarm, θ : Angle between magnetic line and direction of motion, $\theta' = 180-\theta$

Figure 3.20 Schematic representation of the different positions of the bead in a swarm ring during circulation of the swarm ring. Left: the attached bead changes its direction, θ of motion with the circulating swarm ring, whereas the magnetic field lines have the fixed direction. Right: Determination of the acting force F_a on the bead at each position, which depends on the angle θ between F_m and F_a

Figure 3.20 left shows the different positions of the bead attached to the ring and circulating with the swarm under the magnetic field. From the figure, it is seen that the magnetic field line direction is fixed whereas the direction of motion of the bead changes with time as the swarm ring is continuously propelled by kinesin in a circular path. The Acting force F_a on the bead was measured individually depending on the position of the bead where the angle, θ changes with changing the direction of motion of the bead and fixed magnetic field lines.

At position 1 (figure 3.20 right), where the angle between the direction of the bead's motion and the magnetic field's line is θ, shown in figure 3.20 right. Acting force, F_a working on the beads,

$$F_a = F_m \cos\theta \quad \ldots\ldots\ldots\ldots\ldots\ldots\ldots\ldots \text{(i)}$$

First, the angle of each position was estimated (Figure 3.21), and then the acting force was determined.

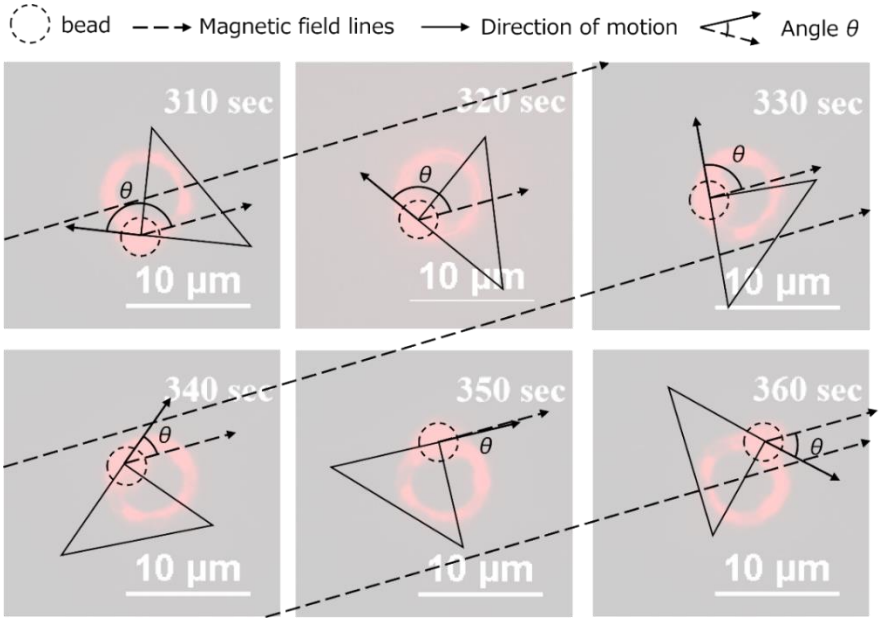

Figure 3.21: Estimation of the angle between the changing direction of the bead's motion with the fixed magnetic field lines

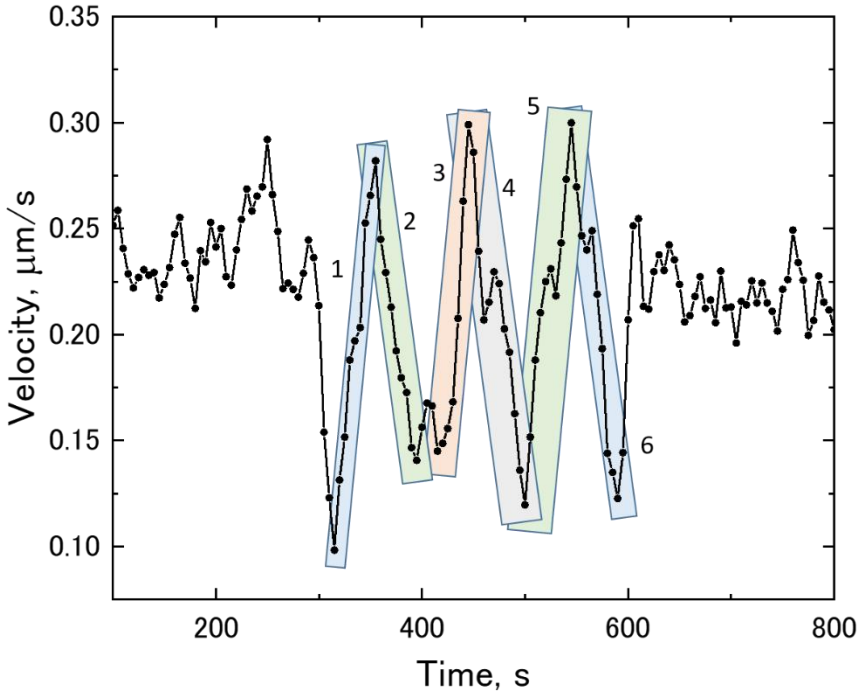

Figure 3.22 Increasing and decreasing of the velocity depending on the positions of the bead to the swarm ring and acting force was estimated from the colored region only at the time EMF was applied

The acting force on the bead was only determined while EMTw was turned on. Figure 3.22 shows the zoomed view of (5 s interval) time versus velocity curve from 100-800 s. The colored parts 1, 3, and 5 show the increasing velocity, and 2, 4, and 6 show the decreasing velocity which is in corresponds to the applied magnetic force and the direction of bead's motion. In these increasing and decreasing velocity region acting force was estimated using equation 1.

3.2.12 Force determination of the circular swarm

The force of the swarm ring was determined by estimating the acting force on the bead. In figure 3.23, the velocity was plotted against the acting force while applying EMF. From the figure, it is seen that the lower velocity (compared to the average velocity) was resulted from the negative acting force whereas the higher velocity was resulted from the positive force applied to the swarm ring depending on the θ value. The velocity at zero force is comparable to the average velocity of the swarm ring.

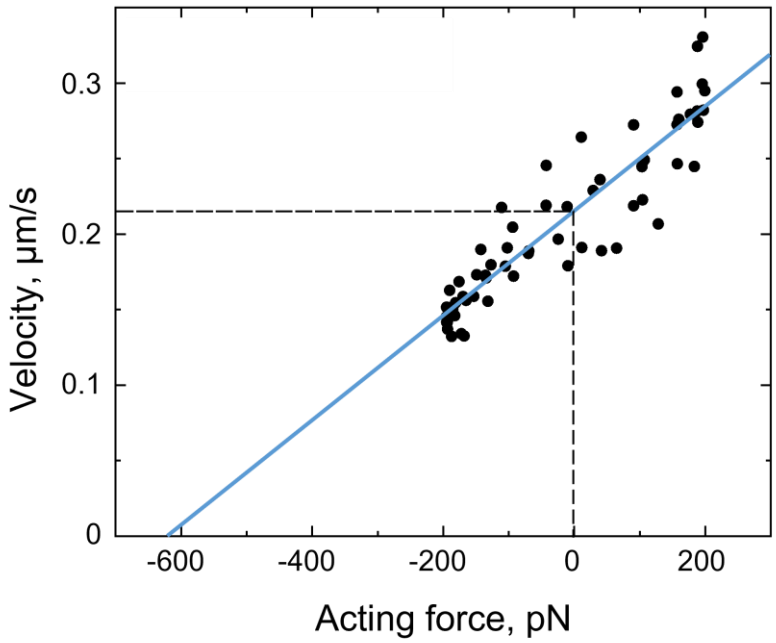

Figure 3.23 Acting force versus velocity curve for bead loaded circulating MT swarm ring and determination of the force of the swarm. The dashed lines represent the average velocity of the swarm ring at zero applied force. The plot was fitted linearly ($Y = mX + c$, R-square~0.84) and the extrapolation of the fitted line towards zero velocity corresponds to the force required to stop the swarm ring i. e. force of the swarm.

To measure the force of the swarm ring the acting force velocity curve was fitted linearly, and the acting force was extrapolated to zero velocity. The acting force at zero velocity represents the force required to stop the swarm ring against the kinesin force which is defined as the force of the swarm. The force obtained in this method for the particular swarm ring is ~625 pN. Forces for the swarm rings of different diameters and widths were estimated from different swarm events.

Change in the force of the swarm ring with different size and widths has been shown in the figure 3.24 (a). From the figure it is seen that the force of the swarm ring increases with the diameter of the swarm ring, however the increasing tendency of the force was random.

For the further realization of the force tendency, we additionally considered the width of the swarm ring. The width of the swarm ring was determined from the fluorescence images converting to the threshold binary images. The area of the swarm ring (except from the inner area) was determined from the diameter and width of the ring and force was plotted against the area in figure 3.24 (b). The force increases with the area of the swarm ring and shows better increasing tendency.

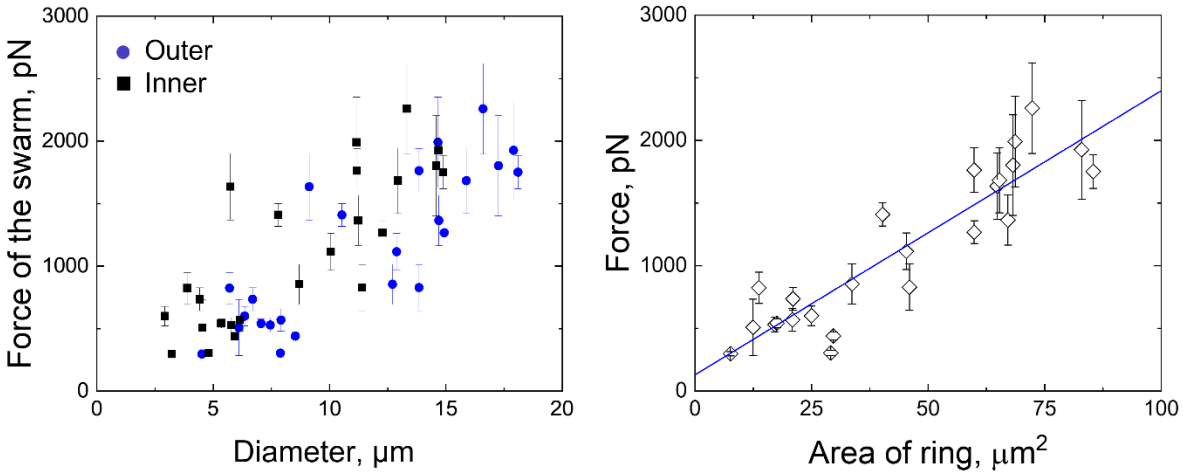

Figure 3.24 (a) Force of the swarm ring with the diameter of the rings. The force of the swarm tends to increase randomly with the higher diameter of the swarm rings. (b) Force of the swarm ring with the area of the swarm. The width of each of the rings were determined from the fluorescence images converting to the threshold binary images. The force of the swarm tends to increase with the increasing area of the MT swarm.

It is obvious that in a larger swarm (with higher area), the number of involved kinesins is higher than in the smaller one. In the nest step we determined the number of kinesins involved in the swarming. The density of the kinesin was determined from the landing rate experiment discussed in the next section.

3.2.13 Landing rate experiment to determine the density of kinesin

Landing rate experiment was performed to determine the density of kinesin.[20] To perform the landing rate experiment, ATTO565 labeled GTP MTs were polymerized. Figure 3.25 shows the fluorescence microscopy image of the successful polymerization of MTs. Length of the MTs was estimated 8.98 ± 5.16 µm (SD).

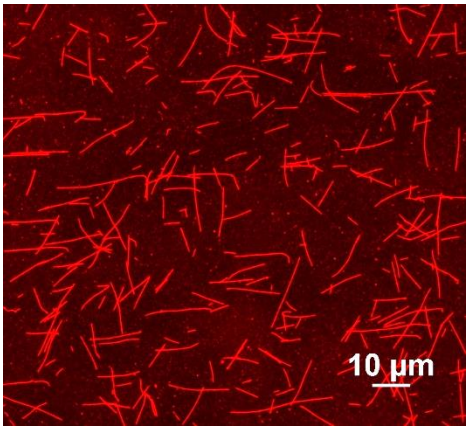

Figure 3.25 Fluorescence microscopy image of ATTO565 labeled GTP MTs.

In the force determination experiment, the kinesin concentration was 400 nM. For the landing rate experiment, the stock kinesin concentration was fixed as the swarming experiment to 400 nM. The stock kinesin (400 nM) solution was diluted according to the different dilution factors, ξ listed in the table 2,

A flow cell was prepared and MTs were added to the kinesin coated glass surface (details in the methods and materials). The time-dependent landing of MTs on the kinesin surface (lower surface) was observed by a fluorescence microscope and time-lapse images were taken for up to 10 minutes. Figure 3.26 shows the MTs landing events in each field of view with time for different concentrations (5 to 180 nM) of kinesin.

Table 2. Different kinesin concentrations depending on the dilution factor of 400 nM kinesin:

Kinesin concentration (nM)	Dilution factor, ξ
1	0.0025
5	0.0125
10	0.025
25	0.0625
50	0.125
75	0.1875
100	0.25
150	0.375
200	0.5

For analysis, the number of the MTs landed on the kinesin surface over time was counted manually. The time versus number of landed MTs was plotted (Figure 3.27) and fitted with the following landing rate equation (ii),

$$N = N_{max}(1 - exp^{(-R(t-t_{ini})/N_{max})}) \quad \text{.....(ii)}$$

Where, N is the number of MTs, N_{max} is the maximum number of MTs landed for each dilution, R is the landing rate for each dilution, t is time, and t_{ini} = 120 s, the time elapsed before imaging started after the addition of MTs to the flow cell. N_{max} and R, are the fitting parameters.

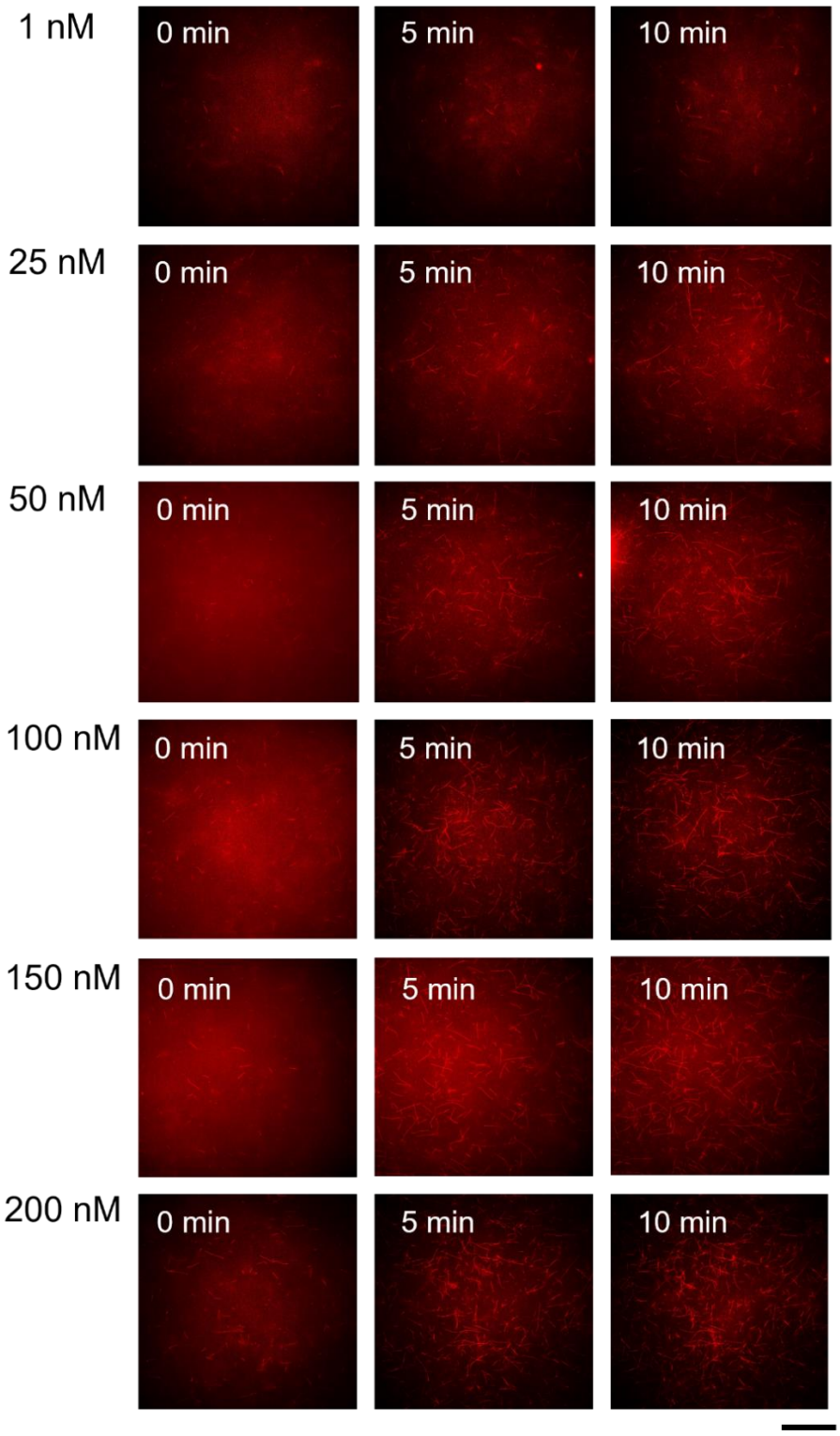

Figure 3.26 Fluorescence microscopy time-lapse images of the landing of MTs on different concentrations of kinesin, Scale bar: 50 μm.

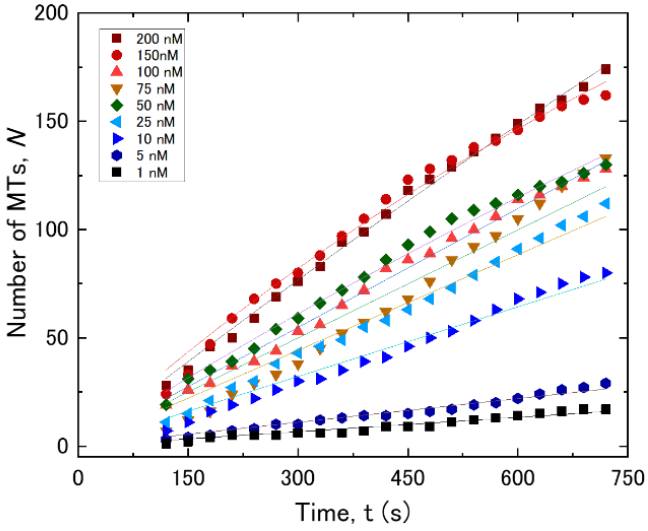

Figure 3.27 MT landing events in a field of view as a function of time for the different dilution factors of kinesin. The regression value of all the curves was over 0.99.

The landing rate *R* was obtained for each of the concentration of kinesin solution from the fitted curve using equation (ii) from figure 3.27. The obtained landing rate R was plotted with the dilution factor ξ in figure 3.28. The plot was fitted with the following landing rate equation (iii) to obtain the density of kinesin.

Landing rate equation (iii),

$$\boldsymbol{R = Z(1 - e^{(-Lw\rho^{o}\xi)})}\text{.....(iii)}$$

Here, *Z* is a constant, ξ is the dilution factor, ρ^{o} represents the kinesin surface density of stock solution (400 nM kinesin), *L*w* is the area of MTs (*L* is the average length and w is the width of MTs, 20 nm)

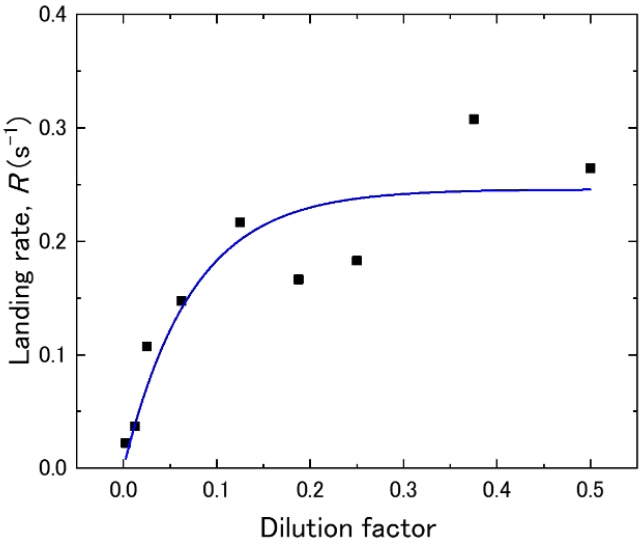

Figure 3.28 Landing rate of MTs, *R* as a function of dilution factor, ξ of stock kinesin (400 nM). The regression value was 0.85.

From the fitted curves of several trials (n = 8) the average kinesin surface density was obtained, ρ^{o} ~ 61.05 ± 22.04 μm^{-2}.

Several trials were performed to measure the density of kinesin. And the average density of the kinesin was obtained from several experiments,~61.05 ± 22.04 μm^{-2}.

3.2.14 Area of the swarm and corresponding kinesin-driven force

The images of the swarm were converted to an 8-bit image followed with the threshold value to estimate the area of the swarm rings using ImageJ software. From the area of the swarm ring (from threshold binary image) and the density of kinesins (from the landing rate experiment) determined in the previous section, the total number of involved kinesins was estimated for each swarm ring encountered to determine force.

The estimated force was plotted against the number of kinesins involved in the swarm rings and shown in figure 3.29. The force of the swarm tends to increase as the number of involved kinesins increases. The slope was 0.42 ± 0.03 and which is less than 1, indicating that all the kinesins did not contribute at the same time. The estimated force of the swarm might be described as sub-additive force while increasing the number of kinesins which is also found while motility of single MTs propelled by multiple kinesins or when the force is applied in the opposite direction.[18,21]

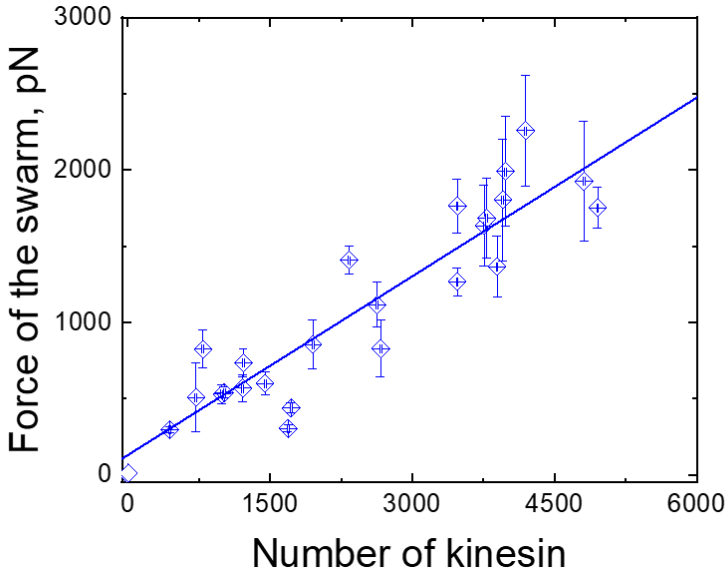

Figure 3.29 Force of the swarm ring with the number of kinesins involved. The number of kinesins was obtained from the landing rate experiment and the force of the swarm ring was obtained from the EMTw's experiment. The plot was fitted linearly with an intercept at zero and a slope value of 0.42 ± 0.03 (R-square, 0.89). The force of the swarm tends to increase with the increasing number of kinesins as well as the increasing size of the MT swarm.

Several theoretical studies on force and velocity were found in the literature for single or only few kinesins (less than 10). The force-velocity curve for multiple motors proposed by Klump and Lipowsky (2005), describes the average velocity of the kinesin and the rate at which it unbinds from the MTs were predicted.[22] According to the model, each kinesin unbind from the microtubules after a finite number of steps but can also rebind to it again, the actual number of pulling motors is not constant but varies with time between zero and N. The number of active kinesins decreases as the opposing force increases. The stall force of a motor is defined as at which the motor stops and the stall force of an object pulled by many motors would increase linearly with the number of motors (*i.e.* stall force for one motor is 6 pN, the stall force for 2 motors is 12 pN) but the velocity of the object would be negligible against higher forces. The detachment rate of the kinesins from the MTs is very low when the applied force is shared equally among all the kinesin motors. This model is comparable with the Shared-Force model proposed by Kunwar *et al.* (2008).[16]

In contrast to these models, Hendricks *et al.* (2009) proposed another mechanistic model where kinesin synchronization increases with increased cargo linker stiffness or opposing force.[17] The kinesin motors are loosely synchronized at normal conditions and under low load, however, the

synchronization increases to overcome obstacles or to deal with higher load. When the kinesin motors experience a higher load, the force against the opposing load increases linearly with the increasing number of kinesins. Another model called the shared-load model was proposed by Hill *et al.* (2004).[23] According to the model, the behavior of multiple motors under load is similar to the single motors when the load is shared equally to the motors.

Furuta *et al.* (2013) experimentally studied the forces generated by a controlled number of kinesin-1 motors in a stationary optical trapping assay and the average collective force was increased sub additively (slope value less than 1) with increasing the number of kinesins.[24] Their simulation results also showed similar results as the mean and median values of the forces generated by less than or equal to four kinesins increase with the number of kinesins, but the collective force generation was clearly sub additive. Another recent study by Mehmet et al. (2020) reported the collective force generation by different motor types and kinesin-1 shows the sub-additive force generation in multiple motor assay.[25] Saurabh *et al.* (2022) studied force generation by the kinesin in driving a MT and also overcoming obstacles. They reported that the kinesin exert less than one pN force in average whiling gliding a MT and occasionally the force might increase while encountering obstacles.[21]

Here I determined the force of thousands of kinesins driving the swarm of hundreds of MTs and the force increases with increasing the number of kinesins. The force of a swarm (F) has been rescaled divided by stall force (Fs) of a single motor (Figure 3.30). The stall force is a force required to stop the propelling of a single kinesin. A linear relationship is found with a slope value of 0.07 (in between 0-1), which represents the sub-additive increase of force.

The obtained slope value was compared with the previously reported force for single kinesin and few kinesins (one to seven kinesin) propelling a cargo or MT. The slope value for the force of the swarm is much lower than the value obtained for at most seven kinesins driving a single MTs.[25] This lower value of the slope represents the lower active state of the kinesins involved at a certain time i. e. the active kinesin is much lower than the total number of kinesins involved in the gliding of the MTs in a swarm.[21] The slope value of the force for few kinesins (one to seven) is lower compared to the single kinesin. In the single state kinesins are most efficient, however total highest force is obtained when higher number of kinesins are generating force together for the MT swarm transportation. The probable reason behind the lower efficiency of the swarm, the individual

kinesins might exert forces occasionally and each kinesin needs to produce much smaller forces on average for transporting the cargo with a higher force.[21]

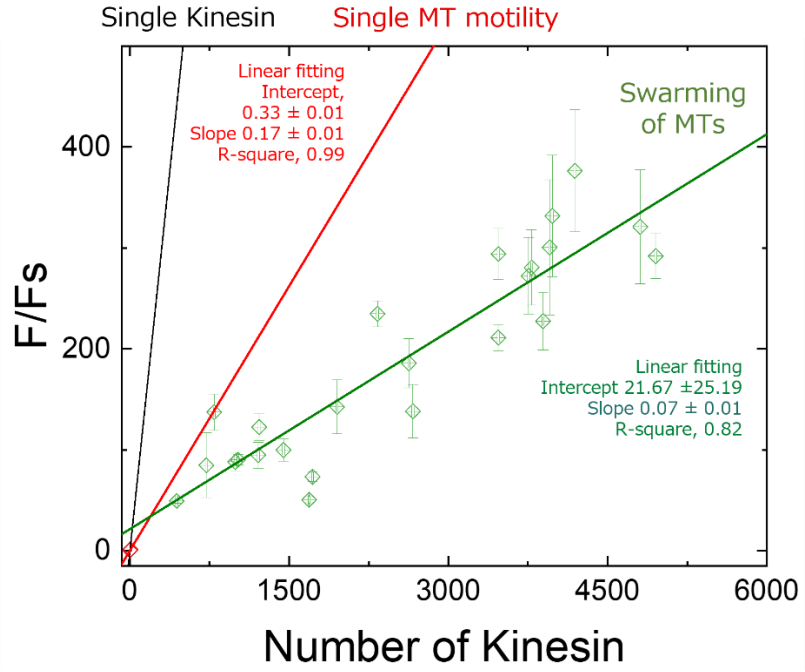

Figure 3.30 The total force of the swarm (higher number of kinesin), cargo transportation by few kinesins (one to seven) and single individual kinesin have been rescaled by the stall force (Fs) of a single kinesin. The linear relationship between the rescaled average forces and the number of motors, i.e., $F/Fs = \eta N$, a pre-factor η having a value of 0.07 ± 0.01 (R-square, 0.89). The fitted curve clearly indicates the sub-additive force generation by the swarm ring of MTs (green line) and force generated by few kinesins (one to seven) (red line).

In the swarming experiment, a higher density of kinesin is required compared to the gliding of single MTs. The effect of the concentration of the kinesin is discussed in section 3.2.5, which implies that a higher kinesin concentration (~400 nM) is required to get a better performance in terms of efficiency, velocity and the number of swarm rings. It might be claimed that in the swarm experiments the kinesins exert their force occasionally to collectively propel the swarm ring.

3.3. Conclusion

In conclusion, I systematically demonstrated the DNA based swarm ring of MTs propelled by kinesin. I investigated the time dependency of the swarm ring regarding the concentration of DNA and kinesin, and their impact on the swarm formation. The beads were successfully loaded and carried by the swarm ring and controlled magnetic force was applied to the bead-carrying swarm ring with changing the direction of motion. The results show that the velocity of the swarm ring increases and decreases in presence of emf. The velocity oscillated by the applied external force to the kinesin motors in positive and negative direction due to the circular motion of the swarm ring. The force of the swarm estimated from the force calibration curve, and it indicates a sub-additive increasing tendency with increasing kinesin numbers. This force estimation revealed the basic properties of MT swarm driving by thousands of kinesins. This work offers a technical advantage for systematic study of the velocity and force of the swarm using electromagnetic tweezer system. This study also helps to understand the cooperative cargo transportation by the MT swarm as it has the capability to supply very high force. It is expected that the results will contribute to understanding the force production of the swarm as well as work done by the swarm, and it expected to rise the new ideas for designing future biomolecular devices to perform nanotechnological tasks.

3.4. Experimental

3.4.1. Purification of tubulin and kinesin

Tubulin was purified from porcine brain using a high-concentration PIPES buffer (1 M PIPES, 20 mM EGTA, and 10 mM $MgCl_2$) and stored in BRB80 buffer (80 mM PIPES, 1 mM EGTA, 2 mM $MgCl_2$, pH adjusted to 6.8 using KOH).[26,27] Azide labeled tubulin was prepared using N_3-PEG_4-NHS following the established protocol of labeling tubulin with fluorescent dye.[19,28] The tubulin concentration was determined by measuring the absorbance at 280 nm using a UV spectrophotometer (Nanodrop 2000c). Recombinant kinesin-1 consisting of the first 573 amino acid residues of human kinesin-1 was prepared as described in the literature.[29]

3.4.2 Complementary DNA sequences for the modification of MTs

Two pairs of complementary DNA sequences were used in this work. For the demonstration of the swarm ring of MTs, the complementary DNAs, TTGTTGTTGTTGTTGTTGTTG (DNA1) and CAACAACAACAACAACAACAACAA (DNA2) were used (SI table 1). The DNA to tubulin labeling ratios were 93% and 102% for DNA1 and DNA2 modified MTs, respectively (SI table 1). The DNAs were purchased from Hokkaido System Science Co. Ltd. The DNAs were modified at the 5′ end with dibenzo cyclooctyne (DBCO).. The molar extinction coefficient of the DNAs was measured by developing a calibration curve of the absorbance with different concentrations of individual DNAs.

3.4.3 Measurement of the melting temperature (*T*m) of the DNA duplex

The DNA duplex (2 μM) was dissolved in 10 mM phosphate buffer (pH 7.0) with 100 mM NaCl. A capillary quarts tube was used as sample cell and melting temperature was determined using a JASCO model V-730 UV-Vis spectrophotometer equipped with programmable temperature controllers. The absorbance at 260 nm was measured at the temperature range from 20 – 90 ^{o}C and the heating rate was 0.5°C/min. T_m was determined from the maximum in the first derivative of the melting curve. Experimental parameters are listed in the Table 3.

Table 3 Experimental parameters for T_m measurement

Concentration of DNA	5 μM
Photometric mode	Absorbance
UV/Vis bandwidth	1.0 nm
Wavelength	260 nm
Temperature slope	1 °C/min
Interval	0.5 °C
Temperature range	20 – 90 °C
Buffer	10 mM phosphate buffer pH 7.0

3.4.4 Preparation of MTs

Dye-labeled tubulin (70 μM) and azide-labeled tubulin (70 μM) were mixed in the molar ration, 1:4 and polymerization buffer (80 mM PIPES, 1 mM EGTA, 1 mM $MgCl_2$, 1 mM guanosine triphosphate (GTP), pH~6.8) was added. Dimethyl sulfoxide (DMSO) was added to adjust a final concentration of 5% to the solution of tubulin and then the solution was incubated at 37 °C for 30 min. 1 μL of 4×BRB80 buffer and 0.5 μL of 1 mM taxol (in DMSO) were added to the MT solution just after polymerization to stabilize the MTs. A copper free click reaction of an azide-alkyne cycloaddition reaction was initiated by adding 3.5 μL DBCO conjugated DNA (250 μM) to the 10 μL azide-MTs (56 μM) and incubating the solution at 37 °C for 6 hours.[30] 100 μL of cushion buffer (BRB80 buffer supplemented with 60% glycerol) was added to separate the tubulin dimers or free DNAs from the DNA modified MTs by centrifugation at 54000 rpm for 1 hour at 37 °C. After discarding the supernatant, the MTs pellet was washed once with 100 μL BRB80P (BRB80 supplemented with 1 mM taxol) and dissolved in 15 μL BRB80P.

3.4.5 Measurement of the labeling ratio of DNA to tubulin

The DNA (DNA1 and DNA2) conjugated MTs in BRB80 were depolymerized to DNA conjugated tubulins by keeping the MTs solution in a tube on ice overnight. The absorption spectrum of the

DNA conjugated tubulin dimers was measured using a spectrophotometer (NanoDrop™ 2000c, Thermo Fisher Scientific Inc.) and deconvoluted using the normal distribution function with Microsoft Excel (Windows Edition, Microsoft Corporation) with peaks at 260 nm and 280 nm. The concentrations of DNA and tubulin dimers were calculated from the Beer-Lambert law using the molar extinction coefficient of tubulin dimers and DNAs from which the labeling ratio was determined and listed in the table 1.[12]

3.4.6 Azide and DNA modification of beads

10 µL beads (dispersed in water) were taken and centrifuged for 1 min to separate the beads from water. 32 µl, 20 mM N_3-PEG_4-NHS ester were added to the bead and mixed properly with micropipette. The solution was incubated on ice for 1 hour. 10 µL, 20 mM glycine added to the solution and kept on ice for 30 minutes. The solution then washed with 10 µl BRB 80 three times to remove free azide by centrifuging in a 0.22 µm porous filter tube. To disperse the beads 10 µl BRB 80 solution was added and then 3.5 µl of 250 µM DNA1 was added to the beads solution and incubated on ice for 12/24 hrs. Then the beads were again washed with BRB 80 solution and centrifuged. Finally, the DNA labelled beads were dispersed in 10 µl of BRB 80 solutions and stored at 4 ^{o} C for 1-2 weeks. For the loading and carrying of the beads to the swarm, the bead solution was further diluted (~ 50 times) using ATP buffer (BRB80 buffer supplemented with dithiothreitol (1 mM), casein (0.5 mg/ml), d-glucose (4.5 mg/ml), glucose oxidase (50 U/ml), catalase (50 U/ml), taxol (10 µM), ATP (5 mM), and methylcellulose (0.2%; w/v)).

3.4.7 Flow cells preparation and motility assays for the swarming ring of MTs

A flow cell was prepared using two cover glasses and a parafilm spacer. A parafilm was taken and cut in a 29×29 mm^2 with a channel 22×1.5 mm^2 in it. A flow cell with dimensions of 18 × 1.5 × 0.45 mm^3 (L × W × H) was assembled from two cover glasses (MATSUNAMI Inc.) using the parafilm as a spacer.

To demonstrate the swarming, first the flow cell was filled with 5 µL casein buffer (BRB80 buffer supplemented with casein (0.5 mg/ml)). After incubating for 3 min, 5 µL, 800 nM kinesin solution was introduced into the flow cell and incubated for 5 min. The flow cell was washed with 10 µL of wash buffer (BRB80 buffer supplemented with dithiothreitol (1 mM), casein (0.5 mg/ml), d-glucose (4.5 mg/ml), glucose oxidase (50 U/ml), catalase (50 U/ml), and taxol (10 µM)) and 5 µL of one of the DNA modified MTs solution (diluted in BRB80P) was introduced and incubated for

2 min. The flow cell then washed with 10 μL of wash buffer and 5 μL of the complementary DNA modified MTs were introduced. After incubating for 2 min, the flow cell was washed with 10 μL of wash buffer and the motility of the MTs was initiated by applying 5 μL of ATP (wash buffer supplemented with ATP (5 mM), and methylcellulose (0.2%; w/v).[11] The time of ATP addition was set as 0 min. Soon after the addition of ATP buffer, the flow cell was placed in an inert chamber system and observed under a fluorescence microscope.[31] To form the complete swarm ring, a waiting time of 30 min was found to be necessary.

3.4.8 Measurement of the association ratio of MTs

The association ratio at a given time *t* was determined by counting the number of single MTs manually and dividing the number at time *t* by the number present initially (t = 0). The time-dependent association ratio, $A(t)$, of red and green MTs was determined as follows:

$$A(t) = \frac{N(0)-N(t)}{N(0)} \times 100\% \quad \ldots\ldots\ldots\ldots\ldots\ldots \quad (3)$$

Here, $N(0)$ is the initial number of the single MTs, and $N(t)$ is the number of the single MTs after time *t*. The mean association ratio was obtained from the average of four regions of interest (2500 μm^{-2}).

3.4.9 Loading and carrying of beads by the swarm ring

After the formation of swarm ring of MTs, 5 μl of beads (dispersed in ATP buffer, 50 times dilution) was introduced into the flow cell. Immediately after adding the beads the flow cell was kept upside down to adsorb the beads on the upper surface. After 5 minutes of incubation, the flow cell was made upright and washed two times by adding 5 μl of ATP buffer into the flow cell to wash the excess beads. Then, the flow cell was immediately taken to the microscopic stage and observation at the upper surface of the flow cell was performed using fluorescence microscope. A single bead loaded swarm ring was with the width in the range of 0.5 – 1.2 μm and without any defects was targeted and observed by fluorescence microscopy for further experiment and analysis.

3.4.10 Application of the emf to the swarm ring by EMTw

The controlled emf was applied to bead attached swarm ring in the flow cell controlling the distance from tip to the swarm ring, the applied current and voltage of the tweezer. The targeted swarm ring in the flow cell was positioned on the observation field of the fluorescence microscope. The EMTw's tip was set on the right side of the observation field keeping the distance between tip

of tweezers to the ring around 200-300 μm. Within this distance the applied force does not fluctuate drastically with a small (~5 um) changes in distance. At first lower emf corresponding to the lower voltages were applied to the swarm ring and observed until a certain period of time.

3.4.11 Analysis of the trajectory, velocity and force determination of circular swarm

To visualize the effect of the application of the EMTw, the trajectory of the bead loaded swarm without and with applying EMF was determined using ImageJ software. The velocity of the bead loaded swarm was determined using the ImageJ software from the displacement with each time interval.

3.4.12 Landing rate experiment

To perform the landing rate experiment, ATTO565 labeled GTP MTs were polymerized. The MTs were diluted in microtubule buffer (BRB80 buffer supplemented with 1 mM AMP-PNP, 10 μM taxol, 1mM $MgCl_2$, 0.5 mg/mL casein, 4.5 mg/mL glucose, 50 U/mL glucose oxidase, and 50 U/mL catalase). The kinesin was diluted in kinesin buffer (BRB80 buffer supplemented with 1 mM AMP-PNP, 10 μM taxol, 1mM $MgCl_2$, and 0.5 mg/mL casein).

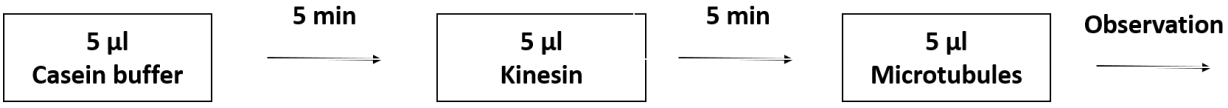

Figure 3.29 Flow cell preparation for the landing rate experiment.

A flow cell was prepared using two glasses and a parafilm as a spacer and the preparation steps are shown schematically in figure 3.29. Casein buffer was employed on the flow cell and waited up to 5 minutes. After that kinesin solution was added to the flow cell and waited up to 5 minutes. In the last step, MT solution was added to the flow cell and the time-dependent landing of MTs on the kinesin surface was observed under an epifluorescence microscope.

3.4.13 Fluorescence Microscopy Image Capture

The samples were visualized by an epifluorescence microscope (Eclipse Ti, Nikon) using an oil-coupled Nikon Plan fluor 60xN.A.1.4 objective (Nikon). UV cut-off filter blocks (TRITC:

EX540/25, DM565, BA605/55; GFP-B: EX460-500, DM50S, BA510-560; Nikon) were used in the optical path of the microscope. Images were captured using a cooled-CMOS camera (NEO CMOS, Andor) connected to a PC.

3.4.14 Image Analysis

The fluorescence microscopy images were analyzed by NIS-Elements software (Nikon) and ImageJ software.[32] Velocity of the gliding MTs and swarms was measured using the Image plugin MTrack. Statistical analysis and graphs were performed with the software OriginPro Version 2019, OriginLab, USA.[33]

3.5 References

1. Whitesides, G. M. & Grzybowski, B. Self-assembly at all scales. *Science.* **295,** 2418–2421 (2002).
2. Beshers, S. N. & Fewell, J. H. Models of division of labor in social insects. *Annu. Rev. Entomol.* **46,** 413–40 (2001).
3. Niven, J. E. How honeybees break a decision-making deadlock. *Science.* **335,** 43–44 (2012).
4. Turgut, A. E., Çelikkanat, H., Gökçe, F. & Şahin, E. Self-organized flocking in mobile robot swarms. *Swarm Intell.* **2,** 97–120 (2008).
5. Wei, H., Chen, Y., Tan, J. & Wang, T. Sambot : A Self-Assembly Modular Robot System. *IEEE/ASME Trans. Mechatronics.* **16,** 745–757 (2011).
6. Palacci, J., Sacanna, S., Steinberg, A. P., Pine, D. J. & Chaikin, P. M. Colloidal Surfers. **339,** 936–941 (2013).
7. Xu, T., Soto, F., Gao, W., Dong, R., Garcia-gradilla, V., Magan, E., Zhang, X. & Wang, J. Reversible Swarming and Separation of Self-Propelled Chemically Powered Nanomotors under Acoustic Fields. **1,** 1–4 (2015).
8. Wang, W., Duan, W., Ahmed, S., Sen, A. & Mallouk, T. E. From One to Many: Dynamic Assembly and Collective Behavior of Self-Propelled Colloidal Motors. (2015). doi:10.1021/acs.accounts.5b00025
9. Keya, J. J., Kabir, A. M. R., Inoue, D., Sada, K., Hess, H., Kuzuya, A. & Kakugo, A. Control of swarming of molecular robots. *Sci. Rep.* **8,** 1–10 (2018).
10. Ishii, S., Akter, M., Murayama, K., Kabir, A. M. R., Asanuma, H., Sada, K. & Kakugo, A. Kinesin motors driven microtubule swarming triggered by UV light. *Polym. J.* (2022).
11. Keya, J. J., Suzuki, R., Kabir, A. M. R., Inoue, D., Asanuma, H., Sada, K., Hess, H., Kuzuya, A. & Kakugo, A. DNA-assisted swarm control in a biomolecular motor system. *Nat. Commun.* **9,** 4–11 (2018).
12. Akter, M., Keya, J. J., Kayano, K., Kabir, A. M. R., Inoue, D., Hess, H., Sada, K., Kuzuya, A., Asanuma, H. & Kakugo, A. Cooperative cargo transportation by a swarm of molecular machines. *Sci. Robot.* **7,** eabm0677 (2022).
13. Ito, M., Kabir, A. M. R., Inoue, D., Torisawa, T., Toyoshima, Y., Sada, K. & Kakugo, A. Formation of ring-shaped microtubule assemblies through active self-organization on

dynein. *Polym. J.* **46,** 220–225 (2014).

14. Hess, H., Clemmens, J., Brunner, C., Doot, R., Luna, S., Ernst, K. H. & Vogel, V. Molecular self-assembly of 'nanowires' and 'nanospools' using active transport. *Nano Lett.* **5,** 629–633 (2005).
15. Bustamante, C. J. & Wang, M. D. Optical tweezers in single-molecule biophysics. *Nat. Rev. Methods Prim.* doi:10.1038/s43586-021-00021-6
16. Kunwar, A., Vershinin, M., Xu, J. & Gross, S. P. Article Stepping , Strain Gating , and an Unexpected Force-Velocity Curve for Multiple-Motor-Based Transport. 1173–1183 (2008). doi:10.1016/j.cub.2008.07.027
17. Hendricks, A. G. & Epureanu, B. I. Collective dynamics of kinesin. 1–12 (2009). doi:10.1103/PhysRevE.79.031929
18. Fallesen, T. L., Macosko, J. C. & Holzwarth, G. Force – velocity relationship for multiple kinesin motors pulling a magnetic bead. *Eur. Biophys. J.* 1071–1079 (2011). doi:10.1007/s00249-011-0724-1
19. Akter, M., Keya, J. J., Kabir, A. M. R., Rashid, M. R., Ishii, S. & Kakugo, A. Functionalization of Tubulin: Approaches to Modify Tubulin with Biotin and DNA. *Methods Mol. Biol.* **2430,** 47—59 (2022).
20. VanDelinder, V., Imam, Z. I. & Bachand, G. Kinesin motor density and dynamics in gliding microtubule motility. *Sci. Rep.* **9,** 1–9 (2019).
21. Shukla, S., Troitskaia, A., Swarna, N., Maity, B. K., Tjioe, M., Bookwalter, C. S., Trybus, K. M., Chemla, Y. R. & Selvin, P. R. High-throughput force measurement of individual kinesin-1 motors during multi-motor transport. 12463–12475 (2022). doi:10.1039/d2nr01701f
22. Klumpp, S. & Lipowsky, R. Cooprative cargo transport by several molecular motors. *Proc. Natl. Acad. Sci. U. S. A.* **102,** (2005).
23. Plaza, D. B. H. Æ. M. J. & Holzwarth, Æ. K. B. Æ. G. Fast vesicle transport in PC12 neurites : velocities and forces. 623–632 (2004). doi:10.1007/s00249-004-0403-6
24. Furuta, A., Toyoshima, Y. Y., Amino, M., Oiwa, K. & Kojima, H. Measuring collective transport by de fi ned numbers of processive and nonprocessive kinesin motors. **110,** (2013).
25. Lipowsky, R. Collective Force Generation by Molecular Motors Is Determined by Strain-

Induced Unbinding. (2020). doi:10.1021/acs.nanolett.9b04445

26. Ishii, S., Akter, M., Keya, J. J., Rashid, M. R., Afroze, F., Nasrin, S. R. & Kakugo, A. Purification of Tubulin from Porcine Brain and its Fluorescence Dye Modification. *Methods Mol. Biol.* **2430,** 3–16 (2022).
27. Castoldi, M. & Popov, A. V. Purification of brain tubulin through two cycles of polymerization- depolymerization in a high-molarity buffer. *Protein Expr. Purif.* **32,** 83–88 (2003).
28. Peloquin, J., Komarova, Y. & Borisy, G. Conjugation of fluorophores to tubulin. *Nat. Methods* **2,** 299–303 (2005).
29. Case, R. B., Pierce, D. W., Hom-Booher, N., Hart, C. L. & Vale, R. D. The directional preference of kinesin motors is specified by an element outside of the motor catalytic domain. *Cell* **90,** 959–966 (1997).
30. Früh, S. M., Steuerwald, D., Simon, U. & Vogel, V. Covalent cargo loading to molecular shuttles via copper-free 'click chemistry'. *Biomacromolecules* **13,** 3908–3911 (2012).
31. Kabir, A. M. R., Inoue, D., Kakugo, A., Kamei, A. & Gong, J. P. Prolongation of the Active Lifetime of a Biomolecular Motor for in Vitro Motility Assay by Using an Inert Atmosphere. *Langmuir* **27,** 13659–13668 (2011).
32. Sheffield, J. B. An introduction to ImageJ: A useful tool for biological image processing and analysis. *Microsc. Microanal.* **14,** 898–899 (2008).
33. Edwards, P. M. Origin 7.0: Scientific graphing and data analysis software. *J. Chem. Inf. Comput. Sci.* **42,** 1270 (2002).

Chapter 4

3D structure of ring-shaped microtubule swarms revealed by high-speed atomic force microscopy

Abstract

The microtubule (MT)-kinesin-based swarms are promising due to their small size, flexibility, and controllability. Such swarms are recently realized as DNA-regulated MT-kinesin systems and are being used for nanotechnological applications, such as in cooperative cargo transportation or in the development of future nanomachines. While the functionality of the MT-kinesin swarm has been proven, the structural details are still unknown. In order to fine-tune the swarms for specific applications, it is necessary to understand the detailed arrangement of the MTs in the swarms. However, conventional fluorescence microscopy – the typical observation technique – is incapable of providing sufficient resolution to analyze MT swarms. In this chapter, high-speed atomic force microscopy was used to observe the detailed structure of the MT swarm rings and estimate the total number of MTs contained within and the fraction of MTs involved in force generation. I performed the photo-dissociation of the MT swarm rings to the single MTs to count the total number of MTs by fluorescence microscope. From these experiments, it is proposed that the microtubules are arranged in multiple layers depending on the sizes of the swarm rings. These findings will specifically impact the understanding of the force generation capability of swarms, as not all MTs contribute equally.

4.1 Introduction

In nature, swarming demonstrates organized structures by multiple moving entities to offer several advantages, such as parallelism, robustness, and flexibility which cannot be achieved by individuals.[1–3] Recently, much effort has been devoted to exploiting the advantages of swarming in an artificial environment.[4,5] Among the various artificial swarm systems, the biomolecular motor-based machine, microtubule (MT)-kinesin has attracted much attention owing to its nanoscale size that confers high scalability of the swarms. Fusion of DNA technology with MT-kinesin swarm robots affords programmability in the swarming behavior while tuning their physical properties allows controlling the morphology of the swarms in the form of linear bundles or rings.[6,7] The bundle-shaped swarm of MTs has been proven useful in transporting cargo in a highly efficient manner, compared to discrete MTs.[8] The ring-shaped swarm of MTs also holds great prospects for future applications by dint of its ability to produce rotational motion and to store bending energy.[9] The circular motion of the ring shaped swarm has the potential as a rotary actuator in energy conversion or performing continuous work without changing its center.[10,11] Although, much attention has been paid to achieve programmability in the swarming of MTs, the detailed organization of MTs in the (ring-shaped) swarms is largely unknown. However, it is critical to tailor their structures to fit the practical applications of the MT swarms.[12–14] So far, only a few efforts were made to investigate the structure of the ring-shaped MT swarms using diffraction limited fluorescence microscopy or transmission electron microscopy (TEM).[9,15,16] The limited resolution of the optical techniques failed to provide adequate information on the spatial arrangement of MTs in swarms. TEM, while providing a much higher resolution than optical methods, cannot be used to observe the swarms in their native state: due to difficulty in the preparation of thin slices of the MT swarms. A different approach offers high-speed atomic force microscopy (HS-AFM). HS-AFM is an improvement upon conventional AFM,[17] specifically developed to image fragile and dynamic biological systems.[18] HS-AFM has been proven to be a powerful tool to investigate MTs at the molecular level.[19–21] In this chapter, I utilized a combined HS-AFM and fluorescence microscopy in a single machine to investigate the packing and alignment of nanometer-scale MTs within the micrometer-scale swarm in an aqueous medium.[22–25] While the HS-AFM was primarily developed to study dynamic systems, I mainly utilize it here to rapidly collect images with nanometer resolution. Supported by fluorescence microscopy with an observational area of tens of micrometers, it was possible to swiftly locate and image MT swarm

rings. I found that in a swarm ring, multiple MTs not only self-organize laterally but also form multiple layers with an increasing number of MTs. These results provide new insight into the structure of the ring-shaped MT swarms and the alignment of MTs in the swarms. Such information will be indispensable in assessing the force associated with MT swarms and allow for further regulation of the force by designing their structure, which will consequently further their applications in nanotechnology and bioengineering.[14]

4.2 Results and discussion

4.2.1 Preparation of MT swarm ring

Single MTs were polymerized from a mixture of fluorescently labelled tubulins (either with ATTO 550 or ATTO 488) and azide labeled tubulins (with a ratio of 1:4) in presence of GTP (see methods for details).[26] Two complimentary DNA strands, DNA1 and DNA2 were chosen to modify the MTs through copper free azide-alkyne cycloaddition reaction (Figure 4.1). The dibenzo cyclooctyne (DBCO) labelled DNA1 and DNA2 at the 5'-end can react with azide functionalized MT.

After the conjugation of DNA to MTs, the labelling ratio of DNA to tubulin was determined using UV-Vis spectrophotometer. The calculated labelling ratio of DNA1 and DNA2 to tubulin dimer was ~90 % and ~100 % respectively (table 1) when the infeed concentration of DNA1 and DNA2 was 250 μM.

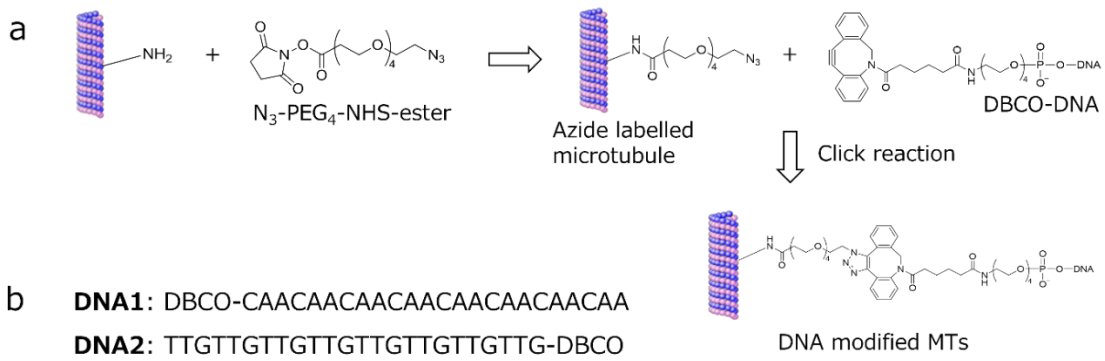

Figure 4.1 (a) Schematic diagram of the preparation of swarm units through conjugation of MT with DNA by click reaction, (b) complementary DNA sequences.

To initiate the swarming, DNA-modified MTs were applied to the kinesin coated glass surface in presence of ATP and monitored using a fluorescence microscope. Figure 4.2 shows the schematic representation of the swarm ring of MTs on the kinesin-coated glass surface. The MTs started gliding on the kinesin surface and the closer MTs started to interact with each other by complementary DNA sequences. The interaction resulted in small groups or bundles of MTs and flexible GTP MTs rotated in a curved path to make a ring swarm.[6,7] The rings grew larger with time as new MTs unites to the existing swarms and stable rings were obtained from the single MTs.

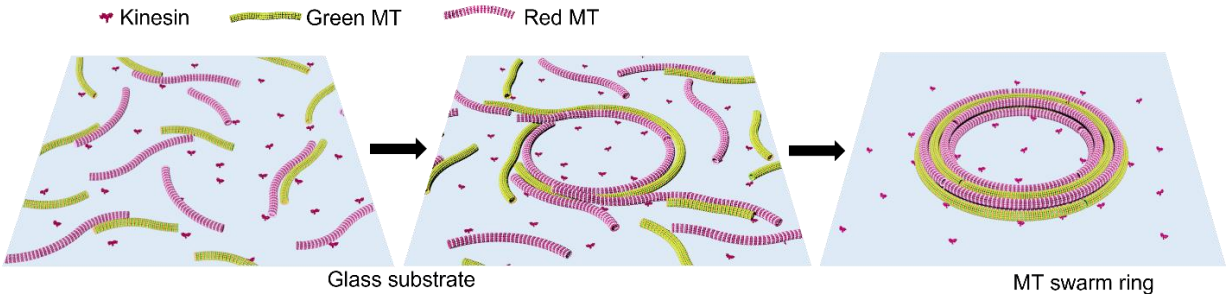

Figure 4.2 Schematic representation of the formation of MT swarm rings using complementary DNA conjugated MTs. The DNA conjugation and the flexibility of the MTs lead to the spooling of the MT swarm ring.

4.2.2 Observation of the single MTs using HS-AFM

In order to study MT swarms in more detail than with fluorescence microscopy, I employed HS-AFM. To fix the single MTs for scanning 1 µL of the stock DNA modified MTs was deposited on a freshly cleaved mica surface and incubated for 10 minutes. After the deposition, the free MTs were washed with 40 µL BRB80 buffer and observed by HS-AFM (Figure 4.3).

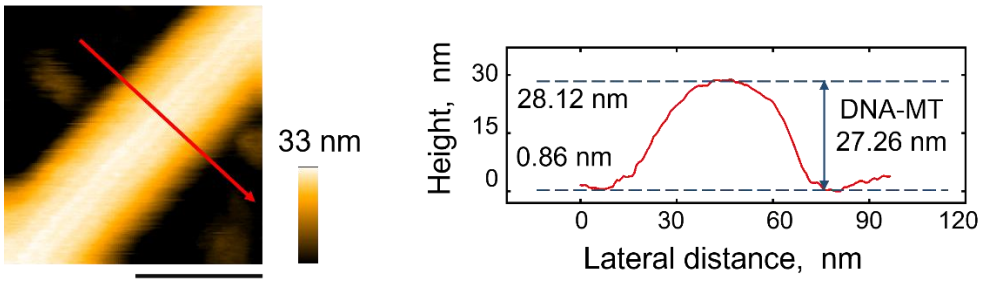

Figure 4.3 HS-AFM image (left) of a DNA-modified single MT, and the MT's height profile (right) through the red line, scale bar: 50 nm.

Since DNA modification was performed after MT polymerization, the DNAs should predominantly modify the outer surface of MTs.[27,28] The mean height of the DNA-modified MTs was 26.84 ± 0.97 nm (mean ± SD, n = 20) which is similar to the height of an unmodified single MT reported previously.[19] Furthermore, the surface is also indistinguishable from an unmodified MT. Short single stranded DNAs (16 nm from 24 bases of single strand DNA) used for this modification may not be observable on MT surfaces because single stranded DNA is not thick and long enough, and the single stranded DNA is very flexible and offers no resistance to even low scanning forces.[29,30] A similar effect was observed when trying to acquire high-resolution images

of kinesin bound to MTs, where kinesin was pushed away by the scanning HS-AFM tip when the scanning forces became too high.[25]

4.2.3 Observation of MT swarm rings using HS-AFM

To visualize the MT swarm rings, I employed an HS-AFM combined with a TIRFM microscope. The HS-AFM observation was performed after locating the sparsely distributed rings using the TIRF microscope. To observe the swarm rings in liquid environment, I used glutaraldehyde as a stabilizing agent to fix the structure.[31,32] HS-AFM images of an MT swarm ring with a width between 100 and 200 nm are given in Figure 4.4a.

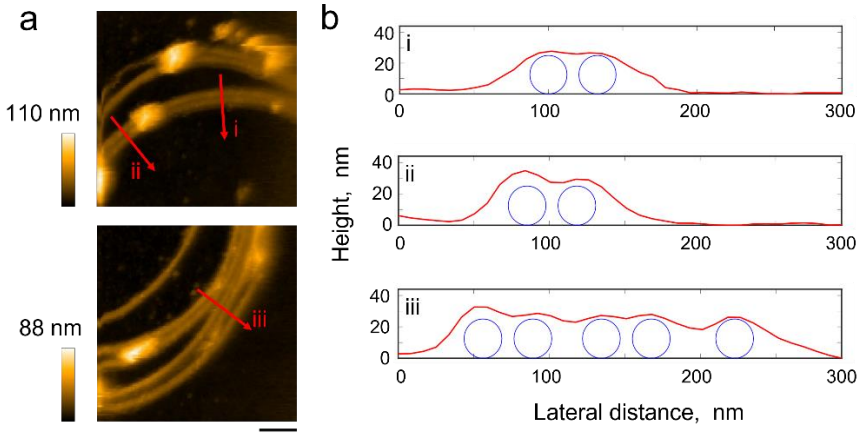

Figure 4.4 HS-AFM observation of MT swarm rings of width between 100 and 200 nm (a) HS-AFM images of the MT swarm rings of the width of 100 nm – 200 nm, scale bar: 100 nm. (b) The height profiles of the swarm rings at the positions (i), (ii), (ii) in (a). Blue circles represent individual MTs in the swarm. The number of MTs was estimated by a custom-made GNU Octave program considering the 25 nm diameter of MTs and the 8 nm distance between the MTs.

The height profiles of the swarm at three different positions (i, ii, iii) were fitted using a custom-made GNU Octave program to estimate the number of MTs and distance between the MTs in a swarm ring (Figure 4.4b).[33] In the program, the diameter of MT and the lateral distance between two adjacent MTs was set to 25 nm and 8 nm, respectively. The 8 nm lateral distance between the DNA conjugated MTs was fixed considering the 24 base pair DNA.[29,30,34] As seen in Figure 4.4a and 4.4b, line profiles with a countable number of microtubules are well fitted with these parameters and were used to estimate number of MTs contained in a swarm, even with a highly complex line profile, henceforth.

Then, I investigated MT swarm rings with different widths and three representative HS-AFM images are shown in Figure 4.5a top, middle, and bottom. The height of the MT swarm rings varied

throughout the cross-section with peaks and valleys and reached up to about 200 nm. In Figure 4.5b, the cross sectional height was filled up with circles using the above-mentioned GNU Octave script. From the HS-AFM images of the MT swarm rings and their height profiles it is clear that MTs are not arranged as a single layer but form a complex 3-dimensional structure, forming multiple layers which numbers vary even within a cross-section.

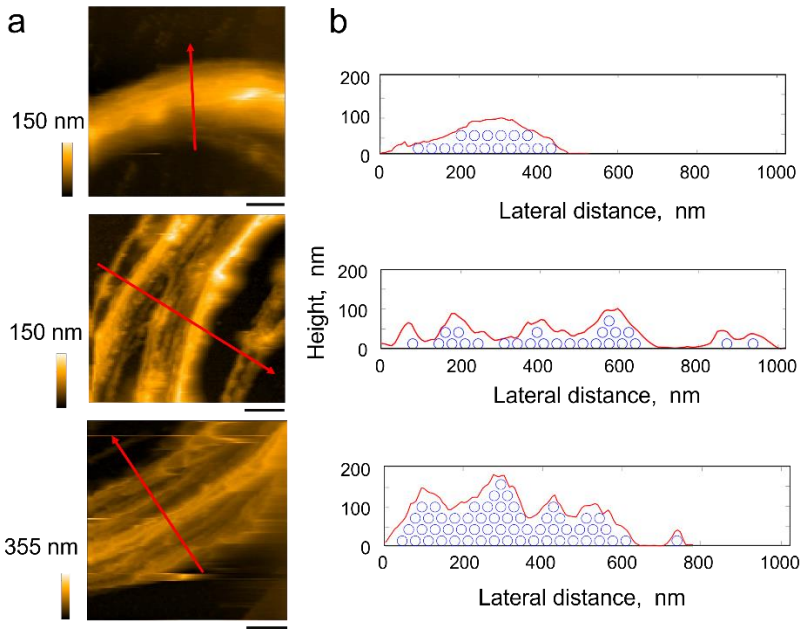

Figure 4.5 (a) HS-AFM images of MT swarm rings with different widths, scale bar: 200 nm. (b) The height profiles of the swarms along the red lines in (a). The number of MTs was estimated by a custom GNU Octave program considering the diameter of MTs 25 nm and the distance between the MTs 8 nm.

In figure 4.5a and 4.5b (middle) a case is presented where the microtubules are not arranged continuously along the radial direction, but a gap is clearly seen between 700 nm and 800 nm. This might be an indication that MT bundles form before a ring is created and join the ring independently instead of forming a ring in a MT-by-MT fashion.

4.2.4 Numbers and layers of MTs in the swarm rings of different widths

In Figure 4.6a, the number of MTs in swarm ring – as estimated above – is plotted against the width of the ring, measured from the HS-AFM images. It is clear that the total number of the MTs as well as the number of MTs in the bottom layer is increasing with increasing ring width. If the ring is narrow – less than 250 nm – the total number of MTs is very similar to the number of bottom layer MTs. This means that MT swarm rings tend to form multiple layers with increasing

width, as is also seen in Figure 4.6b. In Figure 4.6b, the average number of layers is calculated dividing the total number of MTs by the number of MTs at the bottom layer. Naturally, the number of layers varies within a single cross-section. Figure 4.6b clearly demonstrates that wider ring widths tend to form multiple layers.

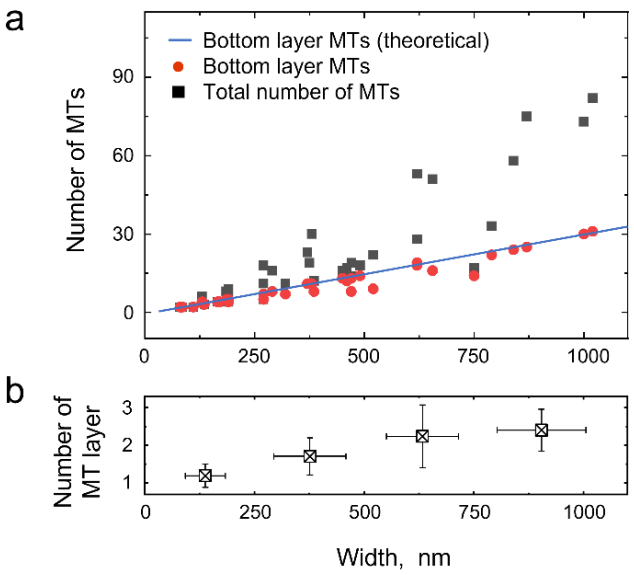

Figure 4.6 (a) The Total number of MTs and MTs at the bottom layer with the width of the MT swarm ring (n =38); The green line of the number of MTs at the bottom layer was calculated theoretically considering 25 nm MT width and 8 nm spacing between two MTs. The circle (red) and square (black) dots represent the experimental values of the number of MTs at the bottom layer and the total number of MTs. (b) The number of MT layers in a swarm ring has been shown with the width. The number of layers was counted from all MTs divided by the number of MTs at the bottom layer of the swarm ring. The number of height profiles used to determine the MT layers is n = 13, n =14, n = 5, and n = 5 for the swarm ring width in the range of 0-250, 251-500, 501-750, and 751-1020 nm respectively. Error bars: Standard error.

4.2.5 Estimation of the MT filaments in a swarm ring by photo-dissociation technique

To confirm the total number of MTs within a swarm ring, a different approach was used: photo dissociation of swarm rings to count the number of MTs. I used azobenzene incorporated complementary DNAs, *p*-DNA1 and *p*-DNA2 instead of DNA1 and DNA2 for DNA modification of microtubules and swarming of MTs was performed on a kinesin coated glass surface.[7,35] A digital mirror device (DMD) mosaic system was used to irradiate UV light (365 nm) at a particular swarm ring dissociate it into single MTs which is shown in Figure 4.7 (see methods for details). After complete dissociation of the swarm rings, single MTs were counted manually.

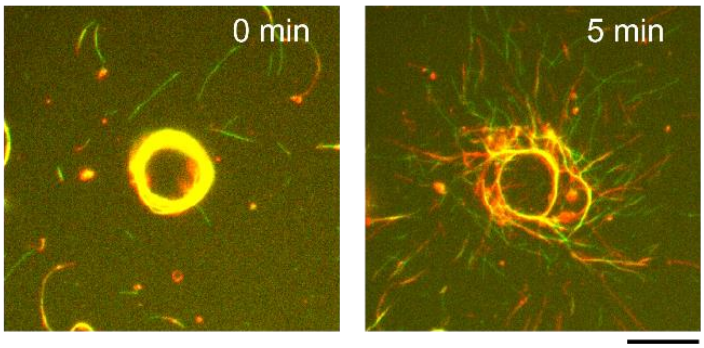

Figure 4.7 Photo-dissociation of the swarm ring to the single MTs. The swarming was performed using photoresponsive complementary DNAs and the swarm ring was dissociated using UV light using the DMD mosaic system. scale bar 10 μm.

4.2.6 Comparison of the number of MTs in a swarm counted from HS-AFM and photo-dissociation

The number of MTs in swarm rings determined from photo dissociation technique is compared with the number estimated from HS-AFM observation and plotted vs. ring width (figure 4.8). The ring width was determined by fluorescence microscopy and HS-AFM, respectively.

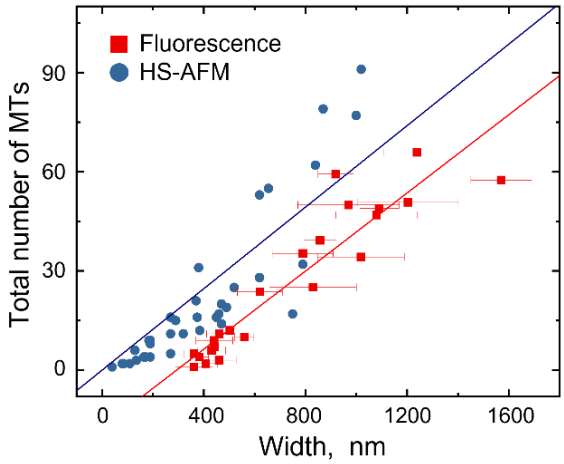

Figure 4.8 The number of MTs in relation to the swarm ring width determined by fluorescence microscopy and compared with data from HS-AFM. The width of single MTs (350 nm) obtained from fluorescence observation is much higher than the actual diameter of MTs (25 nm) due to the diffraction limit of the fluorescence microscope. The number of MTs in a swarm ring was obtained from the HS-AFM study, where the diameter of single MTs coincides with the actual diameter. The plots are fitted with the equation, $y = mx + c$, to guide the eye. The slope values were obtained 0.06 ± 0.003 and 0.06 ± 0.005 with the intercept at 0 and -17.31 ± 4.04 for HS-AFM and UV-dissociation respectively. Error bars: Standard deviation.

In both cases, the plots were fitted with a linear model and show the same trend of increasing number of MTs with an increasing width of the swarm ring. While the fits have similar slopes, as is expected, they yielded different intercept values corresponding to the width of a single MT. From fluorescence observations, the width of single microtubule is about tenfold higher compared with the width of single MT from HS-AFM. This fact is expected and stems from the resolution limit of fluorescence microscopy, which is typically a couple hundred nanometers.[36] Essentially, however, both HS-AFM based estimation of MT numbers within an MT swarm ring and discrete counting of MTs after dissociating the swarm when factoring in the resolution limitation of fluorescence microscopy.

4.3 Conclusions

Using a combination of HS-AFM and fluorescence microscopy, I have presented a detailed investigation about the structure of MT swarm rings on the level of single MTs. HS-AFM proved to be a powerful tool to understand the assembly and spatial arrangement of MT filaments. Compared to conventional fluorescence microscopy HS-AFM allows the visualization of individual MTs in their 3-dimensional arrangement. DNA modified MTs organize themselves in layers to form a swarm ring instead of forming a single-layered sheet. This has the obvious implication that not all of the MTs are in contact with the kinesin-covered substrate and only a part of the MTs contribute to the force generation of the swarm. In order to efficiently use MT swarms as a source for rotational energy, it is necessary to increase the number of load-carrying microtubules. The current findings on the MT swarm ring structure, can contribute to maximize their applications for the development of molecular machines and robots as a power source. As MT swarm rings convert chemical energy into rotational motion, it could be a fundamental power generator for nano or micromachines for future applications like localized surgery on the level of cells or below.[14,37]

4.4 Experimental

4.4.1 Purification of tubulin and kinesin

Tubulin was purified from porcine brain using a high-concentration PIPES buffer (1 M PIPES, 20 mM EGTA, and 10 mM $MgCl_2$) and stored in BRB80 buffer (80 mM PIPES, 1 mM EGTA, 2 mM $MgCl_2$, pH adjusted to 6.8 using KOH).[38,39] Azide labeled tubulin was prepared using N_3-PEG_4-NHS following the established protocol of labeling tubulin with fluorescent dye.[26,40] The tubulin concentration was determined by measuring the absorbance at 280 nm using a UV spectrophotometer (Nanodrop 2000c). Recombinant kinesin-1 consisting of the first 573 amino acid residues of human kinesin-1 was prepared as described in the literature.[41]

4.4.2 Complementary DNA sequences for the modification of MTs

Two pairs of complementary DNA sequences were used in this work. For the observation of the swarm ring of MTs by HS-AFM, the swarming was performed using complementary DNAs, TTGTTGTTGTTGTTGTTGTTG (DNA1) and CAACAACAACAACAACAACAA (DNA2) (table 1). The DNA to tubulin labeling ratios were 93% and 102% for DNA1 and DNA2 modified MTs, respectively (table 1). Other complementary photo responsive DNAs, TTTTTTTTTTTTTTGZTTGZTTG (*p*-DNA1; Z is azobenzene) and CAAZCAAZCAAZCAAZCAAZCAAZCAAZCAA (*p*-DNA2), were used to perform swarming and photodissociation of MTs (table 1). The DNA to tubulin labeling ratios were 41% and 33% for *p*-DNA1 and *p*-DNA2 modified MTs, respectively (table 1). The DNAs were purchased from Hokkaido System Science Co. Ltd. The DNAs were modified at the 5′ end with dibenzo cyclooctyne (DBCO). Quality control of the synthesized DNA was performed by polyacrylamide gel electrophoresis (PAGE). Characterization of the DNA strands was carried out by Liquid Chromatography-Electrospray Ionization-Mass spectroscopy. The molar extinction coefficient of the DNAs was measured by developing a calibration curve of the absorbance with different concentrations of individual DNAs.

4.4.3 Preparation of MTs

MTs were polymerized by adding dye-labeled tubulin and azide-labeled tubulin (molar ration, 1:4) to the polymerization buffer (80 mM PIPES, 1 mM EGTA, 1 mM $MgCl_2$, 1 mM guanosine triphosphate (GTP), pH~6.8) to a final concentration of 56 μM tubulin. Dimethyl sulfoxide

(DMSO) was added to a final concentration of 5% for the polymerization of flexible MTs and incubated at 37 °C for 30 min. 1 μL of 4×BRB80 buffer and 0.5 μL of 1 mM taxol (in DMSO) were added to the MT solution just after polymerization to stabilize the MTs. A copper free click reaction of an azide-alkyne cycloaddition reaction was initiated by adding 3.5 μL DBCO conjugated DNA (200 μM) to the 10 μL azide-MTs (56 μM) and incubating the solution at 37 °C for 6 hours.[42] 100 μL of cushion buffer (BRB80 buffer supplemented with 60% glycerol) was used to separate the tubulin dimers or free DNAs from the DNA modified MTs by centrifugation at 54000 rpm for 1 hour at 37 °C. After discarding the supernatant, the MTs pellet was washed once with 100 μL BRB80P (BRB80 supplemented with 1 mM taxol) and dissolved in 15 μL BRB80P.

4.4.4 Measurement of the labeling ratio of DNA to tubulin

The DNA (DNA1, DNA2, *p*DNA1and *p*DNA2) conjugated MTs were depolymerized to DNA conjugated tubulins by keeping the MTs on ice overnight. The absorption spectrum of the DNA conjugated tubulin dimers was measured using a spectrophotometer (NanoDrop™ 2000c, Thermo Fisher Scientific Inc.) and deconvoluted using the normal distribution function with Microsoft Excel (Windows Edition, Microsoft Corporation) with peaks at 260 nm and 280 nm. The concentrations of DNA and tubulin dimers were calculated from the Beer-Lambert law using the molar extinction coefficient of tubulin dimers and DNAs from which the labeling ratio was determined and listed in the table 1.[8]

4.4.5 Flow cells preparation and motility assays for the swarming ring of MTs

For epifluorescence observation a flow cell was prepared using two cover glasses and a parafilm spacer. A parafilm was taken and cut in a 29×29 mm^2 with a channel 22×1.5 mm^2 in it. A flow cell with dimensions of 18 × 1.5 × 0.45 mm^3 (L × W × H) was assembled from two cover glasses (MATSUNAMI Inc.) using the parafilm as a spacer. For the HS-AFM observation, an open flow cell was prepared by fixing a one-sided PTFE tape with a central circular opening (5 mm diameter) on a MATSUNAMI cover glass.

To demonstrate the swarming, first the flow cell was filled with 5 μL casein buffer (BRB80 buffer supplemented with casein (0.5 mg/ml)). After incubating for 3 min, 5 μL, 800 nM kinesin solution was introduced into the flow cell and incubated for 5 min. The flow cell was washed with 10 μL of wash buffer (BRB80 buffer supplemented with dithiothreitol (1 mM), casein (0.5 mg/ml), d-

glucose (4.5 mg/ml), glucose oxidase (50 U/ml), catalase (50 U/ml), and taxol (10 μM)) and 5 μL of one of the DNA modified MTs solution (diluted in BRB80P) was introduced and incubated for 2 min. The flow cell then washed with 10 μL of wash buffer and 5 μL of the complementary DNA modified MTs were introduced. After incubating for 2 min, the flow cell was washed with 10 μL of wash buffer and the motility of the MTs was initiated by applying 5 μL of ATP (wash buffer supplemented with ATP (5 mM), and methylcellulose (0.2%; w/v).[7] The time of ATP addition was set as 0 min. Soon after the addition of ATP buffer, the flow cell was placed in an inert chamber system.[43] To complete swarm ring formation, a waiting time of 30 min was found to be necessary.

4.4.6 HS-AFM imaging of DNA-modified single MTs on a mica surface

The HS-AFM measurements on mica were performed with a laboratory-built high-speed atomic force microscope of the sample-scanning type.[23] All images were recorded in tapping mode using Olympus BL-AC10DS-A2 cantilevers (Olympus, Tokyo, Japan). These cantilevers have nominal dimensions of 9 μm in length, 2 μm in width, and 130 nm in thickness and the nominal spring constant is 0.1 Nm^{-1}. The resonance frequency of the cantilevers was between 400 kHz and 500 kHz. All measurements were performed in BRB80 buffer, where the cantilevers' resonance frequency was typically between 400 kHz and 500 kHz and the free amplitude was set to 1.5 nm. The tapping mode set point was chosen as 80 % of the free amplitude, so that clear images of the MT's surfaces could be recorded without depolymerizing the MTs due to scanning forces. The tip at the end of the cantilever was a carbon tip grown by electron beam deposition and etched to have an apex radius of typically 2 nm – 5 nm. The imaging rate was set between 300 ms and 500 ms. To fix the MTs for scanning 1 μL of the stock DNA modified MT was deposited on a freshly cleaved mica surface and incubated for 10 minutes. After the deposition, the free MTs were washed with 40 μL BRB80 buffer and observed by HS-AFM.

4.4.7 HS-AFM imaging and analysis of MT swarm rings with the combined HS-AFM/TIRF microscope

The combined high-speed atomic force microscope and total internal reflection microscope (HS-AFM/TIRF microscope) is a laboratory-built system, where the HS-AFM part is of the tip-scanning type.[22] Cantilevers and imaging parameters are equivalent to the sample-scanning HS-AFM procedure described above, except the imaging rate was set between 1 s and 5 s. After

placing the flow-cell prepared as described above on the stage of HS-AFM/TIRF microscope, 20 μL BRB80 buffer was added. After observing the swarm using TIRF microscope the MTs were crosslinked using glutaraldehyde (2.5 %). After 5 minutes, the glutaraldehyde solution was washed away, 200 μL BRB80 buffer was added, and the HS-AFM measurements were started.

To estimate the number of MTs contained in a swarm ring, radial line profiles around the swarm rings were collected. These line profiles were analysed using a custom-made GNU Octave program in the following way. First, starting from the bottom of the line profile, circles with a diameter of 25 nm and a distance of 8 nm between them were aligned within the line profile. The condition of whether to place a circle at a certain position is that it does not intersect with the line profile. After the bottom row is finished, the placement of circles in the next row is conducted in the same fashion. The circles in a following row are always placed so that their centers lie above center point between two circles of the preceding row, with a minimal distance of 8 nm to the circles – essentially forming a hexagonal pattern.

It should be noted, that this counting method is an estimate that has some implicit assumptions. First, it is assumed that the MTs are aligned in a regular fashion, that do not contain any internal voids. Second, it is assumed that each MT is found exactly one time within a line profile – MTs are not so long to wind more than once around the ring or are too short to not reach the full circumference. While the former assumption would lead to an overestimation of the total MTs the latter could be both depending on the ring size in relation to the MT length.

4.4.8 DMD MOSAIC system for the dissociation of MT swarm ring by irradiation of UV light

The swarming of MTs was performed using two *p*-DNAs in the flow channel made by two cover glasses as described earlier. The MT swarm ring was dissociated using a digital mirror device (DMD) mosaic system irradiating UV light (340-390 nm) at a particular area. The DMD system contains 800 × 600 mirrors of about 10 μm. Using the electronic control of the DMD, orientation of the mirrors can be changed one by one. MOSAIC 3 irradiates light (λ = 360-800 nm) at a frame rate of 5000 fps in any region and time. A mirror is installed on the stage of the fluorescence microscope, and ultraviolet light was irradiated through MOSAIC system. After 30 minutes of ATP addition the swarming was completely formed, and the UV light was irradiated to the regions of interest to dissociate the particular swarm. From this dissociation experiment, the number of

MTs were counted manually and the number of MTs in the width of the swarm was calculated from the circumference of the swarm.

4.4.9 Estimation of parameters and statistical analysis

The fluorescence microscopy images were analyzed by NIS-Elements AR (version 5.30.02, Nikon) software. Statistical analysis and profiles were drawn using software OriginPro Version 2019 (OriginLab, USA).[44] The HS-AFM images were analyzed using laboratory-made analysis software Falcon Viewer based on Igor Pro 8. A custom-made GNU Octave program was used to estimate the number of MTs and distance between them in the swarm by fitting into the height profile.[33]

Table 1. The DNA sequences used to demonstrate swarming and labeling ratio of DNA to tubulin

Name of DNA	Sequence (Z is azobenzene)	5' end	3' end	Molar Extinction coefficient, $Lmol^{-1}cm^{-1}$	Labeling ratio %
DNA1	CAACAACAACAACAACAACAACAA	DBCO	-	210200	93
DNA2	TTGTTGTTGTTGTTGTTGTTGTTG	DBCO	-	147400	102
p-DNA1	TTTTTTTTTTTTTTGZTTGZTTG	DBCO	-	205500	41
p-DNA2	CAAZCAAZCAAZCAAZCAAZCAAZ CAAZCAA	DBCO	-	367800	33

4.5 References

1. Whitesides, G. M. & Grzybowski, B. Self-assembly at all scales. *Science.* **295,** 2418–2421 (2002).
2. Beshers, S. N. & Fewell, J. H. Models of division of labor in social insects. *Annu. Rev. Entomol.* **46,** 413–40 (2001).
3. Niven, J. E. How honeybees break a decision-making deadlock. *Science.* **335,** 43–44 (2012).
4. Turgut, A. E., Çelikkanat, H., Gökçe, F. & Şahin, E. Self-organized flocking in mobile robot swarms. *Swarm Intell.* **2,** 97–120 (2008).
5. Wei, H., Chen, Y., Tan, J. & Wang, T. Sambot : A Self-Assembly Modular Robot System. *IEEE/ASME Trans. Mechatronics.* **16,** 745–757 (2011).
6. Keya, J. J., Kabir, A. M. R., Inoue, D., Sada, K., Hess, H., Kuzuya, A. & Kakugo, A. Control of swarming of molecular robots. *Sci. Rep.* **8,** 1–10 (2018).
7. Keya, J. J., Suzuki, R., Kabir, A. M. R., Inoue, D., Asanuma, H., Sada, K., Hess, H., Kuzuya, A. & Kakugo, A. DNA-assisted swarm control in a biomolecular motor system. *Nat. Commun.* **9,** 4–11 (2018).
8. Akter, M., Keya, J. J., Kayano, K., Kabir, A. M. R., Inoue, D., Hess, H., Sada, K., Kuzuya, A., Asanuma, H. & Kakugo, A. Cooperative cargo transportation by a swarm of molecular machines. *Sci. Robot.* **7,** eabm0677 (2022).
9. Liu, H., Spoerke, E. D., Bachand, M., Koch, S. J., Bunker, B. C. & Bachand, G. D. Biomolecular motor-powered self-assembly of dissipative nanocomposite rings. *Adv. Mater.* **20,** 4476–4481 (2008).
10. Oster, G. & Wang, H. Rotary protein motors. *Trends Cell Biol.* **13,** 114–121 (2003).
11. Jülicher, F., Ajdari, A. & Prost, J. Modeling molecular motors. *Rev. Mod. Phys.* **69,** 1269–1281 (1997).
12. Ito, M., Kabir, A. M. R., Inoue, D., Torisawa, T., Toyoshima, Y., Sada, K. & Kakugo, A. Formation of ring-shaped microtubule assemblies through active self-organization on dynein. *Polym. J.* **46,** 220–225 (2014).
13. Hess, H., Clemmens, J., Brunner, C., Doot, R., Luna, S., Ernst, K. H. & Vogel, V. Molecular self-assembly of ‘nanowires’ and ‘nanospools’ using active transport. *Nano Lett.* **5,** 629–633 (2005).

14. Kabir, A. M. R., Inoue, D. & Kakugo, A. Molecular swarm robots: recent progress and future challenges. *Sci. Technol. Adv. Mater.* **21,** 323–332 (2020).
15. Inoue, D., Mahmot, B., Kabir, A. M. R., Farhana, T. I., Tokuraku, K., Sada, K., Konagaya, A. & Kakugo, A. Depletion force induced collective motion of microtubules driven by kinesin. *Nanoscale* **7,** 18054–18061 (2015).
16. Needleman, D. J., Ojeda-Lopez, M. A., Raviv, U., Miller, H. P., Wilson, L. & Safinya, C. R. Higher-order assembly of microtubules by counterions: From hexagonal bundles to living necklaces. *Proc. Natl. Acad. Sci. U. S. A.* **101,** 16099–16103 (2004).
17. Binnig, G. & Quate, C. F. Atomic Force Microscope. *Handb. Phys. Med. Biol.* **56,** 5-1-5–9 (1986).
18. Ando, T., Kodera, N., Takai, E., Maruyama, D., Saito, K. & Toda, A. A high-speed atomic force microscope for studying biological macromolecules. *Proc. Natl. Acad. Sci. U. S. A.* **98,** 12468–12472 (2001).
19. Keya, J. J., Inoue, D., Suzuki, Y., Kozai, T., Ishikuro, D., Kodera, N., Uchihashi, T., Kabir, A. M. R., Endo, M., Sada, K. & Kakugo, A. High-Resolution Imaging of a Single Gliding Protofilament of Tubulins by HS-AFM. *Sci. Rep.* **7,** 1–7 (2017).
20. Ganser, C. & Uchihashi, T. Microtubule self-healing and defect creation investigated by in-line force measurements during high-speed atomic force microscopy imaging. *Nanoscale* **11,** 125–135 (2019).
21. Ganser, C. & Uchihashi, T. Microtubule Preparation for Investigation with High-Speed Atomic Force Microscopy. *Methods Mol. Biol.* **2430,** 337–347 (2022).
22. Fukuda, S., Uchihashi, T., Iino, R., Okazaki, Y., Yoshida, M., Igarashi, K. & Ando, T. High-speed atomic force microscope combined with single-molecule fluorescence microscope. *Rev. Sci. Instrum.* **84,** (2013).
23. Ando, T., Kodera, N., Takai, E., Maruyama, D., Saito, K. & Toda, A. A high-speed atomic force microscope for studying biological macromolecules. *Proc. Natl. Acad. Sci. U. S. A.* **98,** 12468–12472 (2001).
24. Wijeratne, S. S., Marchan, M. F., Tresback, J. S. & Subramanian, R. Atomic force microscopy reveals distinct protofilament-scale structural dynamics in depolymerizing microtubule arrays. *Proc. Natl. Acad. Sci. U. S. A.* **119,** (2022).
25. Nasrin, S. R., Ganser, C., Nishikawa, S., Rashedul Kabir, A. M., Sada, K., Yamashita, T.,

Ikeguchi, M., Uchihashi, T., Hess, H. & Kakugo, A. Deformation of microtubules regulates translocation dynamics of kinesin. *Sci. Adv.* **7,** 1–12 (2021).

26. Akter, M., Keya, J. J., Kabir, A. M. R., Rashid, M. R., Ishii, S. & Kakugo, A. Functionalization of Tubulin: Approaches to Modify Tubulin with Biotin and DNA. *Methods Mol. Biol.* **2430,** 47—59 (2022).
27. Inaba, H., Yamada, M., Rashid, M. R., Kabir, A. M. R., Kakugo, A., Sada, K. & Matsuura, K. Magnetic Force-Induced Alignment of Microtubules by Encapsulation of CoPt Nanoparticles Using a Tau-Derived Peptide. *Nano Lett.* **20,** 5251–5258 (2020).
28. Inaba, H., Sueki, Y., Ichikawa, M. & Kabir, A. M. R. Generation of stable microtubule superstructures by binding of peptide- fused tetrameric proteins to inside and outside. *Sci. Adv.* **8,** 1–30 (2022).
29. Chi, Q., Wang, G. & Jiang, J. The persistence length and length per base of single-stranded DNA obtained from fluorescence correlation spectroscopy measurements using mean field theory. *Phys. A Stat. Mech. its Appl.* **392,** 1072–1079 (2013).
30. Garrido, J. A., Vainrub, A. & Pettitt, B. M. A model for Structure and Thermodynamics of ssDNA and dsDNA Near a Surface: a Course Grained Approach. *NIH Public Access* **181,** 1–7 (2010).
31. Boal, A. K., Tellez, H., Rivera, S. B., Miller, N. E., Bachand, G. D. & Bunker, B. C. The stability and functionality of chemically crosslinked microtubules. *Small* **2,** 793–803 (2006).
32. Turner, D., Chang, C., Fang, K., Cuomo, P. & Murphy, D. Kinesin movement on glutaraldehyde-fixed microtubules. *Anal. Biochem.* **242,** 20–25 (1996).
33. Lemenkova, P. Awk and Gnu Octave Programming Languagesintegrated With Generic Mapping Tools for Geomorphological Analysis. *Geosci. Eng.* **65,** 1–22 (2019).
34. Johnson, E. & Pardue, M. Lou. *Nucleic acid*. *MacGraw-Hill Educ.* (2014).
35. Ishii, S., Akter, M., Murayama, K., Kabir, A. M. R., Asanuma, H., Sada, K. & Kakugo, A. Kinesin motors driven microtubule swarming triggered by UV light. *Polym. J.* (2022).
36. Stelzer, E. H. K. Contrast, resolution, pixelation, dynamic range and signal-to-noise ratio. *R. Microsc. Soc. J. Microsc.* **189,** 15–24 (1998).
37. Kakugo, A. in *Mol. Robot. An Introd.* (ed. Murata, S.) 195–214 (Springer Nature Singapore, 2022).

38. Ishii, S., Akter, M., Keya, J. J., Rashid, M. R., Afroze, F., Nasrin, S. R. & Kakugo, A. Purification of Tubulin from Porcine Brain and its Fluorescence Dye Modification. *Methods Mol. Biol.* **2430,** 3–16 (2022).
39. Castoldi, M. & Popov, A. V. Purification of brain tubulin through two cycles of polymerization- depolymerization in a high-molarity buffer. *Protein Expr. Purif.* **32,** 83–88 (2003).
40. Peloquin, J., Komarova, Y. & Borisy, G. Conjugation of fluorophores to tubulin. *Nat. Methods* **2,** 299–303 (2005).
41. Case, R. B., Pierce, D. W., Hom-Booher, N., Hart, C. L. & Vale, R. D. The directional preference of kinesin motors is specified by an element outside of the motor catalytic domain. *Cell* **90,** 959–966 (1997).
42. Früh, S. M., Steuerwald, D., Simon, U. & Vogel, V. Covalent cargo loading to molecular shuttles via copper-free 'click chemistry'. *Biomacromolecules* **13,** 3908–3911 (2012).
43. Kabir, A. M. R., Inoue, D., Kakugo, A., Kamei, A. & Gong, J. P. Prolongation of the Active Lifetime of a Biomolecular Motor for in Vitro Motility Assay by Using an Inert Atmosphere. *Langmuir* **27,** 13659–13668 (2011).
44. Edwards, P. M. Origin 7.0: Scientific graphing and data analysis software. *J. Chem. Inf. Comput. Sci.* **42,** 1270 (2002).

Chapter 5

Concluding remarks

This dissertation mainly represents the construction of kinesin-propelled swarming of microtubules (MT)s and the force determination of the swarm using a magnetic bead and an electromagnetic tweezer combined with a fluorescence microscope. The structural details of the MT swarm ring were also investigated in detail using high-speed atomic force microscopy.

In chapter 2, the setup of a custom-made electromagnetic tweezer combined with a fluorescence microscope was described briefly and a magnetic bead was introduced for the force calibration. The microactuators and rotary angle were assembled in the tweezers set up for the spatial arrangement and a current source was employed for the controlled emf generation. A swarm of the MT-kinesin was performed by the recognition ability of DNA and chemical energy from ATP. After the successful force calibration of the beads and performing the swarming of MTs, the evaluation of the tweezer to the bead-loaded MT-kinesin swarm system was examined. The detachment of the MT swarms from the kinesin-coated surface was found by applying emf. In addition, the directional manipulation of the MT swarms was also found as the tweezer was applied. This work offers technical advantages for the setup of electromagnetic tweezers and the systematic application of magnetic force spatially to the bead-loaded swarm for distinct purposes. This study will enrich the current understanding of the use of electromagnetic tweezers in biomolecular manipulations and dynamic control over the MT-kinesin swarming system.

In chapter 3, I systematically established the DNA-based swarm ring of MTs propelled by kinesin. DNA-modified microtubules were prepared using click reaction and the time dependency of the swarm ring in terms of the concentration of DNA and kinesin was investigated on the swarm formation. The beads were successfully attached to the swarm ring and controlled magnetic force was applied to the bead-carrying swarm ring by changing the direction of motion. The results show that the swarm ring's velocity increases and decreases according to the angle of applied emf. The velocity oscillation of the swarm ring was obtained by the applied emf to the kinesin motors in a

positive and negative direction due to the circular motion of the swarm ring. The force of the swarm estimated from the force calibration curve shows a sub-additive increasing tendency with increasing kinesins involved. This force estimation revealed the basic properties of the MT swarm driving by thousands of kinesins and helps to understand the cooperative cargo transportation by the MT swarm as it has the capability to supply very high force. It is expected that the results will contribute to understanding the force production of the swarm as well as the work done by the swarm, and it is expected to rise new ideas for designing future biomolecular devices to perform nanotechnological tasks.

In chapter 4, I presented a detailed investigation of the structure of MT swarm rings on the level of a single of MTs using a combination of HS-AFM and fluorescence microscopy. HS-AFM proved to be a powerful tool to understand the assembly and spatial arrangement of MT filaments. Compared to conventional fluorescence microscopy HS-AFM allows the visualization of individual MTs in their 3-dimensional arrangement. DNA-modified MTs organize themselves in multiple layers to form a swarm ring instead of forming a single-layered sheet. This has the obvious implication that not all of the MTs are in contact with the kinesin-covered substrate and only a part of the MTs contribute to the force generation of the MT swarm ring. In order to efficiently use MT swarms as a source of rotational energy, it is necessary to increase the number of load-carrying kinesins. The current findings on the structure of MT swarm rings can contribute to maximizing their applications for the development of molecular machines and robots as power sources.

Finally, I would like to draw a future perspective of my entire work. The incorporation of the magnetic bead and the electromagnetic tweezer made it possible to determine the force in a controlled manner. And the force obtained from the swarm was much higher than the single kinesin and single MT motility systems. The study would serve the knowledge in the viewpoint from biology, physics, and engineering systems not only to realize the force produced by the swarm but also to develop the swarm with different functionalities for future nanotechnological applications. The high force of the MT swarm would be helpful to design and construct an efficient bio-machine to work in a more sophisticated way. Proper utilization of the DNA-based MT swarm ring could be used as a coil to produce energy from the rotational motion for a more complex task. As MT swarm rings convert chemical energy into rotational motion, it could be a fundamental power generator for nano or micromachines for future applications like localized surgery on the level of

cells or below. Despite this ongoing progress, there are several issues to address for the practical applications of molecular robots such as energy efficiency and reusability. From the perspective of sustainable development goals, it would be intriguing to take further initiatives in the future to tackle the challenges related to the energy crisis.

List of Publications

Manuscripts (related to this dissertation)

Chapter 2, 3

Force determination of the kinesin-driven microtubule's swarm using electromagnetic tweezers; M. R. Rashid, M. Akter, A. M. R. Kabir, K. Sada, A. Kakugo; *to be submitted*

Chapter 4

3D structure of ring-shaped microtubule swarms revealed by high-speed atomic force microscopy; M. R. Rashid, C. Ganser, M. Akter, S. R. Nasrin, A. M. R. Kabir, K. Sada, T. Uchihashi, A.Kakugo; Chemistry Letters, 2022, 52, 2.

Manuscripts (not related to this dissertation)

i. Magnetic Force-Induced Alignment of Microtubules by Encapsulation of Co-Pt Nanoparticles Using a Tau-Derived Peptide; H. Inaba, M. Yamada, M. R. Rashid, A. M. R. Kabir, A. Kakugo, K. Sada, and K. Matsuura; Nano letters, 2020, 20, 5251−5258.

ii. Silica fillers for enhancement of dielectric properties of poly(vinylidene fluoride) and its copolymer; M. Khair, M. R. Rashid, S. Ahmed, M. A. B. H. Susan; Materials Today: Proceedings, 2020, 29, 1239–1245.

iii. Control of the porosity and morphology of ordered mesoporous silica by varying calcination conditions; M. R. Rashid, F. Afroze, S. Ahmed, M. S. Miran, M. A. B. H. Susan; Materials Today: Proceedings, 2019, 15, 546–554.

Book Chapters (not related to this dissertation)

i. Functionalization of Tubulin: Approaches to Modify Tubulin with Biotin and DNA; M. Akter, J. J. Keya, A. Md. R. Kabir, M. R. Rashid, S. Ishii, A. Kakugo; Methods in Molecular Biology (Clifton, NJ), 2022, 2430, 47-49.

ii. Purification of Tubulin from Porcine Brain and its Fluorescence Dye Modification; S. Ishii, M. Akter, J. J. Keya, M. R. Rashid, F. Afroze, S. R. Nasrin, A. Kakugo; Methods in Molecular Biology (Clifton, NJ), 2022, 2430, 3-16.

iii. Construction of Molecular Robots from Microtubules for Programmable Swarming; J. J. Keya, M. Akter, A. Md. R. Kabir, M. R. Rashid, A. Kakugo; Methods in Molecular Biology (Clifton, NJ), 2022, 2430, 219-230.

List of conference presentation

Presentation (related to this dissertation)

1. Force estimation of kinesin driven microtubule's swarm using electromagnetic tweezers; M. R. Rashid, M. Akter, A. M. R. Kabir, J. J. Keya, K. Sada, A. Kakugo; The 8th International Life-Science Symposium 2022, 4th November 2022 (Oral).

2. Force measurement of kinesin-propelled microtubules in swarming using electromagnetic tweezers; M. R. Rashid, M. Akter, A. M. R. Kabir, K. Sada, A. Kakugo; Chem-Bio Informatics Society Annual Meeting 2022, 25-27th October 2022 (Oral).

3. Measuring the force generated by the swarm of microtubules driven by multiple kinesins M. R. Rashid, M. Akter, A. M. R. Kabir, K. Sada, A. Kakugo; The 12th CSE-ALP International Autumn School, 13-14th October 2021 (Oral)

4. Force Determination of Circular Shaped Microtubule's Swarm Driven by Kinesin Using Electromagnetic Tweezers; M. R. Rashid, M. Akter, A. M. R. Kabir, K. Sada, A. Kakugo; 第 70 回高分子討論会, 6-8th September 2021 (Oral).

5. Determination of Interaction Force of Circular Swarm Microtubules Driven by Kinesin using Dynabeads and Electromagnetic Tweezers; M. R. Rashid, M. Akter, J. J. Keya, A. M. R. Kabir, K. Sada, A. Kakugo; 2020 55th Hokkaido Branch Research Seminar (2020 年度　第 55 回北海道支部研究発表会), 28th January 2021 (Oral).

6. Force Determination of Circular Swarm Microtubules Driven by Kinesin using Electromagnetic Tweezers; M. R. Rashid, M. Akter, J. J. Keya, A. M. R. Kabir, K. Sada, A. Kakugo; The 11th CSE International Autumn School & The 8th ALP International Symposium, 4-5th November 2020 (Poster).

7. Force Measurement of Microtubules in Swarming Using Electromagnetic Tweezers; M. R. Rashid, M. Akter, J. J. Keya, A. M. R. Kabir, K. Sada, A. Kakugo; 7th International Life-Science Symposium (7th ILSS), 1st November 2019 (Poster).

Presentation (not related to this dissertation)

1. Porous silica for the enhancement of dielectric properties of PVDF based polymers; M. R. Rashid, S. Ahmed, M. A. B. H. Susan; International Conference on Nanotechnology and Condensed Matter Physics 2018 (ICNCMP), January 11-12, 2018 (Poster).

2. Temperature-Dependent Control of the Porosity of Mesoporous Silica, M. R. Rashid, S. Ahmed, M. S. Miran, M. A. B. H. Susan; 1st Symposium on Chemistry for Global Solidarity, October 14, 2016 (Poster).

3. Preparation and Characterization of Polyvinyl Alcohol/Mesoporous Silica Composite; M. R. Rashid, S. Ahmed, M. S. Miran, M. A. B. H. Susan; 16th Asian Chemical Congress (16 ACC), March 16-19, 2016 (Poster).